Digital Signal Processing and Spectrally Efficient Modulation for Short-Range Fiber-Optic and Fiber-Wireless Millimeter-Wave Links

Puerta Ramírez, Rafael

Publication date:
2017

Document Version
Publisher's PDF, also known as Version of record

Digital Signal Processing and Spectrally Efficient Modulation for Short-Range Fiber-Optic and Fiber-Wireless Millimeter-Wave Links

Rafael Puerta

Supervisors:
Professor Idelfonso Tafur Monroy
Adjunct Professor Juan José Vegas Olmos
Professor Jianjun Yu

Delivery Date: 1st September 2017

DTU Fotonik
Department of Photonics Engineering
Technical University of Denmark
Building 343
2800 Kgs. Lyngby
DENMARK

DTU Fotonik
Institut for Fotonik

"In light of photonics, distance is annihilated."
Puerta–Tesla

Abstract

In this thesis several digital signal processing (DSP) techniques and advanced modulation formats are investigated as means of increasing the capacity and spectral efficiency of fiber-optic links and hybrid fiber-wireless millimeter-wave (mmWave) communications systems. Enabled by the fast development of electronics, DSP has become one of the most prospective solutions to enhance the capacity and performance of current communications systems. Currently, the essential devices that allow high-speed DSP are at an advance stage, namely digital-to-analog converters (DACs) and analog-to-digital converters (ADCs), with sampling rates reaching several thousands of millions samples per second (GSa/s). However, to take advantage of these high-speed devices for real-time applications, the digital processing units are required to cope with these speeds, e.g. low-power consumption high-speed arithmetic logic units (ALUs). The further research and development of faster mixed-signal transceiver drivers and high-speed digital processing units have a fundamental role in the next generation of high capacity optical communications systems. This work is devoted to experimentally validate the flexibility and additional degrees of freedom provided by DSP to fiber-optic and photonics-enabled mmWave communications systems, while achieving record data rate transmissions and expanding the state-of-the-art.

Resumé

I denne afhandling undersøges flere digitale signalbehandlingsteknologier og avancerede modulationsformater som middel til at øge kapaciteten og spektral effektiviteten af fiberoptiske forbindelser og hybridfiber-trådløse millimeterbølge (mmWave) kommunikationssystemer. DSPen er muliggjort af den hurtige udvikling af elektronikken, og er blevet en af de mest potente løsninger til at forbedre kapaciteten og ydeevnen i de nuværende kommunikationsnet. I øjeblikket er de væsentlige enheder der tillader højhastigheds-DSP, nemlig digitale til analoge konvertere (DAC'er) og analog-til-digitale konvertere (ADC'er), på et avanceret niveau hvor samplingshastigheder når flere tusinde millioner prøver pr. Sekund (GSa/s). For at udnytte disse højhastigheds-enheder til realtidsapplikationer er de digitale behandlingsenheder imidlertid forpligtet til at klare disse hastigheder, f.eks. lavt strømforbrug højhastigheds aritmetiske logiske enheder (ALU'er). Den videre forskning og udvikling af hurtigere blandede-signal transceiver drivere og højhastighedse digitale behandlingsenheder har en afgørende rolle i den næste generation af optiske kommunikationssystemer med høj kapacitet. Dette arbejde er dedikeret til eksperimentelt at validere den fleksibiliteten og de yderligere frihedsgrader, der leveres af DSP til fiberoptiske og fotonik-aktiverede mmWave-kommunikationssystemer, samtidigt med at der opnås banebrydende dataoverførselsagtigheder og en udvidelse af state-of-the-art.

Acknowledgements

I want to start expressing my full gratitude to my supervisor Idelfonso for his trust in me and for being the enabler of my PhD. Thanks for his advice, motivation, and diligent support during this outstanding experience.

Thanks to Juan José for opening doors to unique opportunities imperative to my PhD.

Thanks to Jarek for sharing his expertise during the first stages of my PhD studies.

Thanks to Jianjun for encouraging me to go beyond my notions.

Thanks to Hoshida-san for the insightful conversations and for sharing his extensive knowledge.

Thanks to my friend Simon for his massive help throughout the course of my PhD.

Thanks to my friends Victor, Lau, Peter and to my colleagues from Metro-access group for making my stay at DTU 'top of the line'.

Thanks to Yamauchi-san for the great teamwork and his friendship during my fruitful stay at Fujitsu.

Thanks to Jose Antonio and Miguel for the valuable technical advice when most needed.

Thanks to Colciencias for providing the means and supporting my research.

Thanks to all the amazing people I had the chance to meet in the last years who contributed to any extend to the completion of this endeavor.

Thanks to my brothers for their genuine support and encouragement.

And overall, my most solemn thanks to my parents for their exemplary righteousness and devotion to me. Therefore, I dedicate this work to them.

Kawasaki, August 2017

Rafael Puerta

Summary of Original Work

This thesis is based on the following original publications:

PAPER 1 R. Puerta, M. Agustin, L. Chorchos, J. Tonski, J.-R. Kropp, N. Ledentsov, V. A. Shchukin, N. N. Ledentsov, R. Henker, I. T. Monroy, J. J. V. Olmos, and J. P. Turkiewicz, "107.5 Gb/s 850 nm multi- and single-mode VCSEL transmission over 10 and 100 m of multi-mode fiber," in *Optical Fiber Communication Conference Post-deadline Papers*, 2016, p. Th5B.5.

PAPER 2 R. Puerta, M. Agustin, L. Chorchos, J. Tonski, J.-R. Kropp, N. Ledentsov, V. A. Shchukin, N. N. Ledentsov, R. Henker, I. T. Monroy, J. J. V. Olmos, and J. P. Turkiewicz, "Effective 100 Gb/s IM/DD 850-nm Multi- and Single-Mode VCSEL Transmission Through OM4 MMF," *J. Light. Technol.*, vol. 35, no. 3, pp. 423–429, Feb. 2017.

PAPER 3 R. Puerta and I. T. Monroy, "Single Photodiode 60 Gb/s 16-QAM and QPSK Coherent Transmission," submitted to *IEEE Photonics Technol. Lett.*, Aug. 2017.

PAPER 4 R. Puerta, T. Yamauchi, T. Tanimura, Y. Akiyama, T. Takahara, I. T. Monroy, and T. Hoshida, "Single-Wavelength, Single-Photodiode per Polarization 276 Gb/s PDM 8-QAM over 100 km of SSMF," submitted to *Optical Fiber Communication Conference*, Oct. 2017.

PAPER 5 R. Puerta, J. Yu, X. Li, Y. Xu, J. J. V. Olmos, and I. T. Monroy, "Single Carrier PDM Radio-over-Fiber 328 Gb/s Wireless Transmission in a D-band Millimeter Wave 2×2 MU-MIMO System," *J. Light. Technol.*, vol. PP, no. 99, pp. 1–1, Sep. 2017.

PAPER 6 R. Puerta, S. Rommel, J. J. V. Olmos, and I. T. Monroy, "Optically Generated Single Side-Band Radio-over-Fiber Transmission of 60Gbit/s over 50m at W-Band," in *Optical Fiber Communication Conference*, 2017, p. M3E.4.

PAPER 7 R. Puerta, J. Yu, X. Li, Y. Xu, J. J. V. Olmos, and I. T. Monroy, "Demonstration of 352 Gbit/s Photonically-enabled D-Band Wireless Delivery in one 2 × 2 MIMO System," in *Optical Fiber Communication Conference*, 2017, p. Tu3B.3.

PAPER 8 R. Puerta, S. Rommel, J. J. V. Olmos, and I. T. Monroy, "Ultra Wideband Technology Comeback: Prospective Solution for 5G Next Generation Networks," submitted to *IEEE Commun. Mag.*, Apr. 2017.

PAPER 9 R. Puerta, S. Rommel, J. J. V Olmos, and I. T. Monroy, "Up to 35 Gbps ultra-wideband wireless data transmission links," in *2016 IEEE 27th Annual International Symposium on Personal, Indoor, and Mobile Radio Communications*, 2016, pp. 1–5.

PAPER 10 R. Puerta, J. J. V Olmos, I. T. Monroy, N. N. Ledentsov, and J. P. Turkiewicz, "Flexible MultiCAP Modulation and its Application to 850 nm VCSEL-MMF Links," *J. Light. Technol.*, vol. 35, no. 15, pp. 3168–3173, Aug. 2017.

Other scientific reports associated with the project:

[PAPER 11] **R. Puerta**, M. Agustin, L. Chorchos, J. Tonski, J.-R. Kropp, N. Ledentsov, V. A. Shchukin, N. N. Ledentsov, R. Henker, I. T. Monroy, J. J. V. Olmos, and J. P. Turkiewicz, "Short-range links beyond 100 Gb/s with vertical-cavity surface-emitting lasers," *SPIE Newsroom*, p. 1–3, 2017.

[PAPER 12] J. P. Turkiewicz, L. Chorchos, **R. Puerta**, J. J. V. Olmos, and N. Ledentsov, "On high speed transmission with the 850nm VCSELs," *Proc. SPIE*, vol. 10031. p. 100311B–100311B–6, 2016.

[PAPER 13] **R. Puerta**, J. J. V. Olmos, I. T. Monroy, J. P. Turkiewicz, "Adaptive MultiCAP modulation for short range VCSEL based transmissions," in *Latin America Optics and Photonics Conference*, 2016, p. LW4C.3.

[PAPER 14] **R. Puerta**, A. Morales, S. Rommel, I. Kim, O. Vassilieva, T. Ikeuchi, and I. T. Monroy, "Physical Layer 1 Gb/s Secret Wireless Data Transmission at W-Band using a Photonic Duffing System," submitted to *Optical Fiber Communication Conference*, Oct. 2017.

[PAPER 15] S. Rommel, **R. Puerta**, J. J. V. Olmos, and I. T. Monroy, "Capacity Enhancement for Hybrid Fiber-Wireless Channels with 46.8Gbit/s Wireless Multi-CAP Transmission over 50m at W-Band," in *Optical Fiber Communication Conference*, 2017, p. M3E.5.

[PAPER 16] **R. Puerta**, S. Rommel, J. J. V Olmos, and I. T. Monroy, "10Gb/s ultra-wideband wireless transmission based on multi-band carrierless amplitude phase modulation" in *2016 IEEE 17th Annual Wireless and Microwave Technology Conference*, 2016, pp. 1–4.

[PAPER 17] J. A. Altabas, S. Rommel, **R. Puerta**, D. Izquierdo, I. Garces, J. A. Lazaro, J. J. Vegas Olmos, and I. T. Monroy, "Non-Orthogonal Multiple Access and Carrierless Amplitude Phase Modulation for Flexible Multi-User Provisioning in 5G Mobile Networks," *J. Light. Technol.*, vol. PP, no. 99, pp. 1–1, Oct. 2017.

[PAPER 18] J. A. Altabas, S. Rommel, **R. Puerta**, D. Izquierdo, I. Garces, J. A. Lazaro, J. J. Vegas Olmos, and I. T. Monroy, "Non-Orthogonal Multiple Access and Carrierless Amplitude Phase Modulation for 5G Mobile Networks," in *European Conference on Optical Communication*, 2017, p. Tu.1.B.2.

[PAPER 19] **R. Puerta**, J. Yu, X. Li, Y. Xu, J. J. V. Olmos, and I. T. Monroy, "Antenna misalignment effects in 100 Gbit/s D-band wireless transmissions," *Microw. Opt. Technol. Lett.*, vol. 59, no. 6, pp. 1431–1434, 2017.

[PAPER 20] **R. Puerta**, S. Rommel, J. A. Altabas, L. Pyndt, R. Idrissa, A. K. Sultanov, J. J. Vegas Olmos, and I. T. Monroy, "Multiband carrierless amplitude/phase modulation for ultrawideband high data rate wireless communications," *Microw. Opt. Technol. Lett.*, vol. 58, no. 7, pp. 1603–1607, 2016.

[PAPER 21] S. Rodriguez, **R. Puerta**, H. Kim, J. J. Vegas Olmos, and I. T. Monroy, "Photonic Up-convertion of carrierless amplitude phase signals for wireless communications on the Ka-band," *Microw. Opt. Technol. Lett.*, vol. 58, no. 9, pp. 2068–2070, 2016.

[PAPER 22] I. F. da Costa, S. Rodriguez, **R. Puerta**, J. J. V. Olmos, A. Cerqueira Jr., L. G. da Silva, D. Spadoti, and I. T. Monroy, "Photonic Downconversion and Optically Controlled Reconfigurable Antennas in mm-waves Wireless Networks," in *Optical Fiber Communication Conference*, 2016, p. W3K.3.

[PAPER 23] I. F. da Costa, A. Cerqueira Jr., S. Rodriguez, **R. Puerta**, J. J. V. Olmos, L. G. da Silva, D. Spadoti, and I. T. Monroy, "Photonics-assisted wireless link based on mm-wave reconfigurable antennas," *IET Microwaves, Antennas Propag.*, Aug. 2017.

[PAPER 24] M. Rico-Martinez, A. Morales, V. Mehmeri, **R. Puerta**, M. Varon, and I. T. Monroy, "Procedure to measure real time latency using software defined radio in a W-band fiber-wireless link," *Microw. Opt. Technol. Lett.*, vol. 59, no. 12, pp. 3147–3151, 2017.

[PAPER 25] G. K. M. Hasanuzzaman, S. Spolitis, T. Salgals, J. Braunfelds, A. Morales, L. E. Gonzalez, S. Rommel, **R. Puerta**, P. Asensio, V. Bobrovs, S. Iezekiel, and I. T. Monroy, "Performance Enhancement of Multi-Core Fiber Transmission Using Real-Time FPGA Based Pre-Emphasis," accepted in *Asia Communications and Photonics Conference*, Sep. 2017.

Contents

Chapter 1

Introduction

1.1 Motivation

Worldwide data traffic is increasing at an unprecedented rate. A clear example is global mobile data traffic which increased 4000-fold from 2005 to 2015 and almost 400-million-fold from 2000 to 2015. It is forecast that annual worldwide internet protocol (IP) traffic will reach 3.3 zettabytes (ZB) by 2021 [1], annual datacenter IP traffic will reach 15.3 ZB by the end of 2020 [2], and mobile data traffic will exceed half a ZB [3].
In light of these numbers, photonics engineers and physicists research is paramount to next generation optical communications systems. Thanks to engineers and physicists thriving collaboration, current optical communication networks were enabled, e.g. wavelength-division multiplexing (WDM) technology [4], [5]. This is such an exemplary synergy, that *good physicists upgrade themselves into system engineers.*[1]

It is challenging to cope with current data traffic growth and data transfer increasing speeds in different scenarios. Global intra-datacenter IP traffic is predicted to grow 3-fold from 2015 to 2020 at a compound annual growth rate (CAGR) of 26.8 percent, mainly due the increase of cloud computing services and internet-of-everything (IoE) technologies and applications. Including the traffic entering, exiting and within the datacenter, the IP traffic will grow 3-fold from 2015 to 2020 as well [2]. Fig. 1.1 summarizes the forecast of datacenter overall IP traffic growth.

Proportionately, the effects of the increasing speeds on traffic growth have defined recent trends on metro-access networks. Broadband speed is an essential enabler of IP traffic, therefore, the adoption and deployment

[1] Dr. Tingye Li remark.

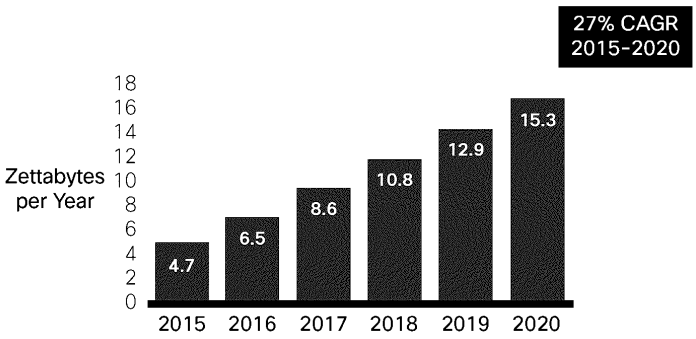

Figure 1.1: Forecast of worldwide datacenter IP traffic growth [2].

of fiber-to-the-home (FTTH) is fundamental to support user cloud storage, allowing the download of large multimedia files as fast as a transfer from a local data storage device. The underlying reason for this accelerated growth in today's homes is the vast increase of streaming media and high definition video-on-demand services. Therefore, it is desirable to carry traffic closer to the end user, however, today most of the traffic is deposited onto regional core networks, thus the percentage of metro networks traffic is lower than the core traffic share. However, traffic from metro networks is growing faster than from core networks and will reach 35 percent of total users' internet traffic by 2021, up from 22 percent in 2016 (Fig. 1.2). Furthermore, in 2016, global households with FTTH connectivity generated 28 percent more traffic than households connected by DSL or cable broadband. The average FTTH user generated 84 Gb per month in 2016 and is forecast to generate 183 Gb per month in 2021. [1]. In addition, the demands on datacenter interconnects (DCIs) are more stringent due the increase of datacenters size and number around the globe. It is forecast that the datacenter-to-datacenter traffic will grow 3-fold from 2015 to 2020 at a CAGR of 31.9 percent [2].

Last but not least, in line to datacenters and metro-access networks trends, global mobile data traffic will continue growing, with nearly a sevenfold increase predicted between 2016 and 2021 [3]. Fig. 1.3 shows the forecast of worldwide overall mobile data traffic growth. The increasing demands for ubiquitous access to information and entertainment at higher data rates are one of the main challenges of future fifth generation (5G) wireless networks. Users are expecting wireless communications to reach the capacity of wired communications.

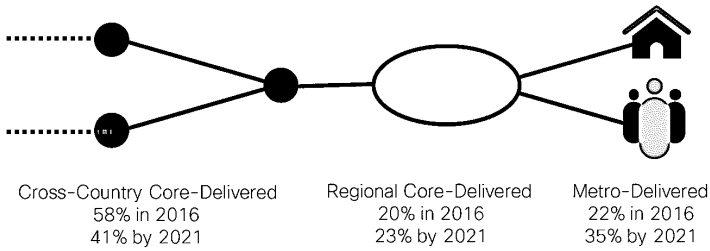

Figure 1.2: Forecast of users' total internet traffic distribution [1].

To cope with this growth, it is expected that upcoming 5G wireless systems will increase the spectral efficiency by a factor of 10 and to increase the capacity by a factor of 1000 of current systems. The rapid evolution of IoE applications and devices has triggered a drastic increase in its number and variety. New technologies must offer an adequate framework for the IoE, which will enable higher capacities and the flexibility to adapt to dynamic scenarios. In addition, in 2015 mobile offload traffic exceeded cellular traffic for the first time, since most of the mobile data activity takes place indoors, e.g. Wi-Fi access points in users' homes and offices. Thus, traffic generated by mobile devices and services is being offloaded from mobile networks, increasing the demand for denser networks with more fixed access nodes [3].

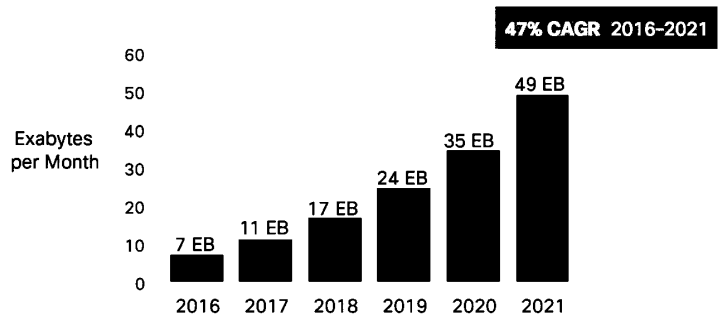

Figure 1.3: Forecast of worldwide overall mobile data traffic growth [3].

1.2 Research Framework

1.2.1 Intra-datacenter Networks

Intra-datacenter optical interconnects are applied to transmit data within information technology (IT) infrastructure, starting from intra-rack links to intra-datacenter connections. The key features required for such applications are high throughput, reduced footprint, low power consumption, and reduced cost of solution [6]–[9]. An appealing solution for intra-datacenter optical links is based on vertical-cavity surface-emitting lasers (VCSELs) and multi-mode fiber (MMF). VCSELs provide advantages of wide bandwidth, low energy consumption and low-cost production, while MMF can be easily coupled to VCSELs [10]. Due to its reduced size and high efficiency, VCSELs can provide tens of mW output power and can be combined in two-dimensional arrays to generate large power outputs from small area wafers (Fig. 1.4). Dense arrays of MMF can be used for inter- and intra-rack connections down to multi-gigabit optical backplanes [11].

However, as optical link length increases, mainly modal dispersion (MD) in MMFs deteriorates the signal quality of conventional multi-mode VCSELs transmissions. MD can be mitigated by reducing the number of modes of these VCSELs, ideally to achieve single-mode operation [12], [13]. VCSEL technology constitutes a low-cost transmission solution desirable for massive deployments, which decreases costs by less than half compared with standard single-mode fiber (SSMF) solutions [14].

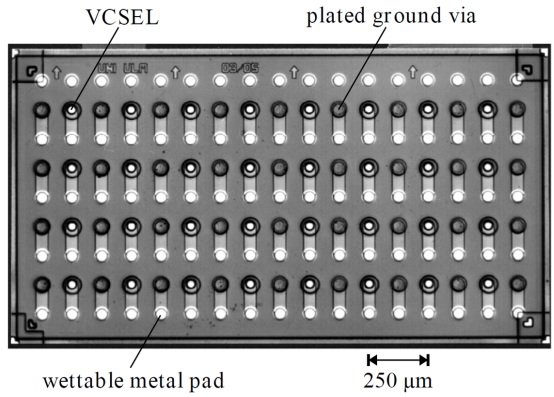

Figure 1.4: Layout of a 4×8 VCSEL array [9].

1.2.2 Metro-Access Networks and Datacenter Interconnects

Digital signal processing (DSP) combined with coherent detection provide the best performance in fiber-optic communications systems. Coherent transceivers capability to linearly transfer the amplitude and phase information of the optical field into the electrical domain, allows full compensation of linear and nonlinear deterministic fiber-optic transmission impairments [15]–[19]. In addition, the accelerated development of electronics has enabled spectrally efficient coherent transceivers reaching bitrates of 400 Gb/s single wavelength [20]–[22]. Therefore, coherent transceivers are the adopted solution for long-haul systems.
On the other hand, point-to-point metro-access range like optical interconnects are more cost-sensitive, therefore less complex intensity modulation and direct detection (IM/DD) based solutions are preferred, however at the expense of a limited reach. Currently, significant research is being performed to realize DCI and metro-access transmission links taking advantage of coherent transceivers' features while using a single photodetector (PD). Thus, the hardware complexity of coherent receivers is reduced to simple single PD direct-detection implementations.

In IM/DD systems, a single PD detects the optical power of a transmitted signal and converts it into an electrical current by square-law detection:

$$|r_s(t)|^2 = |r_x(t)|^2 + \left|r_y(t)\right|^2 \tag{1.1}$$

To achieve single PD coherent detection many challenges arise and new approaches must be explored. Without balanced coherent detection all phase information of the transmitted signal is lost, thus reversal of chromatic dispersion (CD) distortion in the frequency domain is not possible limiting significantly the distance of the link. Furthermore, critical impairments that affect the received signal are the non-Gaussian noise statistics, and the nonlinear distortions due to interaction of CD and square law detection [17], [23], [24].

1.2.3 5G Wireless Networks

The remarkable evolution of wireless networks [25] and the stringent current mobile data growth, drive the research of future 5G networks including cognitive networks, flexible spectrum management, millimeter-wave (mmWave) technology, and network densification, to name a few [26]–[29]. A solution

that has shown promising benefits is cell-shrinking, in which the capacity per unit area can be increased by deploying ultra-dense networks of small cells [26]–[32]. These dense networks are composed mainly by pico- and femto-cells with a wireless range up to 200 m and 10 m, respectively. Thus, by reusing the same frequency bands over different cells, service to more users and higher data rates per user can be provided (Fig. 1.5). In addition, cell-densification not only improves the spectral efficiency but also the radio signal energy efficiency. Reducing the cell size by 10 times the spectral efficiency can be improved by a factor of 100 and the radio energy efficiency by a factor of 3000 [32].

To cope with 5G networks capacity demands in dense networks, mmWave communications systems are a prospective candidate providing high capacity and long wireless reach [34]–[37]. Their main features are: provision of very large bandwidths, i.e. 30–300 GHz, unlike conventional narrowband communications systems which are overcrowded with current radio services; no interference with current mobile networks; and mmWave signals can be generated and processed with current electronics and photonics technologies. Furthermore, radio-over-fiber (RoF) communications systems can be combined with cloud radio access network (C-RAN) architectures, providing a cost-effective solution to achieve network densification [28]–[30], [38]. RoF transmission is a key candidate for next generation mmWave mobile front- and backhaul as well as wireless access, as it effectively combines fiber-optic and wireless transmission to provide large capacity and low latency, while allowing significant fiber distances between the central office and remote radio units (RRUs) [39]. Although mmWave has been used mainly for outdoor point-to-point backhaul links [40], extensive research is being performed to

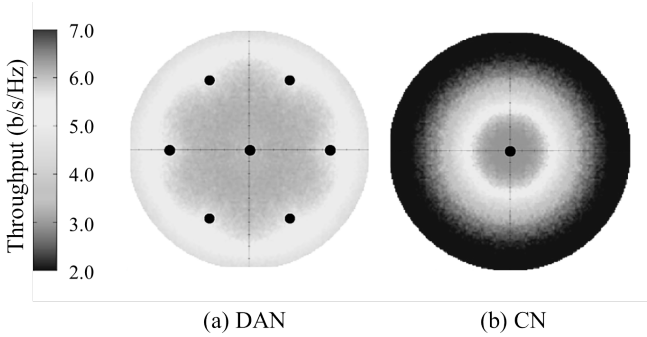

Figure 1.5: Spatial distribution of throughput. (a) Distributed antenna network (DAN) and (b) conventional cellular network (CN) [33].

improve the flexibility of mmWave systems by implementing multiple-input multiple-output (MIMO) schemes [26]–[28], [40]. Frequency bands in the mmWave range are often underutilized with low spectral efficiencies due to the impairments of wireless channels at these high frequencies, e.g. non-flat frequency response, multipath effect, and to the demanding radio frequency (RF) link budget. This is mainly due the strong propagation impairments of millimeter waves such as high free-space path loss (FSPL) and atmospheric and rain absorptions [26], [28].

For shorter wireless distances, e.g. indoor femto-cells, 5G networks are expected to provide new services to cope with future IoE massive device connection. The fast development of machine-to-machine (M2M) technologies, the massive adoption of mobile connectivity by end users, and the need for an optimal management of the bandwidth available are driving the development of new technologies and techniques to ensure a suitable framework for the IoE [3], [26]–[28]. As in larger area mmWave pico-cells, cell-shrinking and cell-densification hold key features which are in accordance with current offload traffic trends and consequently the increasing demands of more fixed access nodes [3], [26]. In these scenarios, ultra-wideband (UWB) technology is a promising alternative which can exploit large bandwidths and has the potential of achieving high-capacity short range wireless transmissions [41]. It can enable from diverse IoE services to high-speed wireless personal area networks (WPANs), where conventional computing and portable devices exchange large amounts of data.

The spectrum bands allocated for current microwave radio services such as cellular and Wi-Fi networks, fixed and mobile-satellite services, global positioning systems, to name a few, is saturated and requires expensive licenses to access. To maximize the capacity of the bandwidth used by these services, worldwide regulatory agencies established regulations enabling to share a wide range of microwave frequency bands on an unlicensed basis. To avoid adding interference to current services, these regulations impose strict limits on the permitted effective isotropic radiated power (EIRP) over a set of frequency bands. Thus, traditional narrowband receivers perceive UWB emissions as ordinary noise [41]. Fig. 1.6 shows the comparison of the UWB regulations established by the United States Federal Communications Commission (FCC), the European Electronic Communications Committee (ECC), and the Russian State Committee for Radio Frequencies (SCRF) [42]–[44]. The main features of UWB technology are its capacity to allow unlicensed operation if regulatory conditions are fulfilled [42]–[44], provision of very large bandwidths, and its ability to coexist with current narrowband

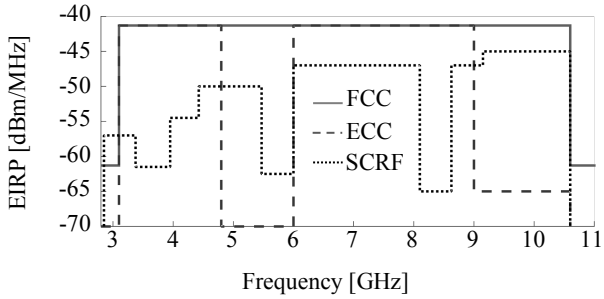

Figure 1.6: Comparison of FCC, ECC and SCRF regulations spectral masks.

wireless communications systems, e.g. Wi-Fi, WiMAX [45]. Furthermore, UWB technology is inherently a low-power solution. As an example, assuming the usage of the whole bandwidth at maximum radiated power defined by the FCC regulation, which is the most generous regulation in terms of power and bandwidth, the total radiated power is only 0.55 mW [41], [46].

1.3 Overview and Main Contributions

Throughout this work, two main modulation formats are investigated for multi-gigabit fiber-optic and wireless communications systems:

- Single-carrier quadrature amplitude modulation (SC-QAM) is used due its simplicity and since it doubles the spectral efficiency by transmitting two orthogonal streams of data simultaneously, namely the in-phase (I) and quadrature (Q) components. By means of a double-nested Mach-Zehnder modulator (MZM), i.e. optical I/Q modulator, in each component multilevel signals are transmitted, e.g. M-ary pulse amplitude modulation (M-PAM).

- Carrierless amplitude phase (CAP) modulation and its mutiband approach (MB-CAP). By means of two orthogonal digital filters, CAP modulation generates suppressed carrier QAM signals. Since CAP signals are generated by modulating a subcarrier in the digital domain, they are transmitted solely via intensity modulation and are demodulated by means of simple non-coherent receivers, e.g. matched filters. Therefore, simple IM/DD schemes are applied. Additionally, MB-CAP modulation is used to exploit the large bandwidths available in optical and mmWave wireless links, while mitigating the impairments of the channel due its non-flat frequency response and the limited bandwidth of electrical and optical devices. On

the other hand, in CAP modulation, when modulating the intensity of the optical carrier or the amplitude of the RF carrier, the resulting spectral efficiency can only reach up to half the spectral efficiency of QAM modulation, i.e. assuming the same baudrate and pulse shaping characteristics. To overcome this drawback, single sideband (SSB) modulation and independent sideband (ISB) modulation are applied by means of digital Hilbert transform filters and optical I/Q modulation. Thus, the spectral efficiency of CAP and MB-CAP modulation is enhanced to match QAM modulation spectral efficiency.
In addition to spectrally efficient modulation formats, pulse shaping and digital pre-distortion (DPD), e.g. de-emphasis to compensate digital-to-analog converters (DAC) frequency response, are applied to further increase the spectral efficiency and minimize the intersymbol interference (ISI).

At the receiver side, the benefits of using digital equalization, e.g. decision feedback equalizers (DFEs), with adaptive training algorithms are presented. These equalizers are used to mitigate the deterministic linear impairments of the channel by cancelling the precursors and postcursors of the channel impulse response. In the case of fiber-optic links, mitigation of CD, MD, and polarization mode dispersion (PMD) is achieved. In the case of wireless transmissions, multipath effects are mitigated. In addition, in both cases, DFEs compensate the ISI due the limited bandwidth of passive and active devices, and modulation I and Q imbalance.

The preceding modulation schemes and DSP techniques are experimentally validated in short-range and metro-access fiber-optic links, in license-free UWB wireless systems, and in hybrid fiber-wireless mmWave systems:

- In short-range IM/DD intra-datacenter links, MB-CAP modulation is used to achieve record data rates by using low-cost directed modulated VCSELs as light source. Multi-mode and quasi single-mode VCSELs are tested achieving a net data rate of 100.47 Gb/s over 10 m and 100 m of OM4 MMF, respectively. To the extent of our knowledge, this is the first experimental demonstration of a VCSEL-based transmission, single wavelength and single polarization, with a net bitrate of 100 Gb/s over up to 100 m of OM4 MMF **[PAPER 1]**, **[PAPER 2]**.

- In optical data links for metro-access networks and DCIs, SC-QAM modulation is used and a promising approach is proposed to take advantage of coherent transceivers' features with the simplicity of single PD direct detection based receivers. By means of heterodyne detection and carrier recovery based on a Costas loop, the I and Q components of the transmitted optical signal are retrieved. Therefore, by using a single PD, both the

amplitude and phase information of the optical field are recovered. The proposed scheme allows frequency domain CD compensation reducing the channel memory length to an ISI of a few symbols due remnant CD and other deterministic impairments, which subsequently can be compensated by a time domain equalizer. First, as a proof of concept, experimental transmissions of QPSK and 16-QAM single polarization signals, with a net bitrate of 60.75 Gb/s, are achieved over 10 km of SSMF **[PAPER 3]**. Then, in further experiments using a single light source and using a single PD per polarization, polarization division multiplexing (PDM) 8-QAM transmissions are achieved over 100 km of SSMF with a net bitrate of 230 Gb/s **[PAPER 4]**. To the extent of our knowledge, this is the first experimental demonstration of single-wavelength PDM coherent detection with a net bitrate of 230 Gb/s over 100 km of uncompensated SSMF by means of a receiver solely composed by two single PDs without an additional laser source as local oscillator (LO).

- In wireless RoF communications systems, UWB wireless systems and fiber-wireless mmWave systems are investigated. CAP and MB-CAP modulation are used to achieve record data rate transmissions, presenting a prospective solution for the upcoming next generation 5G networks. As ultra-dense small cell networks and cell shrinking is becoming a prospective solution for 5G wireless networks, and given that today most of the mobile traffic is offloaded from mobile networks, i.e. most of mobile users are connected to fixed networks, UWB wireless technology and mmWave systems are suitable options for femto- and pico-cells, respectively.

Photonics-enabled fiber-wireless transmissions are performed in two mmWave bands. In the W-band (75–110 GHz), by means of SSB MB-CAP modulation, a net bitrate of 56.08 Gb/s is transmitted over 10 km of SSMF and a wireless distance of 50 m **[PAPER 6]**. In the D-band (110–170 GHz), as a proof of concept, PDM ISB CAP and PDM ISB MB-CAP signals are transmitted over 25 km of SSMF and then transmitted wirelessly achieving net bitrates up to 328.97 Gb/s in a single 2×2 multi-user multiple-input multiple-output (MU-MIMO) system **[PAPER 5]**, **[PAPER 7]**. Wireless distance is limited to 1 m due to limited RF amplification.

Under the UWB indoor regulations established by the United States FCC, the European ECC, and the Russian SCRF, experimental transmissions are performed with record net bitrates up to 32.80 Gb/s, 20.25 Gb/s, and 9.35 Gb/s, respectively. For the FCC and ECC regulations, net bitrates of 1 Gb/s are transmitted over wireless distances up to 8 m and 6 m, respectively **[PAPER 8]**, **[PAPER 9]**.

To the extent of our knowledge, these UWB transmission bitrates are the highest data rates ever achieved in compliance with the FCC, ECC and SCRF regulations. Furthermore, the 328.97 Gb/s D-band wireless transmission is the highest data rate ever achieved in any mmWave band by means of a single 2×2 MU-MIMO system.

Chapter 2

Selected Topics in Fundamentals of Communications Systems

2.1 Spectrally Efficient Modulation

2.1.1 Quadrature Amplitude Modulation

QAM is the two-dimension generalization of PAM in which two streams of data are transmitted independently by modulating the amplitudes of two carriers of the same frequency shifted by 90 degrees, namely the I and Q components. This is equivalent to modulating both the amplitude and phase of a single carrier. A conventional QAM signal is built by two orthogonal basis functions:

$$\varphi_i(t) = p_i(t)\cos(2\pi f_c t) \tag{2.1}$$

$$\varphi_q(t) = p_q(t)\sin(2\pi f_c t) \tag{2.2}$$

where $p(t)$ are multilevel rectangular pulse shaped modulating signals. By adjusting only the amplitude of either signal, the phase and amplitude of the resulting mixed signal are changed [47], [48].

QAM broad adoption in current communication systems relies on its simplicity and capability of increasing spectral efficiency. Amplitude modulation (AM) generates double sideband (DSB) signals requiring twice the bandwidth of the modulating signal, thus underusing the bandwidth available. QAM generates two DSB signals occupying the same bandwidth, thus

it doubles the spectral efficiency compared to AM. To retrieve the I and Q components of QAM, homodyne detection receiver is used. For correct demodulation of QAM signals, a coherent receiver is used to recover the exact phase of the transmitted carrier. If the demodulating phase is not matched to the carrier signal, it results in crosstalk between the demodulated I and Q components [47], [48].

2.1.2 Carrierless Amplitude Phase Modulation

CAP modulation is a variation of QAM in which suppressed carrier QAM signals are generated, i.e. carrierless signals. Consequently, CAP modulation transmits two streams of data separately by means of two orthogonal signals (I and Q). A distinctive feature of CAP modulation is the use of a pulse shaping function to significantly improve the spectral efficiency. Unlike conventional QAM, the generation of the CAP signal is not achieved by modulating two orthogonal carriers with the same frequency, i.e. sine and cosine complementary signals. Instead, two orthogonal filters are used to generate the two components of the signal. These filters are the result of the time-domain multiplication of a pulse shaping function and two orthogonal carriers of the same frequency [47], [49]:

$$\varphi_i(t) = g_i(t)\cos(2\pi f_c t) \tag{2.3}$$

$$\varphi_q(t) = g_q(t)\sin(2\pi f_c t) \tag{2.4}$$

where $g(t)$ are multilevel signals with the spectral characteristics of the pulse shaping function used. CAP modulation can be performed completely in the digital domain, thus reducing its complexity. The orthogonal filters can be implemented as finite impulse response (FIR) filters (Fig. 2.1). In addition, since CAP modulation subcarrier is generated digitally, the resulting digital signal can be transmitted via intensity/amplitude modulation and its I and Q components can be retrieved by means of simple non-coherent receivers, e.g. digital matched filters to retrieve the signal to baseband [47].

The RRC pulse shaping function is a convenient choice to generate the filters, since at the receiver side a pair of matched filters, with the same shape, is used to retrieve the signal. Therefore, by combining both filters at the transmitter and the receiver, the complete response of the system has the characteristics of a raised cosine (RC) function, which minimizes ISI.

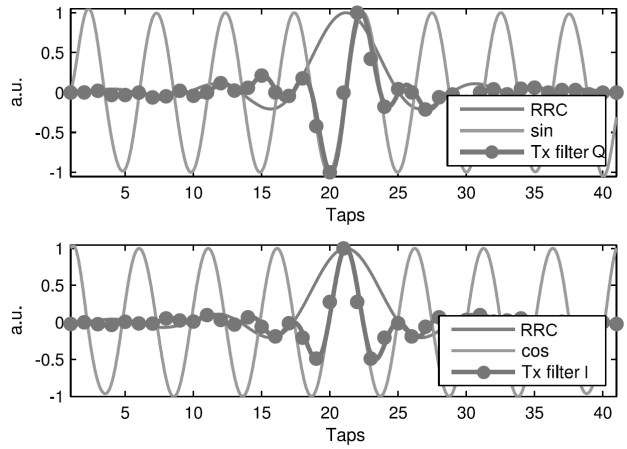

Figure 2.1: Exemplary CAP modulation orthogonal filters with root-raised cosine (RRC) pulse shape [49].

2.1.3 Multiband Carrierless Amplitude Phase Modulation

MB-CAP modulation relies on the simultaneous transmission of several CAP signals assigned to different frequency bands, ensuring that these bands do not overlap. This is achieved by using not only one pair of orthogonal filters, but several pairs with different orthogonal carrier frequencies assigned to each frequency band [49], [50]. Fig. 2.2 shows an exemplary of a 2-band MB-CAP modulation signal orthogonal filters.
The flexibility provided by MB-CAP allows to independently choose the modulation scheme, order, and signal power of each band, i.e. bit loading and power loading [49], [52], [53]. Further, a different baud rate can be assigned to each band [54], [55]. By means of these degrees of freedom, it is possible to compensate for the non-flat frequency response of the channel which is required for a reliable transmission of conventional CAP signals, and to achieve high spectral efficiencies in bandwidth limited systems.

2.2 Channel Deterministic Linear Impairments

2.2.1 Modal Dispersion

MD is an effect of different spatially orthogonal fiber modes travelling at different velocities. In MMFs, several modes propagate through the fiber where the number of modes is determined by the fiber geometry. For short-range applications, MMF based communication systems provide the neces-

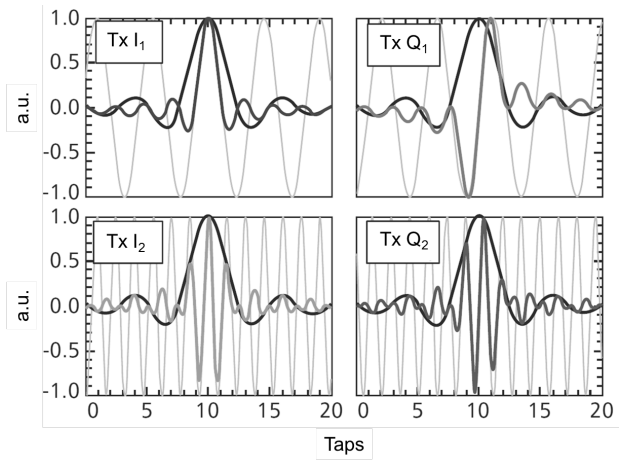

Figure 2.2: Exemplary 2-band MB-CAP modulation orthogonal filters with RRC pulse shape [51].

sary resources at a fraction of the cost of SSMF based solutions, e.g. relaxed optical coupling with light sources.

A simple model for signal propagation in MMFs comprises a set of M_n propagating modes, each of which propagates at different velocities through the fiber. After square-law photodetection, the power of all modes is added together. The following finite-length impulse response model for MMF propagation can be obtained when modal noise and mode coupling is ignored [56]:

$$h(t) = \sum_{k=0}^{M_n-1} e^{-\ln\frac{(10)\alpha L}{20}} h_k(t - \tau_0 - \tau_k) \tag{2.5}$$

where $\sum_{k=0}^{M_n-1} |h_k|^2 = 1$, $|h_k|^2$ is the incident power coupled to the k th mode, τ_k is the differential modal delay (DMD) with respect to the fundamental mode delay of τ_0, α is the attenuation, and L is the fiber length. The DMD is responsible of causing pulse broadening and ISI. Fig. 2.3 shows a numerical simulation where a 200-fs pulse is launched over 0.5 m of MMF, thus multiple modes are excited [57].

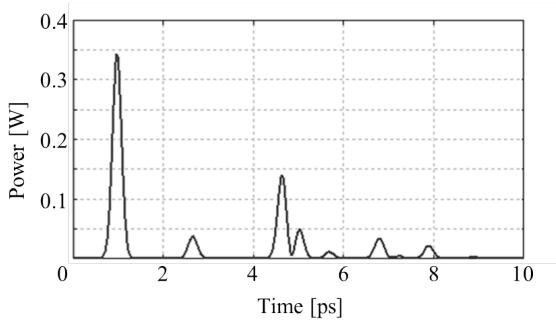

Figure 2.3: Received optical power versus time for a 200-fs input pulse over 0.5 m of MMF [57].

2.2.2 Chromatic Dispersion

The frequency dependence of the refractive index of the fiber is referred as CD. Its simplified transfer function is described by [58]:

$$G(z,\omega) = e^{\frac{j\omega^2\beta_2 z}{2}} \tag{2.6}$$

where ω is the angular frequency, β_2 is the group delay dispersion parameter of the fiber, and z is the propagation distance. From Equation 2.6 it is clear that CD only affects the phase of a signal with a quadratic proportion. In the frequency domain, the effect of CD can be represented as an all-pass filter which imposes different phase shifts to each spectral component. In the time domain, the different spectral components of optical pulses propagate at different group velocities which lead to pulse broadening and consequently ISI [15]–[19], [23], [58]. Since CD effects are proportional to the propagation distance z, the feasible transmission distance without implement a dispersion compensation method is limited. Furthermore, the ISI induced through CD in fiber-optic transmissions scales quadratically with the symbol rate, therefore for high baudrates signals the maximum transmission distance is severely reduced [17], [23].

2.2.3 Multipath Propagation

In wireless communications, multipath is the propagation phenomenon in that a single transmitted radio signal is scattered into various radio sig-

nals reaching the receiver antenna from different directions and with different time delays. Multipath propagation can be caused from atmospheric reflections to buildings and objects reflections. The resultant differential time delay introduces different relative phase shifts between the different components of the received signal. Therefore, depending on these relative phase shifts, constructive and destructive interference occurs resulting in frequency selective channels [47]. Similarly to MD, the finite-length impulse response of multipath phenomenon can be expressed by:

$$h(t) = \sum_{k=0}^{N-1} p_k e^{-j\varphi_k} \delta(t - \tau_k) \tag{2.7}$$

where N is the number of possible paths, δ is the Dirac delta function, τ_k is the time delay of the k th impulse, and $\rho_k e^{j\varphi_k}$ is the complex amplitude which comprises the amplitude and phase of the received pulses.

2.3 Digital Equalization

2.3.1 Carrier Recovery

Advanced modulation formats allow to send information through the amplitude and phase of carriers. Therefore, it is absolutely essential for a receiver to recover the frequency and phase of the transmitted carrier for proper demodulation. The Costas receiver is a practical synchronous receiver, suitable to retrieve suppressed carrier signals and the I and Q components of QAM signals [47], [59]. The general structure the Costas receiver is shown in Fig. 2.4.
The received passband signal $s(t) = m(t)cos(2\pi f_c t + \varphi)$ is multiplied by $cos(2\pi f_c t + \varphi')$ and $sin(2\pi f_c t + \varphi')$, which are generated by a voltage controlled oscillator (VCO), i.e. digitally controlled oscillator in the digital domain. The resulting products are:

$$y_i(t) = m(t)\cos(2\pi f_c t + \varphi)\cos(2\pi f_c t + \varphi') = \frac{m(t)}{2}\cos(\Delta\varphi) + double\ frequency\ terms \tag{2.8}$$

$$y_q(t) = m(t)\cos(2\pi f_c t + \varphi)\sin(2\pi f_c t + \varphi') = \frac{m(t)}{2}\sin(\Delta\varphi) + double\ frequency\ terms \tag{2.9}$$

where $\Delta\varphi = \varphi - \varphi'$ is the phase error. After removing the double frequency terms by lowpass filtering, their product yields a baseband error signal $e(t)$ obtained as:

$$e(t) = \frac{m(t)}{2}\cos(\Delta\varphi)\frac{m(t)}{2}\sin(\Delta\varphi) = \frac{m^2(t)}{4}\cos(\Delta\varphi)\sin(\Delta\varphi) = \frac{m^2(t)}{8}\sin(2\Delta\varphi) \tag{2.10}$$

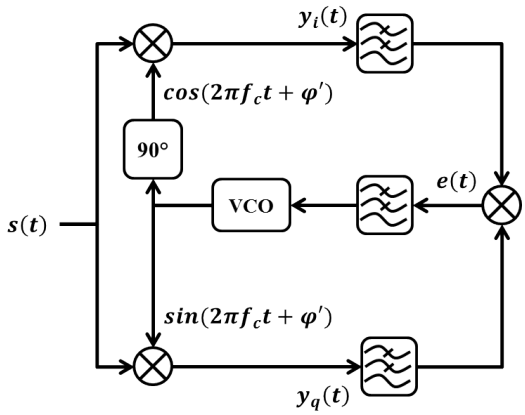

Figure 2.4: Block diagram of Costas receiver.

The latter contains a low-speed component which is entirely dependent on $\Delta\varphi$, which allows the correction of the local phase error through a negative feedback loop capable of tracking the phase of the input carrier.

2.3.2 Decision Feedback Equalizer

As communication channels are stressed with higher data rates, ISI becomes a dominant limiting factor. As described in section 2.2, communication channels can be modeled as linear systems. Linear impairments that only generate amplitude distortions and have a finite duration, i.e. channels with finite memory length, can be extensively mitigated using feedforward equalizers (FFEs) and DFEs, e.g. narrowband filtering due the limited bandwidth of electrical devices. The simplest equalizer is a linear FFE which can be implemented as a FIR filter. Usually the coefficient values of its taps are set to compensate for the low gain at high frequencies, i.e. pre-emphasis. However the performance of FFEs is limited since they amplify noise together with the signal. DFEs are often implemented together with FFE to further improve the quality of the received signal. However, DFE improves the sensitivity at the expense of a higher computational complexity. In general, the feedforward filter is designed to minimize the precursors or convert them into postcursors of the channel impulse response, while the feedback equalizer is used to eliminate the postcursors [60]. The tap

coefficients are set by means of adaptive algorithms such as recursive least squares (RLS) and least mean squares (LMS). In fact, the processing done by a DFE is equivalent to the general problem of linear prediction [61].
The action of DFEs is to feedback a weighted sum of past symbols, i.e. delayed symbols, to cancel out their ISI contributions from the current symbol. Since the ISI due MD in MMFs and wireless multipath propagation can be represented as a deterministic superposition of past scattered pulses, in theory DFEs can mitigate completely the ISI. Both the feedforward and feedback equalizers comprise a FIR filter bank. Each bank consists of a number of taps, which are either T-spaced, i.e. 1 tap/symbol, or n fractionally-spaced, i.e. n samples/symbol. Fractionally-spaced equalizers generally provide better performance than T-spaced equalizers since they serve both as matched filter and as equalizer. However, fractionally-spaced equalizers may not converge due the high correlation of the neighboring symbol taps [23].

2.3.3 Chromatic Dispersion Compensation

For short-range IM/DD links it is possible to compensate the ISI due CD in the time domain, i.e. FIR filters. However, as the channel memory increases so the tap count of the time domain equalizer, and consequently its computational complexity. Furthermore, since all phase information is lost during direct detection process, the amplitude distortions converted from CD phase distortions cannot be completely reversed [62].
For long-haul dispersion uncompensated links, time domain equalization is very challenging if not impossible. Therefore, coherent detection becomes essential to recover the phase of the optical field and enable frequency domain CD compensation. In general, first the incoming signal is transformed into the frequency domain by means of efficient fast Fourier transform (FFT) algorithm. The frequency domain signal is multiplied by $G(-z, \omega)$ (Equation 2.6) reversing the CD effects and then the resulting signal is transformed into the time domain using the inverse FFT (IFFT) [15]–[19], [23].

Chapter 3

Beyond the State of the Art

3.1 VCSEL-based Intra-datacenter Links

Recently, MB-CAP was developed and first introduced for fiber-optic links [49], demonstrating its flexibility to adapt to the large bandwidths available in optical links. As discrete multi-tone (DMT) modulation, the multiband nature of MB-CAP modulation allows the use of bit loading and power loading techniques [49], [52], [53], which is done in accordance to the signal-to-noise ratio (SNR) and channel conditions over the frequency range of each band [49], [63]. Similarly, MB-CAP allows to exploit efficiently the DACs used as electrical generators. As the frequency increases, the DAC effective number of bits (ENOB) decreases, which can be compensated by decreasing the modulation order of high frequency bands, i.e. low order modulation schemes require a low number of quantization levels to construct correctly its corresponding symbol constellation.
By using MB-CAP modulation scheme, the bandwidth provided by VCSEL light sources and the DACs ENOB characteristics can be compensated to maximize the spectral efficiency of transmissions. Alongside, by using the latest advances in quasi single-mode VCSEL technology [12], [13] and by means of digital equalization, i.e. DFE, the dominant deterministic effects of MD in VCSEL based transmissions can be mitigated to maximize the length of MMF links.

In early 2016, by using different modulation schemes, the highest net bitrates reported by using VCSELs as light sources were: 95.8 Gb/s in back-to-back (B2B) transmissions by means of DMT modulation at 1550 nm [52]; 78.51 Gb/s for B2B transmissions by means of DMT modulation at 850 nm [64]; 50.47 Gb/s by using on-off keying (OOK) scheme up to 2.2 km of

OM4 MMF at 850 nm [13], [65]; and 71 Gb/s non-return to zero (NRZ) scheme with no forward error correction (FEC) overhead with a bit error rate (BER) below 1×10^{-12} over 7 m of OM3 MMF at 850 nm [66].
By utilizing state-of-the-art 850 nm VCSEL technology and high-speed DACs, we demonstrated two record experiments with a net bitrate of 100.47 Gb/s, i.e. gross bitrate of 107.5 Gb/s with 7% FEC overhead [63], [67]. The maximum distances reached were 10 m with a multi-mode VCSEL and 100 m with a quasi single-mode VCSEL transmission. Furthermore, by using the quasi single-mode VCSEL, net bitrates of 105.14 Gb/s and 79.44 Gb/s were achieved in B2B transmissions and up to 1000 m of OM4 MMF, respectively. To the best of our knowledge, these results are the first time an effective bitrate of 100 Gb/s is transmitted, at single wavelength, single polarization, and direct detection, over 10 m and 100 m of OM4 MMF with 850 nm multi-mode and single-mode VCSELs respectively. Furthermore, we investigated the power consumption of multi-mode VCSELs under different current bias values. Since VCSEL bandwidth is proportional to its bias, different date rate transmissions were performed by adjusting parameters of MB-CAP modulation. By reducing the VCSEL bias current just above its threshold current value, transmissions with net bitrates up to 10.28 Gb/s were achieved over 100 m of OM4 MMF. Compared to transmissions with VCSEL optimal bias conditions, the received optical power can be decreased up to 6 dB [54], [55].

3.2 Single Photodiode Coherent Detection for Metro-Access and Inter-datacenter Links

Among the most common DSP algorithms used in single PD direct detection receivers are: Linear FFEs or DFEs; nonlinear equalizers, optical field reconstruction algorithms, maximum likelihood sequence estimation (MLSE) [17], [23].
To compensate for the signal distortions, an equalizer can be used to estimate the inverse of the channel impulse response. The simplest equalizer structure is a linear FFE or DFE. However, these equalizers can only compensate for limited signal distortions as direct detection receivers are inherently nonlinear due to the PD square-law. By using a square-root stage before the receiver DSP, the received signal can be partially linearized [68]. However, since all optical phase information is lost during direct detection process, the amplitude distortions converted from CD phase distortions

cannot be completely inversed by using a FFE–DFE. Conversely, impairments that only generate amplitude distortions, can be greatly mitigated by combining a square-root stage after detection and a FFE–DFE, e.g. after linearization the effects of narrowband optical filtering are equivalent to electrical filtering effects. Furthermore, PD nonlinearities can be alleviated through the use of nonlinear equalizers by using structures based on nonlinear models [62]. However, the fact that the phase information of the optical field is lost remains unchanged.

Recently, single PD coherent detection systems have been investigated. The main approach adopted is based on optical heterodyne detection by using a LO generated by optical means or generated in the digital domain. Thus, after photodetection, the transmitted signal is downconverted to an intermediate frequency (IF) to which carrier recovery schemes can be applied, and consequently the amplitude and phase information of the optical field can be retrieved. However, without coherent balanced detection, the main impairment that arises from this approach is the presence of signal-to-signal beating products (SSBP) due to square-law of the PD. In addition, it is to be noted that the price to be paid for using a single PD, in SC-QAM transmissions, is the need of a PD with a bandwidth equal to the entire bandwidth of the transmitted signal, which is twice as in conventional intradyne coherent receivers [15]–[19], [23]. The easiest approach to avoid SSBP interference, is leaving a sufficient frequency gap between the transmitted signal and the LO. Thus, after heterodyne photodetection, no interference is added to the transmitted signal, however, the spectral efficiency is severely decreased [69]. Another appealing approach is to implement digital SSBP cancellation schemes by reversing the PD square-law action [70]. This approach has shown interesting results, where by applying dispersion compensation schemes together with SSBP cancellation, WDM direct-detection systems have been validated up to 100 Gb/s per wavelength over several hundreds of kilometers of SSMF [71], [72]. Recently, from a more mathematical background, Kramers-Kronig (KK) relations have been applied to single PD receiver based systems. These relations allow to determine the phase of the optical field entirely from its intensity, assuming the fulfillment of specific transmission conditions [73].

Remarkable experimental results have been presented by means of the KK scheme and DMT modulation, achieving record bitrates over 125 km of SSMF [74]. Furthermore, it has been experimentally validated in WDM direct-detection systems, a better performance when using the KK scheme over SSBP cancellation schemes [71].

Given the transmitted signal $r_s(t) = |E(t)|e^{i(2\pi f_c t+\varphi_s)}$ and the LO $r_{LO}(t) = |A|e^{i(2\pi f_{LO} t)}$, the resulting signal after photodetection is given by:

$$|r_s(t) + r_{LO}(t)|^2 = |E(t)|^2 + |A|^2 + 2|E(t)||A|\cos\big(2\pi f_{IF} t + \varphi_s(t) + \varphi_n(t)\big) \tag{3.1}$$

where f_{IF} is the IF equal to the frequency separation between the optical carrier and the LO, φ_s is the phase modulation, and φ_n is the total phase noise. Note that the LO amplitude |A| acts as amplification, thus by using a large LO power, i.e. large carrier-to-signal power ratio (CSPR), and a DC blocker, the SSBP term $|E(t)|^2$ and the DC term $|A|^2$ can be neglected. Subsequently, it is possible to track the intermediate frequency carrier phase and restore the signal complex amplitude through DSP on the heterodyne-detected signal [17], [24].

We experimentally validated a scheme using a single PD, which allows the linear transfer of the amplitude and phase information of the optical field into the electrical domain. This is possible by means of optical heterodyne detection and by adjusting the CSPR, thus the undesired SSBP can be considered negligible. Therefore, the receiver computational complexity is significantly reduced since no additional DSP is required to mitigate the SSBP or to estimate the phase of the optical signal. As a proof of concept, the simplicity of QAM is combined with our proposed scheme. Single wavelength and single polarization 16-QAM and QPSK transmissions, both with a net bitrate of 60.75 Gb/s, are transmitted over 10 km of SSMF [75]. Due the short link, frequency domain CD compensation was not required. In further experiments, we extended our concept to PDM transmissions and generate the LO (single sideband) together with an 8-QAM signal solely with the DAC. Therefore, by using a single light source, we transmitted a PDM 8-QAM signal achieving a net bitrate of 230 Gb/s over 100 km of SSMF. Instead of using balanced PDs and 90 degree optical hybrids, a Costas loop is used to retrieve the I and Q components of each polarization, thus a dual polarization coherent receiver is achieved using only 2 PDs [76]. In Fig. 3.1 is shown the experimental setup, and the insets show the eye diagram of the 8-QAM signal Q component, the transmitted optical spectrum, and the symbol constellation of X-polarization before and after frequency domain CD compensation.

It is to be noted that, conversely to conventional coherent receivers, carrier recovery is the first stage of the receiver DSP. Subsequently, radius directed equalization (RDE) based polarization demultiplexing, frequency domain CD compensation, and DFE based time domain equalization are carried

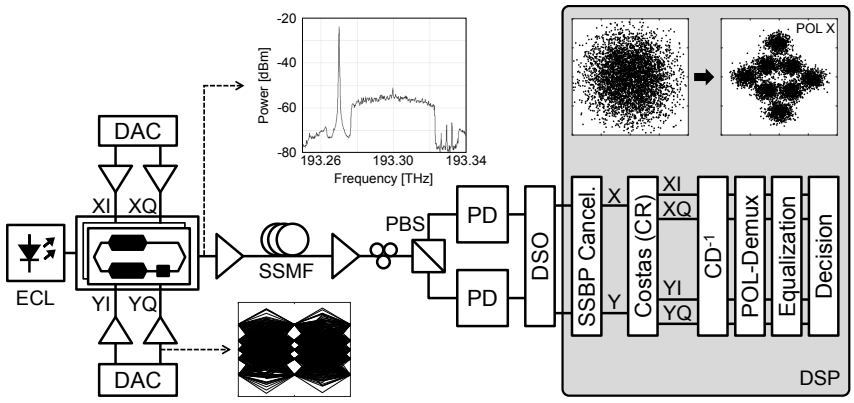

Figure 3.1: Experimental setup. Single light source transmitter and single PD per polarization receiver.

out before demodulation. In addition, due the limited vertical resolution of DACs, a high CSPR is not possible while using high order modulation formats leading to higher SSBP. Therefore, before carrier recovery, SSBP were reduced with a single-stage linearization filter as described in [71].

3.3 High Capacity Hybrid Fiber-Wireless 5G Networks

Recently, enabled by the rapid development of electronics and RoF technology, extensive research on mmWave wireless systems has been made. To increase wireless capacity, complex multi-carrier MIMO systems have been proposed [77], [78], combining the bandwidth available from the Ka-band to the W-band (26.5–110 GHz). By employing 2×2 MU-MIMO spatial multiplexing, maximum net bitrates up to 209.35 Gb/s at a carrier frequency of 37.5 GHz have been reported [77]. Research efforts are now moving to even higher frequency bands: work in the D-band (110–170 GHz) have been reported, achieving gross bitrates up to 60 Gb/s over a wireless distance of 0.4 m [79], [80]. Also, the first demonstration of a D-band 2×2 MU-MIMO optical-wireless system was presented recently, achieving a gross bitrate up to 32 Gb/s [80]. However, these demonstrations fall short on taking advantage of the large bandwidth available in the mmWave D-band.

In the case of short-range UWB technology, multiband orthogonal frequency division multiplexing (MB-OFDM) is the most popular multiband scheme. First, it was adopted by theWiMedia Alliance (no longer operating)

as a standard, and then adopted by the Wireless USB Promoter Group to support high-speed wireless connections, ensuring USB-like user experience. Following FCC regulations, WiMedia's last physical layer (PHY) specification [81], specified the usage of the frequency range between 3.1 GHz and 10.6 GHz reaching date rates up to 1024 Mb/s, supporting transmissions of 480 Mb/s over distances up to 3 m and 110 Mb/s up to 10 m. The MB-OFDM scheme is suitable for wireless communications since it can alleviate the effects of multipath propagation, however MB-OFDM implementation faces some challenges which increase its complexity. The most notorious are the distortion generated due the high peak-to-average power ratio (PAPR) which stresses the limited linear range of power amplifiers, and the time and frequency synchronization relying on the addition of pilot tones or pilot symbols to the signal [82].

MB-CAP modulation multiband features make it suitable to exploit the large bandwidths available in mmWave and UWB wireless communications systems. It can mitigate impairments of wireless channels such as frequency selectivity and non-flat frequency responses, e.g. uneven antenna gain. In addition, MB-CAP modulation has better features than MB-OFDM, such as lower PAPR and lower computational complexity in its implementation [49]. The flexible nature of MB-CAP modulation is highly suitable for UWB wireless communications systems, allowing to adjust the power and bandwidth used to comply with current regulatory UWB standards [42]–[44].

The main advantages of MB-CAP modulation are that it can be transmitted by means of intensity/amplitude modulation, e.g. directly modulated lasers (DMLs), and that the I and Q components of each CAP band can be retrieved by means of simple matched filters instead of coherent receivers. However, since CAP modulation inherently comprises a digital subcarrier, by modulating the intensity of an optical carrier or the amplitude of a RF carrier, the resulting spectral efficiency can only reach up to half the spectral efficiency of QAM, i.e. assuming the same symbol rate and pulse shape. To overcome this disadvantage, SSB modulation and ISB modulation can be applied by means of digital Hilbert transform filters and optical I/Q modulation [35], [83]. Thus, the spectral efficiency of CAP and MB-CAP modulation can be improved to match QAM spectral efficiency.

We demonstrated the feasibility of fiber-like capacity mmWave transmissions in the D-band. As a proof-of-concept, we generated PDM ISB CAP and PDM ISB MB-CAP modulation signals, and transmitted both polarizations first over 25 km of SSMF and then wirelessly by a single 2×2

MU-MIMO system, i.e. one dedicated pair transmitter/receiver antennas per polarization. Net bitrates up to 328.97 Gb/s were achieved at a RF carrier frequency of 141 GHz [83], [84]. Wireless distance was limited to 1 m due I/Q imbalance as described and investigated in [85], and due limited RF amplification at these high frequencies. To the best of our knowledge, this is the highest data rate ever achieved in any mmWave band by means of a single 2×2 MU-MIMO wireless system.
In further experiments at the W-band, by improving the power budget, i.e. high gain antennas, and reducing the optical I/Q imbalance, we successfully transmitted single polarization SSB MB-CAP modulation signals achieving a net bitrate of 56.08 Gb/s over 10 km SSMF and a wireless distance of 50 m [35]. To the best of our knowledge this is first experimental demonstration of a W-band transmission over considerable wireless distance with a net bitrate over 50 Gb/s by means solely of a single transmitter antenna and a single receiver antenna.

For short-range wireless communications, we proposed the inherently low power UWB technology as a prospective solution for next generation networks, which is able to provide multi-gigabit links and large bandwidths suitable for small cell wireless communications and future IoE applications and devices [86]. We used MB-CAP modulation for the first time [87] for wireless transmissions exploiting the large bandwidths defined by UWB regulations, supporting data rates from multiple Gb/s to hundreds of Mb/s. We experimentally validated the capacity of the proposed solution. Wireless transmissions with a gross bitrate of 10 Gb/s were performed in compliance with the regulations established by the United States FCC, the European ECC, and the Russian SCRF. The maximum wireless distances reached were 3.5 m, 2 m, and 1.3 m, respectively [88]. In further experiments, for a set of wireless distances spanning from 0.5 m to 9 m, we experimentally demonstrated transmission bitrates up to 35.1 Gb/s and 21.6 Gb/s complying with the FCC and ECC regulations, respectively [89]. In all transmissions, the mentioned bitrates were achieved with BERs below the commercial 7% overhead FEC threshold of 3.8×10^{-3}. To the best of our knowledge, these experimental demonstrations provide the highest net bitrates ever achieved under the FCC, ECC and SCRF UWB regulations.

Chapter 4

Concluding Remarks

Low-cost VCSEL technology constitutes one of the most prospective solutions for intra-datacenter networks. The presented results demonstrate the feasibility of effective single wavelength IM/DD 100 Gb/s short-range links using cost-effective MMF and 850 nm VCSELs. The flexibility provided by MB-CAP modulation allowed to maximize the transmission data rates with limited power and bandwidth resources. Further research has to be focused in assessing the analog and digital electronics required to develop VCSEL 100G drivers for real-time transmissions. In addition, to further increase the length of MMF links, research is dedicated to improve VCSEL designs to increase its output power. Recently, VCSELs with oxide apertures having a total thickness of 100 nm, the diameter for single-mode operation at >15dB side-mode suppression ratio (SMSR), is increased to 5 μm at electrical currents exceeding 5 mA [90]. Due the increasing data rates of optical interconnects, signal integrity requirements in datacenters are more challenging, e.g. BERs of 1×10^{-15} are considered error free. With alternative low-density parity-check (LDPC) code schemes, it is possible to reduce the post FEC BER floor, however, at the expense of larger the overheads [91]. With the BERs presented, our results are suitable for applications compliant with recent IEEE 802.3 and Fibre Channel standards.

Datacenters have proliferated in recent years requiring low latency and reliable interconnects. Up to date, the most cost-effective point-to-point transport for DCIs is based on WDM coherent optical communications. Due to its low cost, IM/DD solutions are being proposed for DCIs, e.g. PAM-4 [92]. However, their symbol rate per wavelength and link distance are limited by CD, and the operational cost of deploying dispersion-compensating fiber (DCF) is to be avoided, i.e. service providers prefer to use the existing

metro optical networks.

Through simulation and experiments, we validated a scheme in which it is possible to achieve coherent detection using a single PD direct detection based receivers. Optical M-ary QAM signals are transmitted, and the I and Q components of the transmitted optical signal are recovered by means of optical heterodyne detection and carrier recovery based on a Costas loop. Thus, solely with a single PD, the amplitude and phase information of the optical field are recovered, however, at the expense of requiring a PD with twice the bandwidth as in conventional coherent receivers. We experimentally validated our proposed scheme first, transmitting single polarization QPSK and 16-QAM signals with a net bitrate of 60.75 Gb/s over 10 km of SSMF, and then transmitting PDM 8-QAM signals with a net bitrate of 230 Gb/s over 100 km of SSMF, using a single PD per polarization.

Future work will be devoted to reduce hardware complexity and to improve the performance of our scheme while keeping DSP requirements feasible for real-time implementations. One appealing approach is to generate the optical carrier and the LO from a single light source by means of an additional MZM as described in [35]. As a result, no polarization tracking is necessary, and DSP carrier recovery is relaxed since the IF is always constant. In addition, further research will be carried to avoid the use of a polarization controller and make our PDM transmissions completely insensitive to the signal state-of-polarization (SOP).

Lastly, the convergence of radio and optical technologies is imperative to future 5G networks. We experimentally demonstrated high capacity photonically-enabled D-band wireless transmissions with net bitrates up to 328.97 Gb/s. We proposed a scheme that by applying ISB modulation, the benefits of multiband modulation schemes can be maintained while achieving the same spectral efficiency of traditional SC-QAM. This experiment effectively bridges fiber-like capacity in the air using an untapped wireless frequency band. In further demonstrations, we optimized our results in the W-band by minimizing optical I/Q imbalance and therefore the imaging crosstalk between sidebands, achieving high capacity transmissions while relaxing the computational complexity of equalization [35]. Enhancement of mmWave systems is a challenging task for researchers are engineers, which is decisive for the soon to be 5G platform upgrade, e.g. Japan national 5G project [93].

Alongside, by means of simple single-input single-output (SISO) wireless links, we experimentally validated the capabilities of short-range UWB technology and MB-CAP modulation to adapt to different scenarios, i.e. differ-

ent worldwide regulations, while achieving record data rates over distances up to 9 m. High-speed UWB communication systems represent a flexible solution that can be adjusted to current and future regulatory standards and can become a prospective solution for upcoming IEEE 802.11 and IEEE 802.15 high data rate systems standardization.
Both mmWave and UWB wireless communication systems are suitable for ultra-dense networks which can improve the spectral efficiency per unit area. Furthermore, as in mmWave systems, UWB signaling can be transmitted through SSMF by means of RoF technology [94]–[96], therefore fiber-optic networks can supply both systems to reach the end-user. By applying current MIMO technology to our results, i.e. beamforming techniques, intra- and intercell interference can be minimized [26], [28]. In addition, to provide a robust and reliable connectivity, further research is necessary to establish optimal techniques for mobility management, i.e. user mobility from one microcell to another [27]. Data rates can be increased drastically by exploiting spatial diversity multiplexing (SDM), i.e. denser MU-MIMO technology, used in current commercial 802.11ac Wi-Fi standard compliant products [97].

Paper 1: 107.5 Gb/s 850 nm multi- and single-mode VCSEL transmission over 10 and 100 m of multi-mode fiber

R. Puerta, M. Agustin, L. Chorchos, J. Tonski, J.-R. Kropp, N. Ledentsov, V. A. Shchukin, N. N. Ledentsov, R. Henker, I. T. Monroy, J. J. V. Olmos, and J. P. Turkiewicz, "107.5 Gb/s 850 nm multi- and single-mode VCSEL transmission over 10 and 100 m of multi-mode fiber," in *Optical Fiber Communication Conference Postdeadline Papers*, 2016, p. Th5B.5.

DOI: 10.1364/OFC.2016.Th5B.5

107.5 Gb/s 850 nm multi- and single-mode VCSEL transmission over 10 and 100 m of multi-mode fiber

R. Puerta[(1)], M. Agustin[(2)], Ł. Chorchos[(4)], J. Tański[(4)], J.-R. Kropp[(2)], N. Ledentsov Jr.[(2)], V.A. Shchukin[(2)], N.N. Ledentsov[(2)], R. Henker[(3)], I. Tafur Monroy[(1)], J.J. Vegas Olmos[(1)] and J.P. Turkiewicz[(4)]

[(1)] Dpt. Photonics Engineering, Technical University of Denmark (DTU), Akademivej Building 358, 2800 Kgs. Lyngby, Denmark
[(2)] VI-Systems GmbH, Hardenbergstrasse 7, Berlin 10623, Germany
[(3)] Technische Universität Dresden, Chair for Circuit Design and Network Theory, 01062 Dresden, Germany
[(4)] Institute of Telecommunications, Warsaw University of Technology, Nowowiejska 15/19, 00-665 Warsaw, Poland
E-mail: rapur@fotonik.dtu.dk, nikolay.ledentsov@v-i-systems.com, jturkiew@tele.pw.edu.pl

Abstract: First time successful 107.5 Gb/s MultiCAP 850 nm OM4 MMF transmissions over 10 m with multi-mode VCSEL and up to 100 m with single-mode VCSEL are demonstrated, with BER below 7% overhead FEC limit measured for each case.
OCIS codes: (060.2330) Fiber optics communications; (140.7260) Vertical cavity surface emitting lasers

1. Introduction

The ever increasing amount of transmitted data does not only increase of the transmission data rates in the access, metro and core networks but also in the short connections – the optical data interconnects. The key transmission solution for optical interconnects is based on vertical cavity surface emitting lasers (VCSELs) and multimode fiber (MMF). VCSELs have key advantages of wide bandwidth, low-energy consumption and low-cost manufacturing, while MMF can be easily coupled to VCSELs. All of that transforms into a low cost transmission solution, desirable for massive deployments, e.g. within data centers. A significant research effort is devoted to increase the transmission performance of VCSEL interconnects and several remarkable recent transmission experiments have been reported, e.g. [1] 70 Gb/s PAM-4 over 3 m MMF at 850 nm, [2] 71 Gb/s NRZ over 7 m MMF at 850 nm, [3] 105 Gb/s DMT over 500 m SSMF at 1550 nm, [4] 49 Gb/s DMT over 2.2 km MMF at 850 nm, and [5] 84 Gb/s DMT over 100 m MMF at 850 nm.

In this paper, we demonstrate two record experiments utilizing 850 nm VCSEL and MMF at data rate 107.5 Gb/s (100 Gb/s data + 7% FEC overhead) over the distances of 10 m for multi-mode (MM) VCSEL and of 100 m for single-mode (SM) VCSEL. Multi-band approach of carrierless amplitude/phase (CAP) modulation (MultiCAP) [6], with advantages of adaptivity as well as feasible implementation and direct detection was applied. Bit error rate (BER) measurements were below 7% forward error correction (FEC) limit of $3.8 \cdot 10^{-3}$. Additional, SM-VCSEL transmission experiments showed excellent transmission up to 1000 m MMF at data rates of 85 Gb/s.

2. Experimental Setup

Figure 1 shows the experimental setup. The transmitter consisted of a 65 GSa/s arbitrary waveform generator (AWG), a bias-T, a current source and a VCSEL. Standard multiple oxide aperture VCSEL design was applied for MM-VCSEL [7], while a design of the SM-VCSEL allowed oxide-aperture-induced leakage effect to be applied for mode selection [8]. The packaged and pigtailed MM-VCSEL was biased with 8 mA current and driven by 0.7 V_{pp} voltage, while the bare chip SM-VCSEL with 2.8 mA and 1 V_{pp}, respectively. After transmission in the MMF OM4 fiber of different lengths, the optical signal was converted to the electrical domain in a 22 GHz bandwidth photoreceiver (PR) with optional electrical amplifier. The electrical signal was captured in a 100 GSa/s real time oscilloscope (OSC) for further offline digital signal processing (DSP).

A MultiCAP signal with 10 frequency bands was utilized. For each band, decorrelated pseudo random binary sequences (PRBSs) of 2^{11}-1 bit length were mapped into its corresponding symbol constellation. The obtained symbol sequences were upsampled and then filtered by the pair of orthogonal CAP filters corresponding to each band. Power loading was employed by assigning weights to each band. At the receiver, the sequences of each band were retrieved by orthogonal CAP matched filters. Finally, symbols were demodulated employing a decision-feedback equalizer (DFE) and k-means algorithm. BERs and error vector magnitudes (EVMs) were computed offline, for each band separately, from the actual received data stored with the OSC.

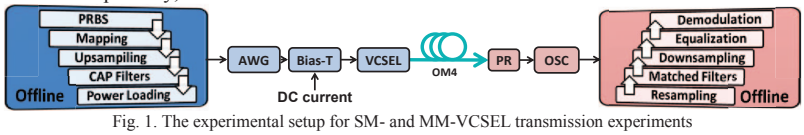

Fig. 1. The experimental setup for SM- and MM-VCSEL transmission experiments

978-1-943580-08-8/16/$31.00 ©2016 Optical Society of America

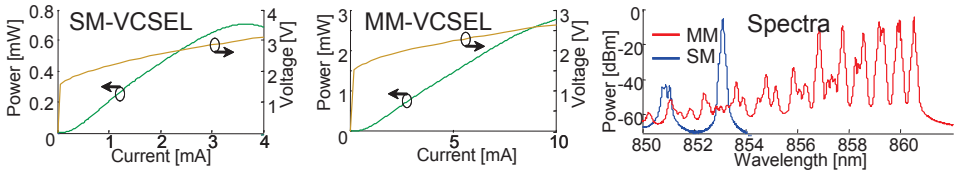

Fig. 2. SM-VCSEL and MM-VCSEL LIV curves together with its corresponding optical spectra

3. Experimental Results

Figure 2 shows the light-current-voltage (LIV) curves and the optical spectra of the utilized SM- and MM-VCSELs. For the SM/MM-VCSEL operating wavelengths were 853.1/860.5 nm, respectively. The MM-VCSEL had over 10 modes and the SM-VCSEL suppression ratio of the strongest mode was 39 dB. The maximum optical power for SM/MM-VCSEL was -1.4 dBm and 4.4 dBm, respectively.

First, transmission with MM-VCSEL was realized. A transmission of 107.5 Gb/s was achieved over 10 m of OM4 MMF with a received optical power of 3.9 dBm. In Table 1 the BER and main parameters of each band are presented. The BER of all bands is below 7% FEC threshold of $3.8 \cdot 10^{-3}$, thus achieving a total effective bit rate of 100.5 Gb/s. Fig. 3 shows the received electrical spectrum of the MultiCAP signal together with the constellations and EVMs of all bands. It is to be noted that thanks to power loading technique, bands with the same modulation order have practically the same EVM.

Table 1. BER and main parameters of MM-VCSEL 107.5 Gb/s transmission over 10 m of OM4

Band	1	2	3	4	5	6	7	8	9	10
Baud rate [Gbaud/s]	2.5	2.5	2.5	2.5	2.5	2.5	2.5	2.5	2.5	2.5
Modulation	64-QAM	64-QAM	32-QAM	32-QAM	32-QAM	32-QAM	16-QAM	16-QAM	QPSK	BPSK
Bitrate [Gb/s]	15	15	12.5	12.5	12.5	12.5	10	10	5	2.5
Power Loading [dB]	2	1	0.3	0.6	1	2.1	1.2	2.6	0.4	2
Transmitted Bits	2174976	2174976	1812480	1812480	1812480	1812480	1449984	1449984	724992	362496
BER	**3.12e-03**	**2.58e-03**	**2.36e-03**	**2.53e-03**	**3.76e-03**	**3.33e-03**	**2.63e-03**	**2.77e-03**	**7.89e-04**	**3.56e-03**

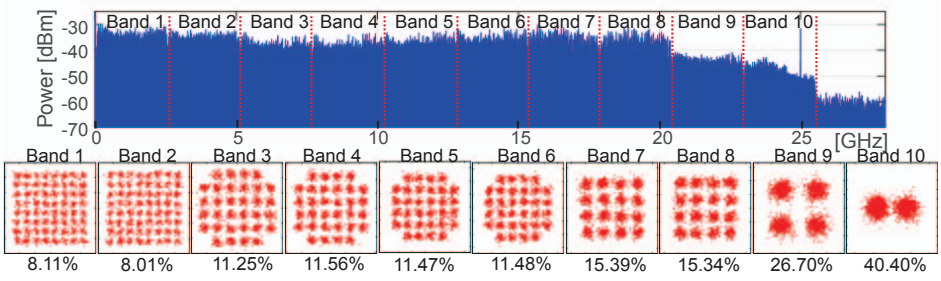

Fig. 3. Received electrical spectrum and constellation diagrams after DFE for 107.5 Gb/s 10 m MM-VCSEL transmission

Next, transmission with SM-VCSEL was realized. An additional electrical amplifier was placed after the photoreceiver to compensate for the limited optical signal power. A transmission of 107.5 Gb/s was achieved over 100 m of OM4 MMF with a received optical power of -2.54 dBm. In Table 2, the BER and main parameters of each band are presented, while Fig. 4 shows the received electrical spectrum of the MultiCAP signal together with the constellations and EVMs of all bands SM-VCSEL 107.5 Gb/s transmission over 100 m of OM4.

Table 2. BER and main parameters of SM-VCSEL 107.5 Gb/s transmission over 100 m of OM4

Band	1	2	3	4	5	6	7	8	9	10
Baud rate [Gbaud/s]	2.5	2.5	2.5	2.5	2.5	2.5	2.5	2.5	2.5	2.5
Modulation	64-QAM	64-QAM	32-QAM	32-QAM	32-QAM	32-QAM	16-QAM	8-QAM	QPSK	QPSK
Bitrate [Gb/s]	15	15	12.5	12.5	12.5	12.5	10	7.5	5	5
Power Loading [dB]	2	2.1	-0.2	0.7	1.7	2.6	2	1.1	-1	2.1
Transmitted Bits	1449984	1449984	1208320	1208320	1208320	1208320	966656	724992	483328	483328
BER	**1.80e-03**	**2.94e-03**	**1.33e-03**	**1.58e-03**	**1.26e-03**	**1.89e-03**	**1.11e-03**	**1.66e-03**	**1.69e-03**	**2.08e-03**

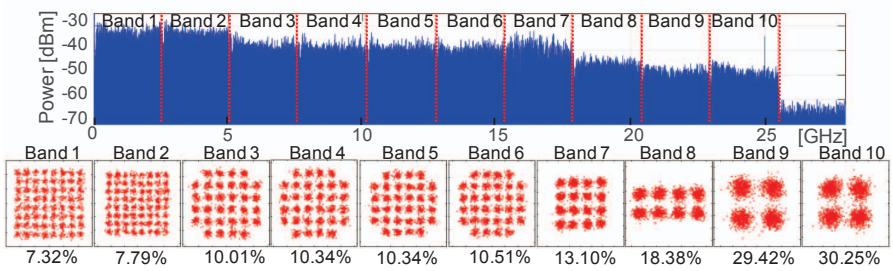

Fig. 4. Received electrical spectrum and constellation diagrams after DFE for 107.5 Gb/s 100 m SM-VCSEL transmission

Finally, the experiments towards maximum bit rate transmission at given distance with adjustable as well as fixed (107.5 Gb/s) bit rate were performed. Fig. 5(a) shows the maximum bit rates achieved below 7% FEC limit in function of MMF length. The maximum bit rate achieved was 112.5 Gb/s in the B2B test, and the maximum length tested was 1 km achieving a bit rate of 85 Gb/s. Fig. 5(b) shows the average BER of all bands for 107.5 Gb/s transmission in function of MMF length. For longer distances high order modulation schemes, such as 64-QAM, degrade considerably increasing the BER as can be noted.

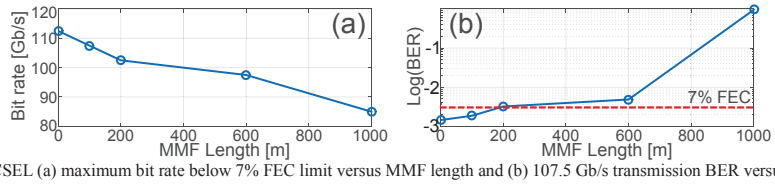

Fig. 5. SM-VCSEL (a) maximum bit rate below 7% FEC limit versus MMF length and (b) 107.5 Gb/s transmission BER versus MMF length

4. Conclusions

To the best of our knowledge, for the first time an effective bit rate over 100 Gb/s is transmitted, at single wavelength, single polarization, and direct detection, with a 850 nm MM-VCSEL over 10 m of OM4 MMF and with a 850 nm SM-VCSEL over 100 m of OM4 MMF. These two records, with comparable hardware constraints and resources as previous works [1–5], are achieved through the use of MultiCAP modulation and BER below FEC limit were measured. The presented results demonstrate that ultra high speed links of over 100 Gb/s with distances up to 100 m can be realized by using cost-effective MMF and 850 nm VCSELs, disruptingly opening a technology solution for the high capacity data interconnects, e.g. in combination with short-WDM (SWDM).

5. Acknowledgements

R. Puerta would like to express his gratitude to the Colombian Administrative Department of Science, Technology and Innovation (COLCIENCIAS). The presented work has been funded by the European Commission under the FP7 grant agreement no. 619197 ADDAPT “Adaptive Data and Power Aware Transceivers for Optical Communications” as well as the Marie-Curie project FENDOI. The laboratory equipment was provided through the Polish Innovative Economy Program POIG.02.01.00-14-197/09 FOTEH project.

6. References

[1] K. Szczerba *et al.*, "70 Gbps 4-PAM and 56 Gbps 8-PAM Using an 850 nm VCSEL," J. Lightw. Technol. **33**(7), 1395-1401 (2015).
[2] D. M. Kuchta *et al.*, “A 71-Gb/s NRZ Modulated 850-nm VCSEL-Based Optical Link,” IEEE Photon. Technol. Lett. **27**(6), 577–580 (2015).
[3] C. Xie *et al.*, "Single-VCSEL 100-Gb/s Short-Reach System Using Discrete Multi-Tone Modulation and Direct Detection," in Optical Fiber Communication Conference, OSA Technical Digest (online) (Optical Society of America, 2015), paper Tu2H.2.
[4] I. C. Lu *et al.*, “Very High Bit-Rate Distance Product Using High-Power Single-Mode 850-nm VCSEL With Discrete Multitone Modulation Formats Through OM4 Multimode Fiber,” IEEE J. Sel. Top. Quantum Electron. **21**(6), 444–452, (2015).
[5] B. Wu *et al.*, “Close to 100 Gbps discrete multitone transmission over 100m of multimode fiber using a single transverse mode 850nm VCSEL,” presented at SPIE Photonics West, San Francisco-California, United States, 13–18 Feb. 2016.
[6] M. I. Olmedo *et al.*, “Multiband Carrierless Amplitude Phase Modulation for High Capacity Optical Data Links,” J. Lightw. Technol. **32**(4), 798–804 (2014).
[7] J.-R. Kropp *et al.*, "Accelerated aging of 28 Gb s−1 850 nm vertical-cavity surface-emitting laser with multiple thick oxide apertures" Semicond. Sci. Technol. 30, 045001 (2015).
[8] V. Shchukin *et al.*, "Single-Mode Vertical Cavity Surface Emitting Laser via Oxide-Aperture-Engineering of Leakage of High-Order Transverse Modes," IEEE J. Quantum Electron. **50**(12), pp.990-995 (2014).

Paper 2: Effective 100 Gb/s IM/DD 850-nm Multi- and Single-Mode VCSEL Transmission Through OM4 MMF

R. Puerta, M. Agustin, L. Chorchos, J. Tonski, J.-R. Kropp, N. Ledentsov, V. A. Shchukin, N. N. Ledentsov, R. Henker, I. T. Monroy, J. J. V. Olmos, and J. P. Turkiewicz, "Effective 100 Gb/s IM/DD 850-nm Multi- and Single-Mode VCSEL Transmission Through OM4 MMF," *J. Light. Technol.*, vol. 35, no. 3, pp. 423–429, Feb. 2017.

DOI: 10.1109/JLT.2016.2625799

Effective 100 Gb/s IM/DD 850-nm Multi- and Single-Mode VCSEL Transmission Through OM4 MMF

Rafael Puerta, *Student Member, IEEE*, Mikel Agustin, Łukasz Chorchos, Jerzy Toński, Jörg R. Kropp, Nikolay Ledentsov Jr., Vitaly A. Shchukin, Nikolay N. Ledentsov, Ronny Henker, Idelfonso Tafur Monroy, *Senior Member, IEEE*, Juan José Vegas Olmos, *Senior Member, IEEE*, and Jarosław P. Turkiewicz, *Senior Member, IEEE*

(Post-Deadline)

***Abstract*—To cope with the ever increasing data traffic demands in modern data centers, new approaches and technologies must be explored. Short range optical data links play a key role in this scenario, enabling very high speed data rate links. Recently, great research efforts are being made to improve the performance of vertical-cavity surface-emitting lasers (VCSELs) based transmission links, which constitute a cost-effective solution desirable for massive deployments. In this paper, we experimentally demonstrate intensity-modulation direct-detection transmissions with a data rate of 107.5 Gb/s over 10 m of OM4 multimode fiber (MMF) using a multimode VCSEL at 850 nm, and up to 100 m of OM4 MMF using a single-mode VCSEL at 850 nm. Measured bit error rates were below 7% overhead forward error correction limit of 3.8e−03, thus, achieving an effective bit rate of 100.5 Gb/s. These successful transmissions were achieved by means of the multiband approach of carrierless amplitude phase modulation.**

***Index Terms*—Multi-band carrierless amplitude phase modulation, optical fiber communication, vertical cavity surface emitting lasers.**

I. Introduction

THE ever increasing amount of transmitted data does not only increase the data rates of the transmission in the access, metro and core networks but also in the short connections, e.g. the optical data interconnects. The optical interconnects are applied to transmit data within information technology (IT) infrastructure, starting from in-rack communication to intra-data center connections. The key features requires for such applications are high throughput, limited footprint, reduced power consumption and reduced cost of the solution [1], [2].

An appealing transmission solution for optical interconnects is based on vertical-cavity surface-emitting lasers (VCSELs) and multi-mode fiber (MMF). VCSELs have key advantages of wide bandwidth, low energy consumption and low-cost manufacturing, while MMF can be easily coupled to VCSELs [3]. However, as optical link length increases, the modal and chromatic dispersion in MMFs deteriorate the transmission quality of traditional multi-mode (MM) VCSELs. The impairments imposed by both dispersions can be mitigated by reducing the number of modes of these VCSELs, ideally to achieve single-mode (SM) operation [4], [5]. VCSEL technology constitute a low-cost transmission solution, desirable for massive deployments, e.g. data center interconnects, which decreases costs by less than half compared with standard single-mode fiber (SSMF) solutions in data centers [6]. The VCSEL data interconnect cost advantage originates from low capital as well as operational, e.g. limited energy consumption, cost [7].

Optical communication systems are evolving from classic spectral inefficient non-return to zero (NRZ) schemes to more advanced and flexible modulation schemes such as quadrature phase shift keying (QPSK) [8], [9], pulse amplitude modulation (PAM) [10], [11], discrete multi-tone (DMT) [12]–[14], multi-band approach of carrierless amplitude phase (MultiCAP) [15], [16], polybinary modulation [17], [18], among others. By combining VCSEL technology with these advanced modulation schemes, spectral efficiency can be boosted up, enabling low-cost 100G links at single wavelength, single polarization, and direct detection.

A significant research effort is devoted to increase the transmission data rates and performance of VCSEL interconnects. The highest bit rates reported by some of these works including both the bit rates before and after forward error

Manuscript received May 31, 2016; revised October 6, 2016; accepted October 23, 2016. Date of publication November 9, 2016; date of current version February 13, 2017.

R. Puerta, and J. J. V. Olmos are with the Department of Photonics Engineering, Technical University of Denmark, Kongens Lyngby 2800, Denmark (e-mail: rapur@fotonik.dtu.dk; jjvo@fotonik.dtu.dk).

M. Agustin, J. R. Kropp, N. Ledentsov Jr., V. A. Shchukin, and N. N. Ledentsov are with the VI Systems GmbH, Berlin 10623, Germany (e-mail: mikel.agustin@v-i-systems.com; joerg.kropp@v-i-systems.com; n.ledentsov@gmail.com; vitaly.shchukin@v-i-systems.com; nikolay.ledentsov@v-i-systems.com).

Ł. Chorchos, J. Tański, and J. P. Turkiewicz are with the Warsaw University of Technology, Institute of Telecommunications, Warsaw 00-665, Poland (e-mail: lukaszchorchos@gmail.com; tonski@tele.pw.edu.pl; jturkiew@tele.pw.edu.pl).

R. Henker is with the Technische Universität Dresden, Dresden 01069, Germany (e-mail: ronny.henker@tu-dresden.de).

I. T. Monroy is with the Department of Photonics Engineering, Technical University of Denmark, Kongens Lyngby 2800, Denmark; he is also with the ITMO University St. Petersburg, 197101, Russia (e-mail: idtm@fotonik.dtu.dk).

Color versions of one or more of the figures in this paper are available online at http://ieeexplore.ieee.org.

Digital Object Identifier 10.1109/JLT.2016.2625799

correction (FEC) decoding are: 115 Gb/s pre-FEC and 95.8 Gb/s post-FEC for back-to-back (B2B) transmissions by means of DMT modulation at 1550 nm [12]; 71.88 Gb/s pre-FEC and 67.18 Gb/s post-FEC for B2B transmission using DMT modulation at 850 nm [13]; 84 Gb/s pre-FEC and 78.51 Gb/s post-FEC for B2B transmissions with DMT modulation at 850 nm [14]; 54 Gb/s pre-FEC and 50.47 Gb/s post-FEC on-off keying (OOK) transmission up to 2.2 km of OM4 MMF at 850 nm [5], [19]; and 71 Gb/s NRZ modulation with no FEC codes with a BER $<$1e-12 over 7 m of OM3 MMF at 850 nm [20].

In this paper, we demonstrate two record experiments utilizing 850 nm VCSEL and OM4 MMF with a post-FEC bit rate of 100.5 Gb/s (i.e. pre-FEC bit rate of 107.5 Gb/s with 7% overhead FEC) over the distances of 10 m for MM-VCSEL transmission and of 100 m for SM-VCSEL transmission [21]. Furthermore, for B2B transmissions with the SM-VCSEL, a pre-FEC and post-FEC bit rates up to 112.5 Gb/s and 105.14 Gb/s were achieved, respectively. MultiCAP modulation, with advantages of adaptivity as well as feasible implementation and direct detection was applied. Bit error rate (BER) measurements were below 7% forward error correction (FEC) limit of 3.8e-03. Additionally, SM-VCSEL transmission experiments showed excellent performance up to 1000 m MMF at data rates of 85 Gb/s.

This paper is organized as follows: Section II gives a brief description of MultiCAP modulation scheme. In Section III the experimental setup is described in detail and in Section IV the experimental results are given. Finally, in Section V conclusions are presented.

II. Multi-band Carrierless Amplitude Phase Modulation

Carrierless amplitude phase modulation (CAP), similarly to quadrature amplitude (QAM) and high order phase shift keying (PSK) modulations, is a multilevel and multidimensional modulation scheme capable of transmitting two channels of data simultaneously [22], namely the in-phase (I) and quadrature (Q) channels. These two channels are generated by means of two orthogonal pass-band filters obtained from the time-domain multiplication between the root raised cosine (RRC) pulse shape function and a pure cosine and sine tones for I and Q components, respectively:

$$p_i(t) = g(t)\cos(2\pi f_c t) \quad (1)$$

$$p_q(t) = g(t)\sin(2\pi f_c t) \quad (2)$$

where *g(t)* is a pulse shaping function that has a RRC spectral characteristic. CAP filters have three main parameters: i. the cosine and sine frequency determining the central frequency of the transmitted band; ii. the roll off factor α of the RRC, which determines the excess bandwidth required, i.e. with an RRC pulse shape the total pass-band bandwidth of a CAP band is $1 + \alpha$ times the baud rate; iii. the filter length in the number of samples which affects both performance and complexity of the system. For short lengths the overall system is simpler, but performance decreases significantly [16].

To generate a CAP signal, the original binary sequence is first mapped using an M-ary QAM or PSK encoder, and then

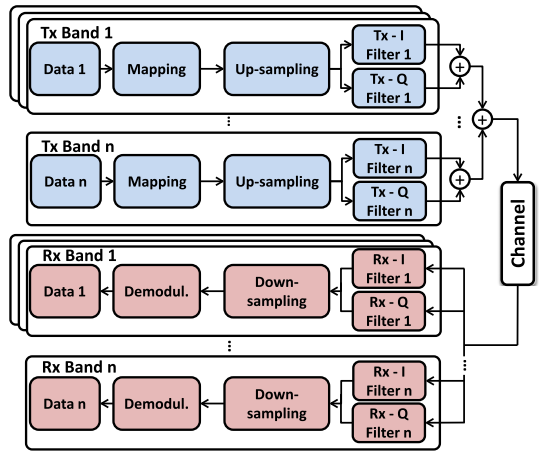

Fig. 1. The block diagram of MultiCAP transmitter and receiver.

the mapped symbols are up-sampled to perform a time-domain convolution with the orthogonal filters. After filtering, the signals from the two channels are added and transmitted. At the receiver first two matched filters separate the I and Q channels. The optimum filters are the ones matched to the passband filters described in (1) and (2), respectively [23]. Finally, the retrieved I and Q signals are down-sampled and the data is decoded. The overall CAP architecture has been demonstrated to be less complex and with better performance than DMT architecture [24].

MultiCAP modulation relies on the simultaneous transmission of several CAP signals assigned to different frequency bands, ensuring that these bands do not overlap. This is achieved by using not only one pair of orthogonal filters, but several pairs with different cosine and sine frequencies assigned to each frequency band [16], [25]. Fig. 1 shows the block diagrams of a MultiCAP transmitter and receiver.

The flexibility offered by MultiCAP allows to independently choose the modulation scheme, order, and signal power, i.e. allows bit loading and power loading in each band [12], [13], [16]. Thanks to these extra degrees of freedom, is possible to overcome the need of a flat frequency response of the channel which is required for reliable transmission of conventional CAP signals. The combination of bit loading and power loading for each band makes MultiCAP an appealing candidate for optical fiber links, where frequency selectivity and uneven gain of the channel cause significant degradations of the transmitted signal. However, it is to be noted that the advantages of this multi-band approach requires higher digital signal processing (DSP) resources. Some studies [26], [27] demonstrate that CAP and DMT have similar DSP complexity (i.e. number of basic real-valued arithmetic operations), therefore when the number of bands used in MultiCAP modulation increases, the DSP complexity increases proportionally as well.

III. Experimental Setup

Figure 2 shows the block diagram of the experimental setup. The transmitter consisted of a 65 GSa/s arbitrary waveform

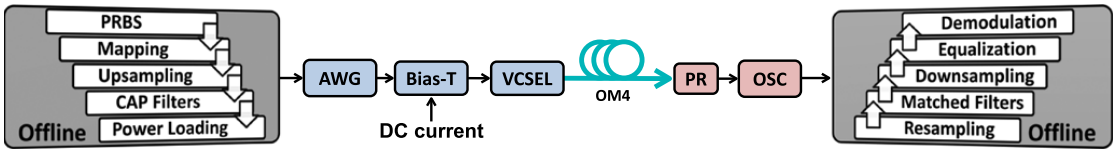

Fig 2. The block diagram of experimental setup. PRBS: pseudo-random binary sequence, AWG: arbitrary waveform generator, VCSEL: vertical cavity surface emitting laser, PR: photoreceiver, OSC: real time oscilloscope.

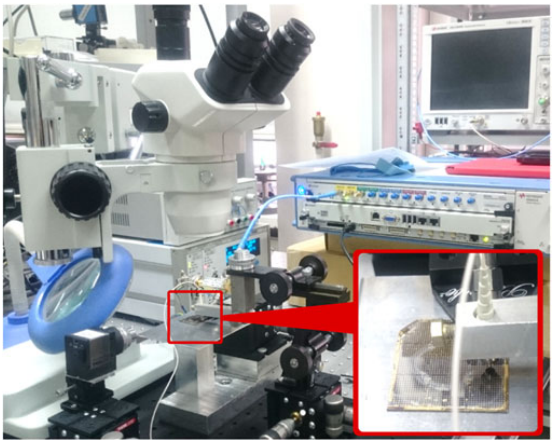

Fig. 3. The precision alignment probe station with SM-VCSEL chip wafer (inset).

generator (AWG), a bias-T, a current source and a VCSEL. Standard multiple oxide aperture VCSEL design was applied for MM-VCSEL [28], while the SM-VCSEL design allowed oxide aperture induced leakage effect to be applied for mode selection [29]. In order to achieve SM operation, thick multiple oxide apertures were used. For such design the optical field distribution of the tilted modes (in the oxidized area) becomes non-orthogonal to the VCSEL cavity mode enabling the optical leakage process. The VCSEL used in the experiments has 3 μm-diameter oxide apertures (total oxide thickness $\sim$70 nm) with which SM operation was achieved.

The packaged and pigtailed MM-VCSEL was biased with 8 mA current and driven by a modulating signal of 0.7 V_{pp}. In Fig. 3 is shown the probe station with the SM-VCSEL wafer. The SM-VCSEL was biased with 2.8 mA and driven by a modulating signal of 1 V_{pp}. No thermal stabilization was applied to both VCSELs. After transmission over the MMF OM4 fiber, which has a bandwidth of 4700 MHz·km, the optical signal was converted to the electrical domain in a 22 GHz bandwidth photoreceiver (PR) with an optional electrical amplifier. The electrical signal was captured in a 100 GSa/s real time oscilloscope (OSC) for further offline DSP.

IV. Experiments

A. MultiCAP Signal Generation and Signal Processing

A MultiCAP signal with 10 frequency bands with a baud rate of 2.5 Gbaud each was utilized. For each band, decorrelated pseudo random binary sequences (PRBSs) of $2^{11}-1$ bit length were independently generated (i.e. a PRBS with a different time shift for each band). Then, the PRBS of each band was repeated several times accordingly to the symbol constellation in which the sequences of each band were mapped, thus the resulting number of symbols of each band was the same. The obtained symbol sequences for each band were up-sampled and then filtered by the pair of orthogonal CAP filters corresponding to each band. Next, power loading was employed by assigning weights to each band in order to mitigate the channel gain unevenness. For all bands its corresponding pair of CAP filters were implemented as finite impulse response (FIR) filters with a length of 45 symbols each and an α of 0.03. The separation between the central frequencies of the bands was 2.55 GHz, starting in 1.3125 GHz as central frequency of the first band. The total bandwidth of all 10 bands was 25.5 GHz achieving a spectral efficiency of 4.21 bit/s/Hz.

At the receiver, to have a sampling rate multiple integer of the baud rates of the signal at the transmitter, the signal stored by the OSC with a sampling rate of 100 GSa/s was resampled to 130 GSa/s. Subsequently, I and Q channels of each band were retrieved by filtering with the filters matched to the CAP filters at the transmitter. After filtering, each channel was down-sampled to construct the corresponding symbol constellations, from which the symbols were demodulated employing a decision-feedback equalizer (DFE) and the k-means algorithm. The equalizer employed used the recursive least squares (RLS) adaptive algorithm, 30 feed-forward and feed-back taps, a forget-factor of 0.9999, and a value of 0.1 to initialize the diagonal elements of the inverse correlation matrix for Kalman gain computation. BERs and error vector magnitudes (EVMs) were computed offline, for each band separately, from the actual received data stored with the OSC.

B. VCSEL Characterization

Figure 4 shows the light-current-voltage (LIV) curves and the optical spectra of the utilized SM- and MM-VCSELs. For the SM/MM-VCSEL operating wavelengths were 853.1/860.5 nm, respectively. The MM-VCSEL had over 10 modes and the SM-VCSEL suppression ratio of the strongest mode was 39 dB. The maximum optical power for SM/MM-VCSEL was -1.4 dBm and 4.4 dBm, respectively. Fig. 5 shows the normalized (to the first trace measurement point) frequency response of the MM and SM-VCSELs based transmission link for various OM4 fiber lengths [5]. The frequency responses were measured with a 50 GHz network analyzer, which was connected to the VCSELs input and the PD output. The

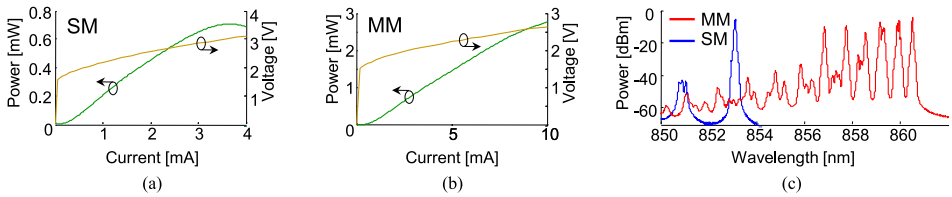

Fig 4. Light-current-voltage curves of (a) SM-VCSEL and (b) MM-VCSEL, and (c) optical spectra of SM and MM VCSELs.

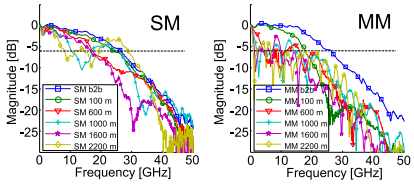

Fig. 5. Frequency response of the MM and SM-VCSELs based link.

measurements were performed with the SM-VCSEL similar to the one used in the MultiCAP experiments. While the B2B curves are similar for both lasers (i.e. the 6 dB electrical bandwidth of about 26 GHz), a clear improvement of the SM laser is visible for lengths >100 m. For the MM-VCSEL the 6 dB electrical bandwidth does not exceed 5 GHz for the lengths >100 m, while for the SM-VCSEL it is over 15 GHz for the lengths up to 1600 m (excluding 1000 m) and over 8 GHz for all lengths.

It is to be noted that for all characterization tests and fiber optic transmissions in the experiments, the VCSELs did not have any kind of thermal stabilization and all tests were performed at ambient temperature within the laboratory.

C. Transmission Experiments

First, transmission with MM-VCSEL was performed. A transmission of 107.5 Gb/s was achieved over 10 m of OM4 MMF with a received optical power of 3.9 dBm. For low frequencies, the link had a fairly flat frequency response which allowed to employ 64-QAM modulation scheme in the first two bands. Contrary, at high frequencies, the link frequency response was uneven and had a lower gain. Consequently, it was necessary to decrease the modulation order of the high frequency bands to maintain a low BER, e.g. binary phase shift keying (BPSK) modulation scheme for the last band. In Table I the BER and main parameters of each band are presented. The BER of all bands was below 7% FEC threshold of 3.8e-03, thus achieving a total effective bit rate of 100.5 Gb/s. Fig. 6 shows the received electrical spectrum of the MultiCAP signal together with the constellations and EVMs of all bands. Due the link frequency response, bands 9 and 10 had considerable lower power than the other bands, which not even with power loading could be compensated enough to increase its modulation order.

Next, transmission with SM-VCSEL was performed. An additional 25 dB gain electrical amplifier was placed after the PD to compensate for the limited optical signal power. A transmission of 107.5 Gb/s was achieved over 100 m of OM4 MMF with a received optical power of −2.54 dBm. With a similar trend as in the MM-VCSEL transmission, the highest modulation order scheme used was 64-QAM for the bands at low frequencies and the lowest modulation order scheme used was quadrature phase shift keying (QPSK) for the last two bands. In Table II, the BER and main parameters of each band are presented, while Fig. 7 shows the received electrical spectrum of the MultiCAP signal together with the constellations and EVMs of all bands. The frequency response of the 10 m MM-VCSEL link and the 100 m SM-VCSEL link are quite similar to the extent that, with the proper power assignment of each band, only the modulation order scheme of bands 8 and 10 were changed. It is to be noted that, for both VCSELs, thanks to power loading technique bands with the same modulation order have practically the same EVM. Additionally, depending on the modulation order of each band (i.e. the spectral efficiency), the processed bits per band range from 362496 to 2174976 and from 483328 to 1449984, for the MM-VCSEL and SM-VCSEL transmissions, respectively, validating the reliability of the BER results presented.

Finally, with the SM-VCSEL, the experiments towards maximum bit rate transmission at a given distance with adjustable as well as fixed (107.5 Gb/s) bit rate were performed. Fig. 8(a) shows the maximum bit rates achieved below 7% FEC limit as a function of the MMF length. The maximum bit rate achieved was 112.5 Gb/s in the B2B test, and the maximum length tested was 1 km achieving a bit rate of 85 Gb/s. Fig. 8(b) shows the average BER of all bands for 107.5 Gb/s transmission in function of MMF length. For longer distances the higher order modulation schemes, such as 64-QAM, degrade considerably increasing the BER as can be noted. For the maximum bit rate transmission experiment, Table III presents a summary of all MMF links lengths and the modulations schemes of all bands. As the link length increases, the link bandwidth and the received optical power decrease. Therefore, the EVMs of all bands worsen and the modulation order of some bands must be decreased accordingly in order to ensure a BER below 7% FEC limit.

TABLE I
BER AND MAIN PARAMETERS OF MM-VCSEL 107.5 GB/S TRANSMISSION OVER 10 M OF OM4

Band	1	2	3	4	5	6	7	8	9	10
Baud rate [Gbaud]	2.5	2.5	2.5	2.5	2.5	2.5	2.5	2.5	2.5	2.5
Modulation	64-QAM	64-QAM	32-QAM	32-QAM	32-QAM	32-QAM	16-QAM	16-QAM	QPSK	BPSK
Bit rate [Gb/s]	15	15	12.5	12.5	12.5	12.5	10	10	5	2.5
Central Freq. [GHz]	1.3125	3.8625	6.4125	8.9625	11.5125	14.0625	16.6125	19.1625	21.7125	24.2625
Power Loading [dB]	2	1	0.3	0.6	1	2.1	1.2	2.6	0.4	2
Transmitted Bits	2174976	2174976	1812480	1812480	1812480	1812480	1449984	1449984	724992	362496
BER	**3.12e-03**	**2.58e-03**	**2.36e-03**	**2.53e-03**	**3.76e-03**	**3.33e-03**	**2.63e-03**	**2.77e-03**	**7.89e-04**	**3.56e-03**

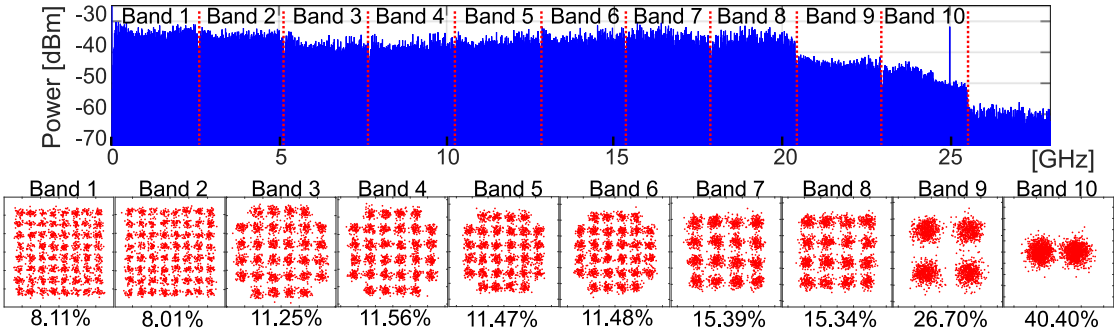

Fig 6. Received electrical spectrum and constellation diagrams after DFE for 107.5 Gb/s 10 m MM-VCSEL transmission.

TABLE II
BER AND MAIN PARAMETERS OF SM-VCSEL 107.5 GB/S TRANSMISSION OVER 100 M OF OM4

Band	1	2	3	4	5	6	7	8	9	10
Baud rate [Gbaud]	2.5	2.5	2.5	2.5	2.5	2.5	2.5	2.5	2.5	2.5
Modulation	64-QAM	64-QAM	32-QAM	32-QAM	32-QAM	32-QAM	16-QAM	8-QAM	QPSK	QPSK
Bit rate [Gb/s]	15	15	12.5	12.5	12.5	12.5	10	7.5	5	5
Central Freq. [GHz]	1.3125	3.8625	6.4125	8.9625	11.5125	14.0625	16.6125	19.1625	21.7125	24.2625
Power Loading [dB]	2	2.1	−0.2	0.7	1.7	2.6	2	1.1	−1	2.1
Transmitted Bits	1449984	1449984	1208320	1208320	1208320	1208320	966656	724992	483328	483328
BER	**1.80e-03**	**2.94e-03**	**1.33e-03**	**1.58e-03**	**1.26e-03**	**1.89e-03**	**l.lle-03**	**1.66e-03**	**1.69e-03**	**2.08e-03**

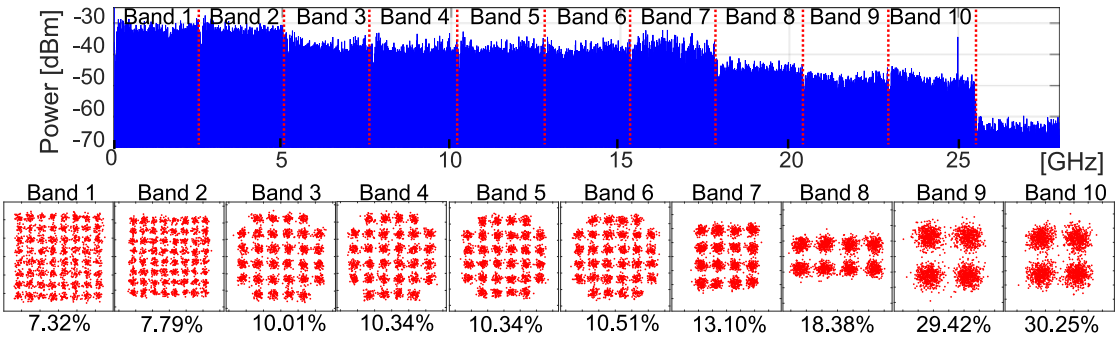

Fig 7. Received electrical spectrum and constellation diagrams after DFE for 107.5 Gb/s 100 m SM-VCSEL transmission.

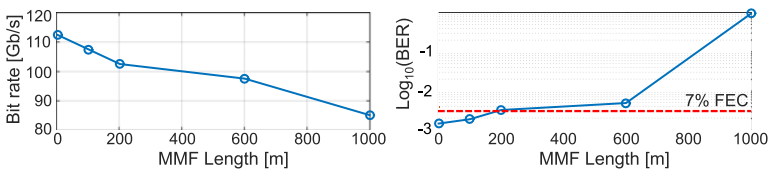

Fig 8. SM-VCSEL (a) maximum bit rate below 7% FEC limit versus MMF length and (b) 107.5 Gb/s transmission BER versus MMF length.

TABLE III
SM-VCSEL SET OF MODULATION SCHEMES FOR EACH MMF LENGTH

Distance [m]	Band 1	Band 2	Band 3	Band 4	Band 5	Band 6	Band 7	Band 8	Band 9	Band 10	Bit Rate [Gb/s]
0	64-QAM	64-QAM	64-QAM	64-QAM	32-QAM	32-QAM	16-QAM	8-QAM	QPSK	QPSK	112.5
100	64-QAM	64-QAM	32-QAM	32-QAM	32-QAM	32-QAM	16-QAM	8-QAM	QPSK	QPSK	107.5
200	64-QAM	64-QAM	32-QAM	32-QAM	32-QAM	16-QAM	16-QAM	8-QAM	QPSK	BPSK	102.5
600	32-QAM	32-QAM	32-QAM	32-QAM	32-QAM	16-QAM	16-QAM	8-QAM	QPSK	BPSK	97.5
1000	32-QAM	32-QAM	32-QAM	16-QAM	16-QAM	8-QAM	8-QAM	QPSK	QPSK	BPSK	85

V. CONCLUSION

To the best of our knowledge, for the first time an effective bit rate over 100 Gb/s is transmitted, at single wavelength, single polarization, and direct detection, with an 850 nm MM-VCSEL over 10 m of OM4 MMF and with an 850 nm SM-VCSEL over 100 m of OM4 MMF. These two records, with comparable hardware constraints and resources as previous works [12]–[14], [20], were achieved through the use of MultiCAP modulation. BERs below 7% FEC limit were measured.

To be able to increase the length of optical links, work is dedicated to develop more advanced designs to increase the output power of VCSELs. Recently, with oxide apertures having a total thickness of 100 nm, the oxide apertures diameter for SM operation was increased to 5 μm at currents exceeding 5 mA with >15 dB Side-Mode Suppression Ratio (SMSR) [30].

Due the high data rates of optical interconnects, signal integrity requirements in data centers are getting more stringent (e.g. a BER of 1e-15 is considered error free). With alternative low-density parity-check (LDPC) code schemes [31] is possible to reduce the post-FEC BER floor, however, the overhead required is larger. With the BERs achieved, our results are suitable for applications with bit rates over 50 Gb/s compliant with recent IEEE 802.3 and Fibre Channel standards (i.e. BER<1e-13).

The presented results demonstrate that ultra-high speed links over 100 Gb/s with distances up to 100 m can be realized by using cost-effective MMF and 850 nm VCSELs, disruptingly opening a technology solution for the high capacity data interconnects that can be further increased by combination with short-WDM (SWDM).

REFERENCES

[1] C. Kachris and I. Tomkos, "A roadmap on optical interconnects in data centre networks," in *Proc. 2015 17th Int. Conf. Transp. Opt. Netw.*, 2015, pp. 1–3.
[2] C. F. Lam, H. Liu, and R. Urata, "What devices do data centers need?," in *Proc. Opt. Fiber Commun. Conf.*, 2014, Paper M2K.5.
[3] J. A. Tatum *et al.*, "VCSEL-based interconnects for current and future data centers," *J. Lightw. Technol.*, vol. 33, no. 4, pp. 727–732, Feb. 2015.
[4] C. Caspar, J. R. Kropp, V. A. Shchukin, N. N. Ledentsov, V. Jungnickel, and R. Freund, "High speed transmission over multimode fiber with direct modulated single-mode VCSEL," in *Proc. Broadband Coverage Germany. 9th ITG Symp.*, 2015, pp. 1–4.
[5] G. Stepniak *et al.*, "54 Gbit/s OOK transmission using single-mode VCSEL up to 2.2 km MMF," *Electron. Lett.*, vol. 52, no. 8, pp. 633–635, 2016.
[6] D. Coleman. (2012). Optical trends in the data center. [Online]. Available: https://www.bicsi.org/uploadedfiles/bicsi_conferences/canada/2012/presentations/concses_2a.pdf
[7] J. P. Turkiewicz, J. R. Kropp, N. N. Ledentsov, V. A. Shchukin, and G. Schäfer, "High speed temperature insensitive optical data transmission with compact 850 nm TO-can assemblies," in *Proc. Opt. Fiber Commun. Conf. Exhib.*, 2014, pp. 1–3.
[8] J. Sakaguchi *et al.*, "109-Tb/s (7 × 97 × 172-Gb/s SDM/WDM/PDM) QPSK transmission through 16.8-km homogeneous multi-core fiber," in *Proc. Opt. Fiber Commun. Conf. Expo./Nat. Fiber Opt. Eng. Conf.*, 2011, Paper PDPB6.
[9] G. Meloni, A. Malacarne, F. Fresi, and L. Potì, "6.27 bit/s/Hz spectral efficiency VCSEL-based coherent communication over 800 km of SMF," in *Proc. Opt. Fiber Commun. Conf.*, 2015, Paper Th2A.30.
[10] N. Eiselt *et al.*, "First real-time 400G PAM-4 demonstration for inter-data center transmission over 100 km of SSMF at 1550 nm," in *Proc. Opt. Fiber Commun. Conf.*, 2016, Paper W1K.5.
[11] R. van der Linden, N.-C. Tran, E. Tangdiongga, and T. Koonen, "Increasing flexibility and capacity in real PON deployments by using 2/4/8-PAM formats," in *Proc. Opt. Fiber Commun. Conf.*, 2016, Paper Tu3C.4.
[12] C. Xie *et al.*, "Single-VCSEL 100-Gb/s short-reach system using discrete multi-tone modulation and direct detection," in *Proc. Opt. Fiber Commun. Conf. Exhib.*, 2015, pp. 1–3.
[13] I. C. Lu *et al.*, "Very high bit-rate distance product using high-power single-mode 850-nm VCSEL with discrete multitone modulation formats through OM4 multimode fiber," *IEEE J. Sel. Topics Quantum Electron.*, vol. 21, no. 6, pp. 444–452, Nov. 2015.
[14] B. Wu *et al.*, "Close to 100 Gbps discrete multitone transmission over 100 m of multimode fiber using a single transverse mode 850 nm VCSEL," *Proc. SPIE*, vol. 9766, 2016, Art. no. 97660K.
[15] R. Puerta *et al.*, "Multiband carrierless amplitude/phase modulation for ultrawideband high data rate wireless communications," *Microw. Opt. Technol. Lett.*, vol. 58, no. 7, pp. 1603–1607, 2016.
[16] M. I. Olmedo *et al.*, "Multiband carrierless amplitude phase modulation for high capacity optical data links," *J. Lightw. Technol.*, vol. 32, no. 4, pp. 798–804, Feb. 2014.
[17] J. J. V. Olmos, L. F. Suhr, B. Li, and I. T. Monroy, "Five-level polybinary signaling for 10 Gbps data transmission systems," *Opt. Express*, vol. 21, no. 17, pp. 20417–20422, Aug. 2013.

[18] L. F. Suhr, J. J. V Olmos, B. Mao, X. Xu, G. N. Liu, and I. T. Monroy, "112-Gbit/s x 4-lane duobinary-4-PAM for 400GBase," in *Proc. 2014 Eur. Conf. Opt. Commun.*, 2014, pp. 1–3.

[19] K. L. Chi *et al.*, "Single-mode 850-nm VCSELs for 54-Gb/s ON-OFF keying transmission over 1-km multi-mode fiber," *IEEE Photon. Technol. Lett.*, vol. 28, no. 12, pp. 1367–1370, Jun. 2016.

[20] D. M. Kuchta *et al.*, "A 71-Gb/s NRZ modulated 850-nm VCSEL-based optical link," *IEEE Photon. Technol. Lett.*, vol. 27, no. 6, pp. 577–580, Mar. 2015.

[21] R. Puerta *et al.*, "107.5 Gb/s 850 nm multi- and single-mode VCSEL transmission over 10 and 100 m of multi-mode fiber," in *Proc. Opt. Fiber Commun. Conf. Exhib.*, 2016, Paper Th5B.5.

[22] D. D. Falconer, "Carrierless AM/PM," Bell Laboratories, Murray Hill, NJ, USA, Internal Memorandum, Tech. Rep., Jul. 1975.

[23] S. Haykin, *Communication Systems*, 4th ed. New York, NY, USA: Wiley, 2001.

[24] J. L. Wei, J. D. Ingham, D. G. Cunningham, R. V Penty, and I. H. White, "Performance and power dissipation comparisons between 28 Gb/s NRZ, PAM, CAP and optical OFDM systems for data communication applications," *J. Lightw. Technol.*, vol. 30, no. 20, pp. 3273–3280, Oct. 2012.

[25] T. Zuo *et al.*, "O-band 400 Gbit/s client side optical transmission link," in *Proc. Opt. Fiber Commun. Conf.*, 2014, Paper M2E.4.

[26] J. Wei, Q. Cheng, R. V Penty, I. White, and D. Cunningham, "Analysis of complexity and power consumption in DSP-based optical modulation formats," in *Proc. Adv. Photon . Commun.*, 2014, Paper SM2D.5.

[27] K. Zhong *et al.*, "Experimental study of PAM-4, CAP-16, and DMT for 100 Gb/s short reach optical transmission systems," *Opt. Express*, vol. 23, no. 2, pp. 1176–1189, Jan. 2015.

[28] J. R. Kropp *et al.*, "Accelerated aging of 28 Gb s^{-1} 850 nm vertical-cavity surface-emitting laser with multiple thick oxide apertures," *Semicond. Sci. Technol.*, vol. 30, no. 4, pp. 45001–45005, Apr. 2015.

[29] V. Shchukin *et al.*, "Single-mode vertical cavity surface emitting laser via oxide-aperture-engineering of leakage of high-order transverse modes," *IEEE J. Quantum Electron.*, vol. 50, no. 12, pp. 990–995, Dec. 2014.

[30] N. Ledentsov Jr., V. A. Shchukin, J.-R. Kropp, M. Agustin, and N. N. Ledentsov, "Oxide-confined leaky vertical-cavity surface-emitting lasers for single mode operation," SPIE Newsroom, May 2016.

[31] D. A. Morero and M. R. Hueda, "Efficient concatenated coding schemes for error floor reduction of LDPC and turbo product codes," in *Proc. IEEE Global Commun. Conf.*, 2012, pp. 2361–2366.

Authors' biographies not available at the time of publication.

Paper 3: Single Photodiode 60 Gb/s 16-QAM and QPSK Coherent Transmission

R. Puerta and I. T. Monroy, "Single Photodiode 60 Gb/s 16-QAM and QPSK Coherent Transmission," submitted to *IEEE Photonics Technol. Lett.*, Aug. 2017.

DOI: -

Single Photodiode 60 Gb/s 16-QAM and QPSK Coherent Transmission

Rafael Puerta, *Student Member, IEEE*, Idelfonso Tafur Monroy, *Senior Member*

***Abstract*—In this letter, we investigate an optical transmission scheme using a single photodetector (PD) which, as in conventional coherent detection systems, allows the linear transfer of the amplitude information and phase information of the optical field into the electrical domain. This is possible by means of optical heterodyne detection and by adjusting the carrier-to-signal power ratio (CSPR), thus the undesired signal-to-signal beating products (SSBP) due to the PD square-law, can be considered negligible. After photodetection, carrier recovery is performed by a Costas loop. Through simulation, the CSPR impact on the proposed scheme is determined. Then, we experimentally validate our scheme for a single wavelength and single polarization transmission with a net bitrate of 60.75 Gb/s over 10 km of standard single-mode fiber (SSMF).**

***Index Terms*—Coherent detection, digital signal processing, heterodyne receiver, optical fiber communication, quadrature amplitude modulation (QAM).**

I. Introduction

DIGITAL signal processing (DSP) combined with coherent detection provide the best performance in fiber-optic communications systems. Coherent transceivers capability to linearly transfer the amplitude and phase information of the optical field into the electrical domain, allows full compensation of linear and nonlinear deterministic fiber-optic transmission impairments. In addition, the accelerated development of electronics has enabled spectrally efficient coherent transceivers reaching bitrates of 400 Gb/s single wavelength. Therefore, coherent transceivers are the adopted solution for long-haul systems. On the other hand, point-to-point metro-access range like optical interconnects are more cost-sensitive, therefore less complex intensity modulation and direct detection (IM/DD) based solutions are preferred, however at the expense of a limited reach.

Currently, significant research is being performed to realize datacenter interconnects (DCI) and metro-access transmission links taking advantage of coherent transceivers' features while using a single photodetector (PD). Thus, the hardware complexity of coherent receivers is reduced to simple single PD direct-detection implementations.

To realize single PD coherent detection, the main approach adopted is based on optical heterodyne detection by using a local oscillator (LO) digitally generated or generated by optical means, e.g. Mach-Zehnder Modulator (MZM) based frequency shifter or an additional light source. Thus, after photodetection, the transmitted signal is downconverted to an intermediate frequency (IF) to which carrier recovery schemes can be applied, and consequently the full information of the optical field is retrieved. However, without coherent balanced detection, the main impairment that arises from this approach is the presence of signal-to-signal beating products (SSBP) due to square-law photodetection, which introduce distortion to the signal. In addition, it is to be noted that the price to be paid for using a single PD, for single-carrier quadrature amplitude modulation (SC-QAM), is the requirement of a PD with a bandwidth equal to the entire bandwidth of the transmitted signal, which is twice as in conventional intradyne coherent receivers [1]–[5].

The more straightforward approach to avoid SSBP interference, is leaving a sufficient frequency gap between the transmitted signal and the LO. Thus, after heterodyne photodetection, no interference is added to the transmitted signal, however, the spectral efficiency (SE) is severely decreased [6]. Another appealing approach is to implement digital SSBP cancellation schemes by reversing the PD square-law action [7]. This approach has shown interesting results, where by applying transmitter- and receiver-based dispersion compensation together with SSBP cancellation, wavelength-division multiplexing (WDM) direct-detection systems have been validated up to 100 Gb/s per wavelength over several hundreds of kilometers of standard single-mode fiber (SSMF) [8], [9]. Recently, from a more theoretical background, Kramers-Kronig (KK) relations have been applied to single PD receiver based systems. These relations allow to determine the phase of the optical field entirely from its intensity, assuming the fulfillment of specific transmission conditions [10]. Remarkable experimental results have been presented by means of the KK scheme and discrete multitone (DMT) modulation, achieving record bitrates over 125 km of SSMF [11]. Furthermore, it has been experimentally validated in WDM direct-detection systems, a better performance when using the KK scheme over SSBP cancellation schemes [9].

Given the transmitted signal $r_s(t) = |E(t)|e^{i(2\pi f_c t + \varphi_s)}$ and

This letter was submitted for publication August 21, 2017. R. Puerta expresses his gratitude to the Colombian Administrative Department of Science, Technology and Innovation (Colciencias) for partly funding his research.

R. Puerta is with the Technical University of Denmark, Ørsted Plads, Building 343, Kongens Lyngby, 2800, Denmark (e-mail: rapur@fotonik.dtu.dk).

I. Tafur Monroy is with the Institute for Photonic Integration, Dept. of Elec. Eng, Eindhoven Univ. of Technology, PO Box 513, 5600 MB Eindhoven, The Netherlands (e-mail: i.tafur.monroy@tue.nl).

the LO $r_{LO}(t) = |A|e^{i(2\pi f_{LO}t)}$, the result after photodetection is given by

$$|r_s(t) + r_{LO}(t)|^2 = |E(t)|^2 + |A|^2 + 2|E(t)||A|\cos\big(2\pi f_{IF}t + \varphi_s(t) + \varphi_n(t)\big) \quad (1)$$

where f_{IF} is the IF equal to the frequency separation between the optical carrier and the LO, φ_s is the phase modulation, and φ_n is the total phase noise. Note that the LO amplitude $|A|$ acts as amplification, thus by using a large LO power, i.e. large CSPR, and a DC blocker, the SSBP term $|E(t)|^2$ and the DC term $|A|^2$ can be neglected. Subsequently, it is possible to track the intermediate frequency carrier phase and restore the signal complex amplitude through DSP on the heterodyne-detected signal [3], [12].

In this letter, we propose and experimentally validate a scheme that, by only adjusting the CSPR and performing digital carrier recovery after heterodyne detection, coherent detection is achieved using a single PD. Therefore, the receiver computational complexity is significantly reduced since no additional DSP is required to mitigate the SSBP or to estimate the phase of the optical signal. As a proof of concept, the simplicity of QAM modulation is combined with our proposed scheme. Single wavelength and single polarization 16-QAM and QPSK transmissions, both with a gross bitrate of 65 Gb/s, are transmitted over 10 km of SSMF with a bit error rate (BER) below 3.8×10^{-3}. Due the short link tested, frequency domain chromatic dispersion (CD) compensation is not necessary, however, since the amplitude and phase of the optical field are fully retrieved, it can be applied for metro-access and long-haul links [1]–[5].

II. Numerical Simulations

To determine the trade-off between optical signal-to-noise ratio (OSNR) requirements and feasible values of CSPRs, first, a set of simulations are performed. In Fig. 1 is shown the block diagram used in simulations.

At the transmitter side, in accordance to the digital-to-analog converter (DAC) to be used in the experiments and since the transmissions baud rates are over 30 Gbaud, a sampling rate of 65 GSa/s, an electrical bandwidth of 20 GHz, and an effective number of bits (ENOB) of 5 bits are set. To generate the data, pseudo random binary sequences (PRBSs) of 2^{11}-1 bits of length are mapped into QPSK symbol constellation using gray coding. The generated symbol sequences are upsampled to 2 samples per symbol (sps), i.e. 32.5 Gbaud, and raised cosine (RC) pulse shape with a roll-off factor of 0.01 is applied. Subsequently, the in-phase (I) and quadrature (Q) components of the signal are quantized and low-pass filtered. No further bandwidth restrictions are imposed by the optical I/Q modulator since its bandwidth is greater than 20 GHz. Given the baudrate and pulse shape characteristics, a frequency separation of 16.25 GHz between the transmitter laser and the LO is set.

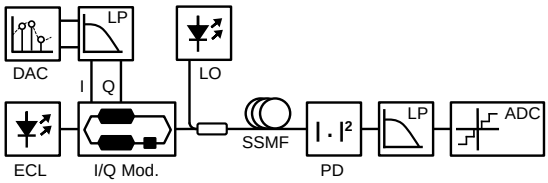

Fig. 1. Simulation setup block diagram.

To effectively have a receiver based solely on a single PD, the LO for heterodyne detection is generated at the transmitter side and sent through the fiber together with the modulated optical carrier. It is chosen to generate the LO with an additional light source, thus the CSPR can be easily adjusted [11]. In simulations, both light sources are polarization matched. It is assumed that the lasers phase noise accumulated during a sample interval T has a Gaussian distribution with a variance $\sigma^2 = 2\pi(\delta f)T$, where δf corresponds to the 3 dB linewidth of the transmitter light source and LO [12]. For lasers with a linewidth of 100 KHz, the phase noise standard deviation σ is 3.11×10^{-3}. In addition, it is assumed that the transmitted signals are contaminated by additive white Gaussian noise (AWGN).

After transmission over 10 km of SSMF with a dispersion parameter D of 17 ps/(nm·km) and subsequent square-law photodetection, the signal is digitized by an analog-to-digital converter (ADC). In accordance to the ADC to be used in the experiments, the signal is filtered by a 33 GHz Gaussian low-pass filter and quantized with an ENOB of 5 bits at a sampling rate of 80 GSa/s. Subsequently, the signal is resampled to 4 sps and a Costas loop [13] is used to retrieve the I and Q components of the IF carrier. Both components are downsampled to construct the QPSK symbol constellation and a decision-feedback equalizer (DFE), with 7 feedforward and 8 feedback T-spaced complex taps, is applied to compensate for the intersymbol interference (ISI) due the deterministic linear channel impairments.

First simulations are done setting a fixed OSNR of 15 dB and 40 dB for the transmitter laser and the LO, respectively. In Fig. 2 is shown the simulated BER performance of a 32.5 Gbaud QPSK transmission calculated as a function of the CSPR between the LO and the QPSK signal. As expected, there is minimum value (18 dB) where the SSBP distortion is minimized while the best trade-off between the OSNR and the CSPR occurs. In further simulations, for several values of

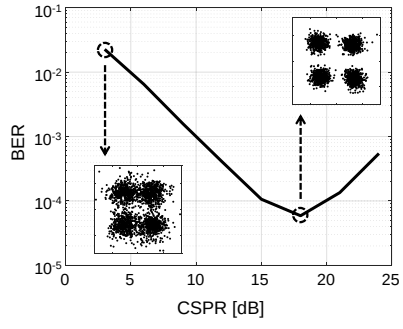

Fig. 2. BER versus CSPR simulations results.

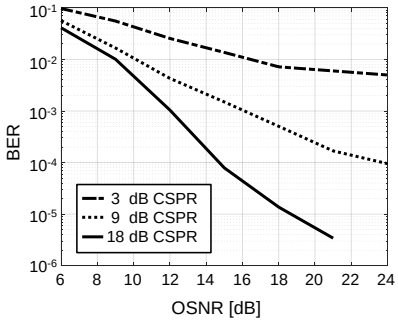

Fig. 3. BER versus OSNR simulations results for several values of CSPR.

CSPR, in Fig. 3 is shown the BER performance as a function of the OSNR of the transmitter laser. It can be noted that for low values of CSPR there is no significant performance improvement when the OSNR is increased due the dominant SSBP in these cases.

III. Experimental Setup

In Fig. 4 is shown the experimental setup. An external cavity laser (ECL) at 1548.94 nm, with a linewidth of 100 KHz, is used as light source. An additional ECL at 1549.07 nm is used to generate the LO, to easily adjust the desired CSPR. By means of polarization controllers (PC) the polarization of both light sources is matched. An arbitrary waveform generator (AWG) with a sampling rate of 65 GSa/s and 20 GHz of bandwidth is used as electrical generator. A set of attenuators and a pair of drivers with 26 dB gain and 38 GHz of bandwidth, are used to adjust the amplitude of the AWG outputs to drive an optical I/Q modulator with 33 GHz of bandwidth. To generate an optical QPSK signal, the two nested MZMs of the optical modulator

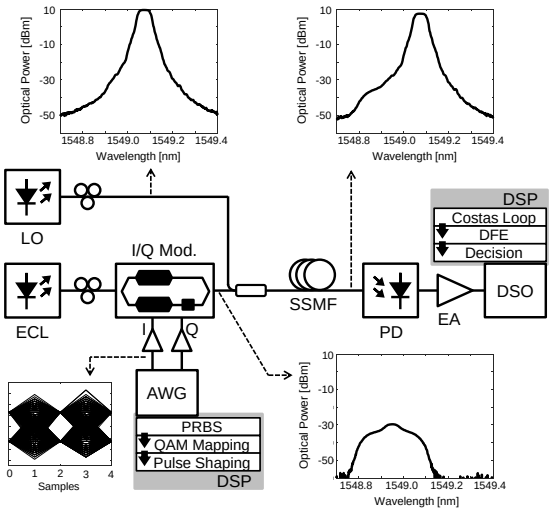

Fig. 4. Experimental setup.

are biased at its null point. After transmission through 10 km of SSMF, the optical signal is converted into the electrical domain by a PIN PD with 40 GHz of bandwidth and a responsivity of 0.6 A/W. After conversion, the electrical signal is amplified by a 26 dB gain electrical amplifier (EA) and subsequently recorded by a 33 GHz digital storage oscilloscope (DSO) at a sampling rate of 80 GSa/s for further offline DSP.

The output power of the ECL is set to 13 dBm and the power of the LO is adjusted to achieve the best CSPR in accordance to simulations. As insets, in Fig. 4 are shown the eye diagram of one of the components generated by the AWG, and the transmitted and received optical spectra.

IV. Results

The best BER results are achieved by setting the output power of the LO to 12 dBm. Due to more stringent bandwidth restrictions of the experimental setup, it was determined experimentally that by slightly reducing the frequency separation between the transmitter laser and the LO, i.e. ~0.75 GHz, the BER performance is improved.

As in simulations, a 32.5 Gbaud QPSK signal is transmitted. The received optical power is 7.3 dBm after transmission over 10 km of SSMF, with an OSNR of 20 dB (Fig. 4). After processing 1174978 bits the BER achieved is 3.68×10^{-3}. Compared to simulations, there is a penalty of ~8 dB which can be attributed to the more stringent bandwidth conditions, the additional distortion added by reducing the frequency separation between both lasers, i.e. reducing the IF, and extra sources of noise not included in simulations. In Fig. 5 is shown the electrical spectrum after photodetection and amplification, and the QPSK constellation diagrams after and before equalization.

To exhibit the negligibility of the SSBP, a transmission of 16.25 Gbaud 16-QAM is done, while keeping the same IF. Since the baudrate is halved, the RC pulse shape roll-off factor is relaxed to 0.6. In addition, the DFE feedback taps are increased to 23. After processing 1392640 bits the BER achieved is 3.34×10^{-3}. In Fig. 6 is shown the electrical spectrum

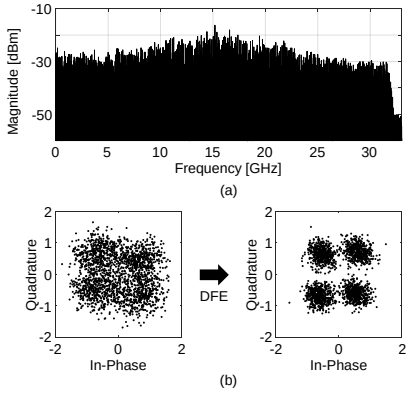

Fig. 5. (a) QPSK signal electrical spectrum after photodetection, and (b) constellation diagrams before and after equalization.

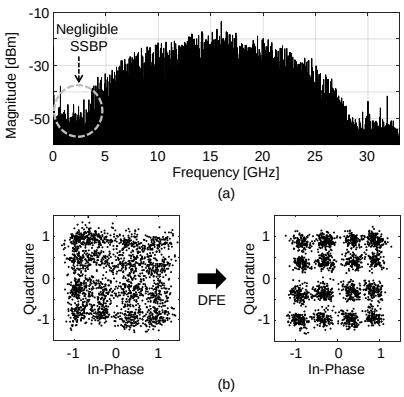

Fig. 6. (a) 16-QAM signal electrical spectrum after photodetection, and (b) constellation diagrams before and after equalization.

after photodetection and amplification, and the 16-QAM constellation diagrams before and after equalization. As can be clearly seen, the SSBP $|E(t)|^2$ are negligible.

For both transmissions, the BER is below the 7% overhead forward error correction (FEC) threshold of 3.8×10^{-3}, thus achieving a net bitrate of 60.75 Gb/s. It is to be noted that the slight asymmetry of the constellation diagrams is due residual I/Q imbalance after equalization and, to a lesser extent, to small distortion contributions of the SSBP, even when negligible.

V. Concluding Remarks

In this letter, through simulation and experiments, we validated a promising scheme in which it is possible to take advantage of coherent transceivers' features with the simplicity of single PD direct detection based receivers. Optical M-ary QAM signals are transmitted, and the I and Q components of the transmitted optical signal are retrieved by means of optical heterodyne detection and carrier recovery based on a Costas loop. Therefore, by using a single PD, both the amplitude and phase information of the optical field are recovered, however, at the expense of requiring a PD with twice the bandwidth as in conventional coherent receivers. Furthermore, the proposed scheme allows eventual frequency domain CD compensation reducing the channel memory length to an ISI of a few symbols due remnant CD and other deterministic channel impairments, which subsequently can be compensated by a time domain equalizer, e.g. DFE.

By having an additional light source as LO, there is more flexibility in setting the CSPR, however this increases hardware cost and complexity, e.g. polarization tracking mechanism is required. In addition, due to frequency instability of the lasers, the IF after optical heterodyne detection is not constant and therefore carrier recovery for signal downconversion to baseband is more demanding, e.g. carrier recovery based on pilot tones.

Future work will be devoted to address the preceding issues and to improve the performance of our scheme while keeping hardware and DSP requirements feasible for real-time implementations. One appealing approach is to generate the optical carrier and the LO from a single light source by means of an additional MZM as described in [14]. As a result, no polarization tracking is necessary, and DSP carrier recovery is relaxed since the IF is always constant. By means of DSP, another interesting approach is to generate a single sideband LO together with the M-ary QAM signal solely with the DAC. Only a single light source is required therefore the same advantages as in the previous approach are achieved. Due the limited vertical resolution of DACs, a high CSPR might not be possible while using high order modulation formats, leading to higher SSBP. These can be mitigated by means of SSBP cancellation techniques at the receiver as described in [8] together with digital pre-distortion (DPD).

References

[1] M. Kuschnerov, F. N. Hauske, K. Piyawanno, B. Spinnler, M. S. Alfiad, A. Napoli, and B. Lankl, "DSP for Coherent Single-Carrier Receivers," *J. Light. Technol.*, vol. 27, no. 16, pp. 3614–3622, Aug. 2009.

[2] S. J. Savory, "Digital Coherent Optical Receivers: Algorithms and Subsystems," *IEEE J. Sel. Top. Quantum Electron.*, vol. 16, no. 5, pp. 1164–1179, Sep. 2010.

[3] F. N. Hauske, *The Importance of Digital Signal Processing in High Speed Optical Receivers: Equalization, Impairment Compensation and Performance Monitoring*, 1st ed. Verlag Dr. Köster, 2013.

[4] K. Kikuchi, "Fundamentals of Coherent Optical Fiber Communications," *J. Light. Technol.*, vol. 34, no. 1, pp. 157–179, Jan. 2016.

[5] M. S. Faruk and S. J. Savory, "Digital Signal Processing for Coherent Transceivers Employing Multilevel Formats," *J. Light. Technol.*, vol. 35, no. 5, pp. 1125–1141, 2017.

[6] A. J. Lowery and J. Armstrong, "Orthogonal-frequency-division multiplexing for dispersion compensation of long-haul optical systems," *Opt. Express*, vol. 14, no. 6, pp. 2079–2084, Mar. 2006.

[7] S. Randel, D. Pilori, S. Chandrasekhar, G. Raybon, and P. Winzer, "100-Gb/s discrete-multitone transmission over 80-km SSMF using single-sideband modulation with novel interference-cancellation scheme," in *2015 European Conference on Optical Communication (ECOC)*, 2015, pp. 1–3.

[8] Z. Li, M. S. Erkilinc, L. Galdino, K. Shi, B. C. Thomsen, P. Bayvel, and R. I. Killey, "Comparison of digital signal-signal beat interference compensation techniques in direct-detection subcarrier modulation systems," *Opt. Express*, vol. 24, no. 25, pp. 29176–29189, Dec. 2016.

[9] Z. Li, M. S. Erkilinc, K. Shi, E. Sillekens, L. Galdino, B. C. Thomsen, P. Bayvel, and R. I. Killey, "SSBI Mitigation and the Kramers–Kronig Scheme in Single-Sideband Direct-Detection Transmission With Receiver-Based Electronic Dispersion Compensation," *J. Light. Technol.*, vol. 35, no. 10, pp. 1887–1893, 2017.

[10] A. Mecozzi, C. Antonelli, and M. Shtaif, "Kramers-Kronig coherent receiver," *Optica*, vol. 3, no. 11, pp. 1220–1227, Nov. 2016.

[11] X. Chen, C. Antonelli, S. Chandrasekhar, G. Raybon, J. Sinsky, A. Mecozzi, M. Shtaif, and P. Winzer, "218-Gb/s single-wavelength, single-polarization, single-photodiode transmission over 125-km of standard singlemode fiber using Kramers-Kronig detection," in *2017 Optical Fiber Communications Conference and Exhibition (OFC)*, 2017, pp. 1–3.

[12] K. Kikuchi, "Coherent Optical Communications: Historical Perspectives and Future Directions," in *High Spectral Density Optical Communication Technologies*, 1st ed. Springer-Verlag Berlin Heidelberg, 2010, ch. 2.

[13] S. Haykin, *Communication Systems*, 4th ed. Wiley Publishing, 2001.

[14] R. Puerta, S. Rommel, J. J. V. Olmos, and I. T. Monroy, "Optically Generated Single Side-Band Radio-over-Fiber Transmission of 60Gbit/s over 50m at W-Band," in *Optical Fiber Communication Conference*, 2017, p. M3E.4.

Paper 4: Single-Wavelength, Single-Photodiode per Polarization 276 Gb/s PDM 8-QAM over 100 km of SSMF

R. Puerta, T. Yamauchi, T. Tanimura, Y. Akiyama, T. Takahara, I. T. Monroy, and T. Hoshida, "Single-Wavelength, Single-Photodiode per Polarization 276 Gb/s PDM 8-QAM over 100 km of SSMF," submitted to *Optical Fiber Communication Conference*, Oct. 2017.

DOI: -

Single-Wavelength, Single-Photodiode per Polarization 276 Gb/s PDM 8-QAM over 100 km of SSMF

Rafael Puerta[1,2,*], Tomohiro Yamauchi[1], Takahito Tanimura[1], Yuichi Akiyama[1], Tomoo Takahara[1], Idelfonso Tafur Monroy[3], and Takeshi Hoshida[1]

[1]*Fujitsu Laboratories Ltd., 4-1-1 Kamikodanaka, Nakahara-ku, Kawasaki 211-8588, Japan*
[2]*Dpt. Photonics Engineering, Technical University of Denmark, Ørsteds Plads Building 343, 2800 Kgs. Lyngby, Denmark*
[3]*Institute for Photonic Integration, Eindhoven University of Technology, PO Box 513, 5600 MB Eindhoven, The Netherlands*
*E-mail: *rapur@fotonik.dtu.dk, ing.puerta@gmail.com*

Abstract: We demonstrate heterodyne detection of 46 Gbaud polarization-multiplexed QAM signaling using a transmitter based on a conventional dual-polarization I/Q modulator and a receiver consisting of two single-photodiodes without a local oscillator.

OCIS codes: (060.1660) Coherent Communications; (060.2330) Fiber optics communications

1. Introduction

Digital signal processing (DSP) combined with optical coherent communications provide the best performance in metro-core networks, datacenter interconnects (DCIs), and long-haul fiber-optic links. Coherent transceivers capability to linearly transfer the amplitude and phase information of the optical field into the electrical domain, allows full compensation of linear and nonlinear deterministic fiber-optic transmission impairments.

Recently, major research is being performed to realize DCIs and metro-access transmission links taking advantage of coherent transceivers' features while using a single photodiode (PD). To achieve single PD single polarization coherent detection, the main approach adopted is based on optical heterodyne detection by transmitting the modulated signal together with a co-propagating tone with a sufficient frequency separation to ensure no overlapping [1–6]. Thus, after photo-detection, the transmitted signal is downconverted to an intermediate frequency (IF) to which carrier recovery schemes can be applied, and consequently the full information of the optical field is retrieved. However, for quadrature amplitude modulation (QAM), the price to be paid for using a single PD combined with heterodyne detection is the requirement of a PD with a bandwidth equal to the entire bandwidth of the transmitted signal, which is twice as in conventional intradyne coherent receivers [7, 8]. In addition, without balanced detection, the main impairment of this approach is the presence of signal-to-signal beating products (SSBP) due to the square-law photo-detection that adds distortion to the signal. To mitigate this impairment, SSBP cancellation schemes [2, 5] and Kramers-Kronig (KK) relations based receivers [1–6] have been applied. In single-wavelength and single polarization transmissions using a single PD receiver, the highest net bitrate reported using both SSBP mitigation approaches is 215 Gb/s over 160 km of standard single-mode fiber (SSMF), considering the 20 percent overhead soft-decision forward error correction (SD-FEC) threshold of 2×10^{-2} [5].

In this paper, we extend the concept of single polarization and single PD coherent detection to polarization division multiplexing (PDM) transmissions [3]. We effectively transmitted 46-Gbaud PDM 8-QAM signals over 100 km of SSMF, achieving a net bitrate of 230 Gb/s, i.e. 276 Gb/s including 20 percent FEC overhead.

2. Proposed Framework

Given the transmitted signal $r_s(t) = |E(t)|e^{i(2\pi f_s t+\varphi_s)}$ and the co-propagating tone $r_{ct}(t) = |A|e^{i(2\pi f_{ct}t)}$, the result after photo-detection is given by:

$$|r_s(t) + r_{ct}(t)|^2 = |E(t)|^2 + |A|^2 + 2|E(t)||A|\,cos\big(2\pi f_{IF}t + \varphi_s(t) + \varphi_n(t)\big) \quad (1)$$

where f_{IF} is the IF equal to the frequency separation between the modulated optical carrier and the co-propagating tone, φ_s is the phase modulation, and φ_n is the total phase noise. Note that the tone amplitude $|A|$ acts as amplification, thus by using a large power tone, i.e. large carrier-to-signal power ratio (CSPR), and a DC blocker, the SSBP term $|E(t)|^2$ and the DC term $|A|^2$ can be minimized. Subsequently, it is possible to track the IF carrier phase and restore the signal complex amplitude through DSP on the heterodyne-detected signal [7, 8].

In this context, transmission of single polarization single sideband (SSB) QAM subcarrier modulation (SCM) signals has been recently reported [2, 4]. By using an optical I/Q modulator based transmitter, and by adjusting the bias point of the dual-nested Mach-Zehnder Modulators (MZMs) in the I/Q modulator, the CSPR can be controlled. Conversely, we generate baseband QAM signals and add a digital SSB tone. Thus, we adjust the CSPR by changing the amplitude ratio of the SSB tone and the QAM signal in the digital domain while keeping the bias of the two

nested MZMs at their null point [5]. By digitally generating a SSB tone instead of performing digital SCM, the Euclidean distance between symbols is maximized since the MZMs are biased in the null point, and since the digital-to-analog converter (DAC) used generates the QAM signals in baseband, higher baudrates can be reached. On the other hand, due to the limited vertical resolution of DACs, a high CSPR might not be possible to set while using high order modulation formats leading to high SSBP.

In our scheme, we generate the co-propagating tone as a digital SSB tone together with a QAM signal in each polarization solely by means of a DAC. Therefore, by using a single light source and a receiver consisting of two single-PDs and no local oscillator (LO), we achieve dual-polarization coherent detection. Instead of using 90 degree optical hybrids and balanced PDs, a digital Costas loop [9] is used to retrieve the in-phase (I) and quadrature (Q) components of each polarization, and a SSBP cancellation stage is applied to mitigate the PD square-law distortion.

3. Experimental Setup and Results

An external cavity laser (ECL) at 1550.9 nm with a linewidth of <100 kHz is used as light source, and a 32 GHz analog bandwidth arbitrary waveform generator (AWG) at a sampling rate of 92 GSa/s is used as a four-channel DAC. A set of drivers with 11 dB gain and 67 GHz bandwidth are used to adjust the amplitude of the AWG outputs to drive a dual-polarization optical I/Q modulator with a 3-dB bandwidth of 35 GHz. To generate an optical 8-QAM signal for each polarization, each inner MZM of the optical modulator is biased at its null point. Before transmission, the optical signal is amplified using an erbium-doped fiber amplifier (EDFA) with a noise figure <6 dB. After transmission over 100 km of SSMF and amplification using a second EDFA, the received optical power is set to 9.5 dBm and the signal is divided into its two polarization components by a polarization beam splitter (PBS). Subsequently, each component is converted into the electrical domain using a PIN PD with 60 GHz of bandwidth and a responsivity of 0.7 A/W. After conversion, the electrical signals are recorded by a 63 GHz digital storage oscilloscope (DSO) at a sampling rate of 160 GSa/s for further offline DSP. It is to be noted that a polarization controller (PC) is used before the PBS to make coarse adjustment of the received optical power at each PD to be comparable, while a polarization demultiplexing DSP stage is still employed. Fig. 1 shows the experimental setup and the insets show the eye diagram of the 8-QAM signal Q component (excluding the SSB tone) at the DAC input, the measured transmitted optical spectrum, and the electrical spectrum of X-polarization after SSBP cancellation.

For each polarization, the SSB co-propagating tone is generated together with an 8-QAM signal solely by means of the AWG. To generate the data, binary sequences of 4640 bits are mapped into 8-QAM symbol constellation. The generated symbol sequences are upsampled to 2 samples per symbol (sps), and raised cosine (RC) pulse shape with a roll-off factor of 0.01 is applied. Subsequently, the I and Q components of the SSB tone are added to the QAM signal. To reduce the interference from the SSBP, a frequency gap equivalent to the 14 percent of the symbol rate of 46Gbaud is left between the SSB tone and the signal (Fig. 1(b)). The generated I and Q components of one polarization are delayed for a thousand symbols to provide a decorrelated driving signal for the other polarization.

At the receiver side, first signals are resampled to 4 sps. Then the non-negligible SSBP, resulting from the optimum but finite CSPR as a compromise under the limited vertical resolution of the AWG, is mitigated by a single-stage linearization filter [2]. Subsequently, carrier recovery (CR) is done by a Costas loop to retrieve the I and Q components from the IF carrier of each polarization. Due to chromatic dispersion (CD), the channel memory length after 100 km of uncompensated SSMF at 1550 nm and a baudrate of 46-Gbaud is ~29 symbols [8], therefore

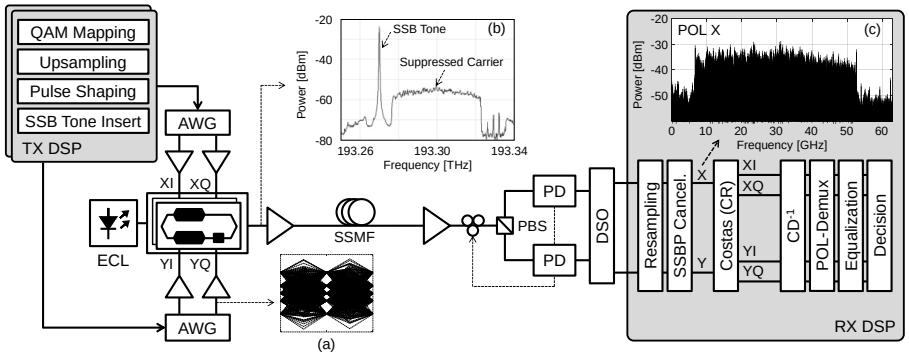

Fig. 1. Experimental setup. Insets: (a) 2 samples per symbol 8-QAM signal Q component eye diagram (excluding SSB tone); (b) transmitted optical spectrum; and (c) X-polarization electrical spectrum after single-stage linearization SSBP cancellation.

CD is compensated in the frequency domain. Radius directed equalizer (RDE) based polarization demultiplexing is performed. Then, the I and Q components of both polarizations are downsampled to construct the 8-QAM symbol constellations. Lastly, a decision-feedback equalizer (DFE), with 9 feedforward and 19 feedback T-spaced complex taps, is applied to each polarization signal to compensate for the intersymbol interference (ISI) due to additional deterministic transmission impairments before demodulation. In all BER measurements, 1252800 bits are processed in each polarization.

The CSPR value which provides the best trade-off between the optical signal-to-noise ratio (OSNR) and the interference due to the SSBP is determined experimentally. Fig. 2(a) shows the symbol constellations of both polarizations in back-to-back (B2B) tests with a CSPR of 14 dB and when SSBP cancellation is applied. In Fig. 2(b) is shown the average bit error rate (BER) of both polarizations as a function of the CSPR with and without the SSBP cancellation stage. For CSPR values of 12 dB and 14 dB the BER is minimized, where the latter is preferred since the SSBP are slightly lower. For a CSPR of 14 dB in 100 km transmissions, Fig. 2(c) shows the received symbol constellations of X-polarization with and without frequency domain CD compensation, RDE, and DFE.

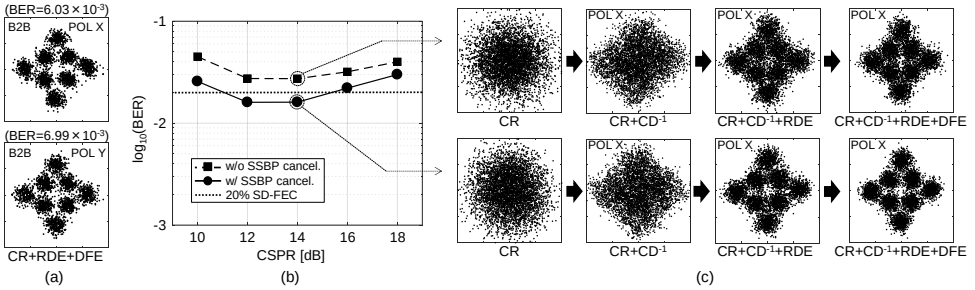

Fig. 2. (a) Received symbol constellations of X- and Y-polarization in B2B tests with a CSPR of 14 dB and SSBP cancellation; (b) BER versus CSPR of 276 Gb/s PDM 8-QAM transmissions over 100 km of SSMF, and (c) received symbol constellation of X-polarization after 100 km of SSMF with and without frequency domain CD compensation, RDE, and DFE.

It is to be noted that as the CSPR value increases, the SSBP are less dominant and therefore the BER improvement by means of SSBP cancellation schemes is reduced. For the optimum CSPR value of 14 dB, the BER is reduced from 2.74×10^{-2} to 1.61×10^{-2} which is below the 20 percent overhead SD-FEC threshold of 2×10^{-2}.

4. Conclusions

We have experimentally validated PDM heterodyne detection by means of a single PD per polarization, transmitting a gross bitrate of 276 Gb/s achieving a spectral efficiency of 5.25 b/s/Hz. To the extent of our knowledge, this is the first experimental demonstration of single-wavelength PDM coherent detection with a net bitrate of 230 Gb/s over 100 km of uncompensated SSMF by means of a receiver solely composed by two single PDs without an additional laser source as LO.

5. Acknowledgments

R. Puerta expresses his gratitude to the Colombian Department of Science, Technology and Innovation (Colciencias) for supporting his research. We would like to thank Hideyuki Minami for his assistance with the experimental setup.

6. References

[1] X. Chen *et al.*, "218-Gb/s Single-Wavelength, Single-Polarization, Single-Photodiode Transmission Over 125-km of Standard Singlemode Fiber Using Kramers-Kronig Detection," in *Optical Fiber Communication Conference* (OFC, 2017), Th5B.6.

[2] Z. Li *et al.*, "SSBI Mitigation and the Kramers–Kronig Scheme in Single-Sideband Direct-Detection Transmission With Receiver-Based Electronic Dispersion Compensation," J. Lightwave Technol. **35**(10), 1887–1893 (2017).

[3] X. Chen *et al.*, "4 x 240 Gb/s Dense DWM and PDM Kramers-Kronig Detection with 125-km SSMF Transmission," in *European Conference on Optical Communication* (ECOC, 2017), W.2.D.4.

[4] Z. Li *et al.*, "168 Gb/s/λ Direct-Detection 64-QAM SSB Nyquist-SCM Transmission over 80 km Uncompensated SSMF at 4.54 b/s/Hz net ISD using a Kramers-Kronig Receiver," in *European Conference on Optical Communication* (ECOC, 2017), Tu.2.E.1.

[5] S. T. Le *et al.*, "8x256Gbps Virtual-Carrier Assisted WDM Direct-Detection Transmission over a Single Span of 200km," in *European Conference on Optical Communication* (ECOC, 2017), Th.PDP.B.1.

[6] A. Mecozzi *et al.*, "Kramers–Kronig coherent receiver," Optica **3**(11), 1220-1227 (2016).

[7] K. Kikuchi, "Coherent Optical Communications: Historical Perspectives and Future Directions" in *High Spectral Density Optical Communication Technologies,* 1st ed. (Springer-Verlag Berlin Heidelberg, 2010).

[8] F. N. Hauske, *The Importance of Digital Signal Processing in High Speed Optical Receivers* (Verlag Dr. Köster, 2013).

[9] J. P. Costas, "Synchronous Communications," Proc. IRE **44**(12), 1713–1718 (1956).

Paper 5: Single Carrier PDM Radio-over-Fiber 328 Gb/s Wireless Transmission in a D-band Millimeter Wave 2 × 2 MU-MIMO System

R. Puerta, J. Yu, X. Li, Y. Xu, J. J. V. Olmos, and I. T. Monroy, "Single Carrier PDM Radio-over-Fiber 328 Gb/s Wireless Transmission in a D-band Millimeter Wave 2 × 2 MU-MIMO System," *J. Light. Technol.*, vol. PP, no. 99, pp. 1–1, Sep. 2017.

DOI: 10.1109/JLT.2017.2756089

Single Carrier PDM Radio-over-Fiber 328 Gb/s Wireless Transmission in a D-band Millimeter Wave 2×2 MU-MIMO System

Rafael Puerta, *Student Member, IEEE*, Jianjun Yu, *Senior Member*, Xinying Li, Yuming Xu, Juan José Vegas Olmos, *Senior Member, IEEE*, Idelfonso Tafur Monroy, *Senior Member*

***Abstract*—Next generation wireless communication systems face many challenges to increase the capacity and spectral efficiency of current solutions. The worldwide mobile data traffic increased 4000-fold over the last decade, and is forecast a sevenfold increase between 2016 and 2021. To cope with these stringent demands, prospective solutions are millimeter-wave (mmWave) technology and ultra-dense small cell networks, given that today most of the mobile traffic is offloaded from mobile networks, i.e. most of mobile users are connected to fixed networks. In addition, enabled by the fast development of electronics, digital signal processing (DSP) has become essential to enhance the capacity and performance of current communication systems. In this paper, by using the benefits of multiband modulation schemes and independent sideband (ISB) modulation, high-speed mmWave wireless transmissions in the D-band (110-170 GHz) are reported. D-band radio frequency carrier is generated by means of optical heterodyning, and ISB modulation is applied by means of the Hilbert transform and a double-nested Mach-Zehnder modulator (MZM). Total data rates up to 352 Gb/s and spectral efficiencies up to 7.7 bit/s/Hz are experimentally achieved in a single 2×2 multiuser multiple-input multiple-output (MU-MIMO) system.**

***Index Terms*—Carrierless amplitude phase modulation, Independent sideband modulation, Millimeter wave, Optical fiber communication, Wireless communications.**

I. Introduction

UPCOMING fifth generation (5G) of wireless networks have as main challenge to increase the capacity and spectral efficiency of systems by a factor of 1000 and 10, respectively [1]. Therefore, several approaches are being investigated such as flexible spectrum management, cognitive networks, millimeter-wave (mmWave) technology, network densification, among others [2]–[5]. A solution that has shown promising benefits is cell-shrinking, in which the capacity per unit area can be increased by deploying ultra-dense networks of small cells [2]–[7]. These dense networks are composed mainly by pico- and femto-cells with a wireless range up to 200 m and 10 m, respectively. Thus, by reusing the same frequency bands over different cells, service to more users and higher data rates per user can be provided. In addition, this approach is consistent with current trends which focus on implementing a suitable framework for the internet of things (IoT) and high-capacity fixed networks, i.e. offload traffic. In 2015, mobile offload traffic exceeded cellular traffic for the first time [1], since most of the mobile data activity takes place indoors, e.g. Wi-Fi access points in users' homes and offices. Thus, traffic generated by mobile devices and services is being offloaded from mobile networks, increasing the demand for denser networks with more fixed access nodes [1].

In dense networks scenarios, to cope with 5G systems capacity demands, mmWave communications systems are a prospective candidate providing high capacity and long wireless reach [8]–[11]. Their main features are: provision of very large bandwidths, i.e. 30–300 GHz, unlike conventional narrowband communications systems which are overcrowded with current radio services; no interference with current mobile networks; and mmWave signals can be generated and processed with current electronics and photonics technologies. Furthermore, mmWave communications systems can be combined with centralized/cloud radio access network (C-RAN) architectures, providing a cost-effective solution to achieve network densification [4]–[6], [12]. Although mmWave has been used mainly for outdoor point-to-point backhaul links [13], extensive research is being performed to improve the flexibility of mmWave systems by implementing MIMO schemes [2]–[4], [13].

MmWave frequency bands are often underutilized with low spectral efficiencies due to, the impairments of wireless channels, e.g. non-flat frequency response, multipath effect, and to the demanding radio frequency (RF) link budget. This is mainly due the strong propagation impairments of millimeter waves such as high free-space path loss (FSPL) and atmospheric and rain absorptions [2], [4], and to the scarce and expensive electronics operating at these high frequencies. To partly alleviate these impairments, digital signal processing

This paper was submitted for publication June 30, 2017. R. Puerta would like to express his gratitude to the Colombian Administrative Department of Science, Technology and Innovation (COLCIENCIAS) for partly funding his research.

R. Puerta and I. Tafur Monroy are with the Technical University of Denmark, Ørsted Plads, Building 343, Kongens Lyngby, 2800, Denmark (e-mail: rapur@fotonik.dtu.dk, idtm@fotonik.dtu.dk).

Jianjun Yu, Xinying Li are with ZTE(TX) Inc., NJ 07960, USA (e-mail: yu.jianjun@ztetx.com, xinying.li@ece.gatech.edu).

J.J. Vegas Olmos is with Mellanox Technologies A/S, Ledreborg Alle 130B, 4000, Roskilde, Denmark (e-mail: juanj@mellanox.com).

Yuming Xu is with Fudan University, MoE, Shanghai 200433, China (e-mail: 13110720072@fudan.edu.cn).

(DSP) techniques and advanced modulation formats have been investigated to enhance the capacity and performance of mmWave communications systems [9], [14]–[16]. In addition, to optimize the management of mmWave large bandwidths, multiband modulation schemes provide the flexibility to split these bandwidths into several bands and adjust them independently. Thus, non-flat frequency responses, e.g. uneven antenna gain, can be compensated to maximize spectral efficiency [17]–[20]. Furthermore, data rates can be increased by exploiting spatial division multiplexing (SDM), more specifically multiuser multiple-input multiple-output (MU-MIMO) technology [21].

Carrierless amplitude phase (CAP) modulation and its multiband approach (MB-CAP) are modulation formats that have shown remarkable transmission speeds in fiber-optic and wireless links [9], [16], [18]–[20], [22]. In CAP modulation, by means of two orthogonal digital filters, a digitally generated subcarrier is modulated resulting in suppressed-carrier quadrature amplitude modulation (QAM) signals. Since CAP modulation is done in the digital domain, the resulting modulated subcarrier can be transmitted via intensity/amplitude modulation and can be demodulated by means of simple non-coherent receivers, e.g. matched filters. MB-CAP modulation is suitable to exploit the large bandwidths available in optical and mmWave wireless links, while mitigating the impairments of the channel due its non-flat frequency response and the limited bandwidth of electrical and optical devices. Additionally, MB-CAP modulation has appealing features such as no need of time and frequency synchronization relying on pilot tones or pilot symbols, low peak-to-average power ratio (PAPR), e.g. alleviating the restrictions on the operation range of electrical amplifiers, and a low computational complexity in its implementation [19]. Adversely, a disadvantage of CAP and MB-CAP modulation is its reduced spectral efficiency when modulating an optical/RF carrier, which in the best of the cases, is only up to half of QAM modulation efficiency. However, given that multiband modulation schemes signals can be transmitted via intensity/amplitude modulation, this drawback can be overcome by means of single sideband (SSB) modulation and independent sideband (ISB) modulation [9], [23–25].

In this paper, enabled by photonics technologies, we present ultra-high capacity mmWave transmissions in the D-band (110-170 GHz). As a proof-of-concept, we generate optically ISB CAP and ISB MB-CAP polarization division multiplexed (PDM) signals, and transmit wirelessly both polarizations by a single 2×2 MU-MIMO system, i.e. one dedicated pair transmitter/receiver antennas per polarization. Net bitrates up to 328.97 Gb/s are achieved [26]. Particularly, we discuss the large number of taps required in the equalization stage at the receiver, due to I/Q imbalance as described and investigated in [27]. To the extent of our knowledge, this is the highest data rate ever achieved in any mmWave band by means of a single 2×2 MU-MIMO system.

II. Modulation and Digital Signal Processing

CAP modulation is a variation of QAM modulation in which suppressed carrier QAM signals are generated, i.e. carrierless signals. Instead of generating the in-phase (I) and quadrature (Q) components of the transmitted signal by modulating the amplitude of two orthogonal carriers of the same frequency, the signal is generated in the digital domain by using two orthogonal filters. These filters are the result of the time-domain multiplication of two orthogonal carriers and a pulse shaping function [28], which are implemented as finite impulse response (FIR) filters. CAP modulation is executed in two stages. First, the signal modulates a subcarrier in the digital domain, and then this digital modulated subcarrier modulates an optical or RF carrier. Thus, two main advantages are attained:

- Since I and Q orthogonal components of CAP signals are comprised in the digitally generated subcarrier, they can be transmitted by means of intensity/amplitude modulation, e.g. amplitude modulation (AM) radio communications, directed modulated lasers (DMLs), intensity modulation via MZMs.
- At the receiver side, the I and Q components of CAP signals can be retrieved by means of simple matched filters instead of coherent receivers or fast Fourier transform (FFT) based receivers.

Given the benefits of CAP modulation, MB-CAP modulation has been proposed for wireless and optical links, achieving high spectral efficiencies over large bandwidths. MB-CAP modulation allows the use of bit- and power-loading techniques for each band independently, which is done in accordance to the signal to noise ratio (SNR) and the channel conditions over the frequency range of each band [19], [20]. The I and Q components of each band are generated by its own pair of FIR orthogonal filters, and then the components of all bands are added together into a single signal.

Although CAP modulation signals exhibit several desirable advantages [19], [20], [28], however, when used to modulate the intensity of an optical carrier or the amplitude of a RF carrier, the resulting spectral efficiency can only reach up to half the spectral efficiency of QAM modulation, i.e. assuming the same baudrate and pulse shaping function. To overcome this disadvantage, SSB modulation and ISB modulation can be applied by means of digital Hilbert transform filters and optical I/Q modulation [9], [26]. Thus, the spectral efficiency of CAP and MB-CAP modulation can be enhanced to match QAM modulation spectral efficiency.

To produce an ISB modulation signal, first two independent SSB signals are generated. To generate each SSB signal, first the original signal is filtered using a FIR Hilbert transform filter, and then its corresponding analytical signal, i.e. its SSB version, is generated as a complex signal with the original signal as the real part and its Hilbert transform as the imaginary part. By adding or subtracting the Hilbert transform as imaginary part to the original signal, it is determined if the lower sideband (LSB) or the upper sideband (USB) is cancelled. It is to be noted that, the real and imaginary parts of the analytical signal are the I and Q components that drive the optical I/Q modulator, respectively. By filtering two

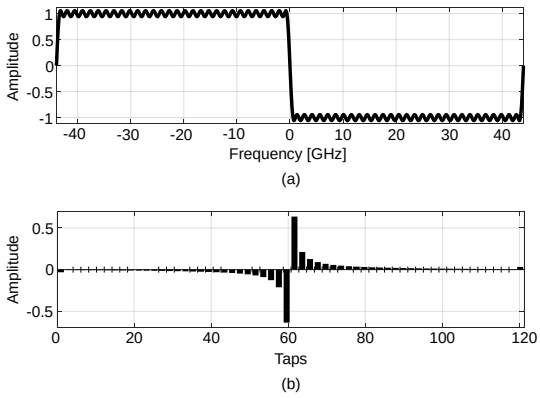

Fig. 1. FIR Hilbert transform filter (a) frequency reponse, and (b) impulse response taps

independent CAP/MB-CAP signals, i.e. decorrelated signals, and cancelling a different sideband each time, two analytical signals are produced which are added to produce the ISB signal. It should be noted as well that, FIR Hilbert transform filters estimates the actual analytical signal, therefore the spectral efficiency of ISB CAP signals is slightly lower than QAM modulation, since a frequency gap has to be left between the optical carrier and the CAP band(s) to avoid signal distortions. This is due the frequency response of the digital Hilbert filter as shown in Fig. 1(a), which has a transition band from its negative to positive frequency spectral components.

To maximize the output power of the optical I/Q modulator, the peak-to-peak voltage (V_{pp}) of its driving signals must be V_{π}, i.e. when biased in its quadrature point. However, due to variability of the system, e.g. temperature changes, the quadrature point of the I/Q modulator double-nested MZMs changes over time. As consequence, occasionally the modulation index of the optically generated signals is not less than or equal to 1, i.e. overmodulation occurs and carrier exhibits phase reversal. Therefore, after optical heterodyning and wireless transmission, a digital Costas loop [28], [29] is implemented to always ensure proper RF carrier recovery, even if the carrier is slightly suppressed, i.e. modulation index is slightly greater than 1 [9], [16].

At the receiver side, digital equalization with adaptive training algorithms is used. A decision feedback equalizer (DFE) is used to partly mitigate the deterministic impairments of the channel by cancelling the precursors and postcursors of the channel impulse response [30], [31]. In the fiber-optic transmission segment, mitigation of chromatic dispersion (CD) is achieved, and in the wireless transmission segment, multipath effect is mitigated. In addition, in both cases, the DFE compensates as well the intersymbol interference (ISI) due the limited bandwidth of electrical and optical devices, and I/Q imbalance [23].

III. Experimental Setup

In this section a description of the experimental setup used to validate our fiber-wireless transmission is described.

Figure 2(a) shows the main blocks used to generate the ISB modulation signals. First, two decorrelated pseudo-random binary sequences (PRBSs) of length 2^{11}-1 bits are mapped into the corresponding symbol constellations of each sideband, i.e. LSB and USB. The resulting multilevel symbol sequences are upsampled and then filtered by CAP root raised cosine (RRC) shaped orthogonal filters, with a roll-off factor of 0.03. Next, by applying the Hilbert transform to the CAP signal of each sideband, the I and Q components of the resulting LSB and USB analytical signals are produced. To avoid distortion due the transition band of the FIR Hilbert filter, during generation of baseband CAP signals, a frequency gap of 500 MHz is left between DC and the start of the CAP band(s).

The laser source used for transmission is a free-running external cavity laser (ECL), with a linewidth <100 kHz and an output power of 13 dBm. Its output is modulated by a double-nested MZM modulator, i.e. optical I/Q modulator. A two-channel 88 GSa/s digital to analog converter (DAC), with 22 GHz of electrical bandwidth, is used as electrical generator to drive the optical I/Q modulator. Each channel is loaded with the I and Q components of the analytical signals produced by the FIR Hilbert transform filters. The generated optical ISB

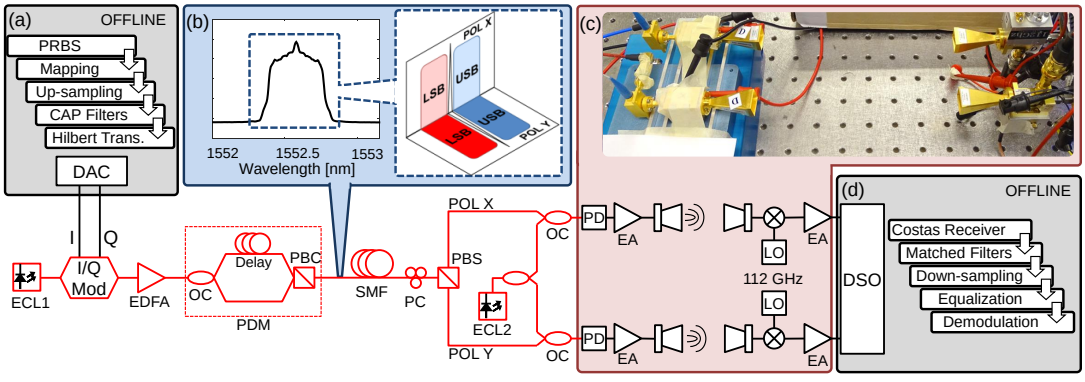

Fig 2. Block diagram of experimental setup. ECL: external cavity laser, PRBS: pseudo-random binary sequence, DAC: digital to analog converter, EDFA: erbium doped fiber amplifier, PBC: polarization beam coupler, PC: polarization controller, PBS: polarization beam splitter, PDM: polarization division multiplexing, EA: electrical amplifier, PD: photodetector, LO: local oscillator, DSO: digital storage oscilloscope, LSB: lower sideband, USB: upper sideband.

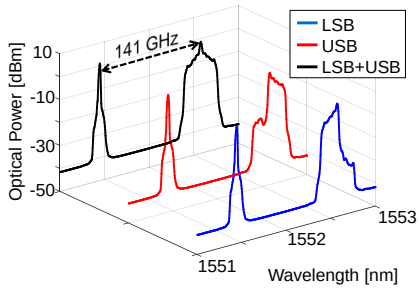

Fig. 3. Comparison of optical spectra for a transmission of 22 Gbaud CAP signals per sideband in both polarizations.

signal is amplified by an erbium-doped fiber amplifier (EDFA). After amplification, a PDM stage is performed by splitting the output of the EDFA using a polarization-maintaining optical coupler (PM-OC), adding an optical delay line in one of its outputs to decorrelate both polarizations, and then combining both polarizations again using a polarization beam combiner (PBC). After the PDM stage, the optical signal is transmitted over 25 km of standard single-mode fiber (SMF). In Fig. 2(b) is illustrated the optical spectrum of each polarization with its corresponding ISBs. Before wireless transmission, each polarization is retrieved by a polarization beam splitter (PBS). A second ECL is used as optical local oscillator, with 141 GHz frequency spacing relatively to the ECL at the transmitter side, thus, generating a D-band mmWave RF carrier by means of optical heterodyning at the photodetectors (PDs). In Fig. 3 is shown the comparison of the optical spectra of a signal with 22 Gbaud per sideband, when transmitting only the LSB, when transmitting only the USB, and when transmitting both sidebands, respectively.

The generated mmWave signals from each polarization, are first amplified by 15 dB gain D-band electrical amplifiers (EAs) and then transmitted wirelessly by two transmitter/receiver horn antenna (HA) pairs, where each HA has a gain of 25 dBi. In Fig 2(c) the 2×2 MU-MIMO antenna setup is shown. After wireless transmission, the received signals are downconverted to an intermediate-frequency (IF) of 29 GHz by means of two parallel balanced mixers and two 112 GHz electrical local oscillators. The downconverted signals are amplified and stored by a digital storage oscilloscope (DSO) with 65 GHz of bandwidth and 8 bits of vertical resolution, at a sampling rate of 160 GSa/s for further offline DSP. The main DSP receiver blocks include (Fig. 2(d)): carrier and phase recovery by a Costas loop, CAP matched filters, downsampling to construct symbol constellations, and equalization by means of a DFE.

IV. Experimental Results

To present the flexibility and capacity enhancement achieved by the proposed ISB modulation scheme, several CAP and MB-CAP signals are transmitted. Since ISB modulation makes each sideband independent from each other, to show our results clearly, we present four sets of results: bit error rates (BERs) of the LSB and USB for each polarization, i.e. X and Y.

In first transmissions, a 22 Gbaud CAP signal, i.e. 4 samples per symbol at 88 GSa/s, is allocated in both sidebands in both polarizations. By transmitting a QPSK symbol constellation in both sidebands in both polarizations, a total bitrate of 176 Gb/s is achieved. At the receiver side digital equalization is done by a DFE with 25 feedforward and 51 feedback T-spaced complex taps. In Fig. 4(a) is shown the measured BER versus wireless distance for a fixed SMF length of 25 km. At 20 cm the BER is below the 7% forward error correction (FEC) threshold of 3.8×10^{-3}, and up to 80 cm (only the USB) the BER is below the 20% FEC threshold of 2×10^{-2}. Keeping the same baudrate, by increasing drastically the DFE number of taps to 51 feedforward and 525 feedback taps, transmission of 16-QAM symbol constellation in both sidebands is possible reaching a total bitrate of 352 Gb/s. In Fig. 4(b) is shown the BER versus the wireless distance. At 20 cm the BER is below the 7% FEC threshold. Up to 60 cm, only the USB BER (for both polarizations) is below the 20% FEC threshold. In Fig. 4(c) is shown the measured BER versus the SMF length for a fixed wireless distance of 20 cm. For all SMF lengths, the received optical power at the input of the PDs is kept to 9 dBm by adjusting the EDFA gain before fiber transmission. Up to 50 km the BERs are below FEC thresholds, but for longer lengths, EDFA saturation degraded the performance of the system.

In further transmissions, a 2 band MB-CAP signal (11 Gbaud per band) is allocated in both sidebands in both polarizations. In Fig. 5(a) is shown the measured BER versus the aggregated bitrate of different symbol constellations per

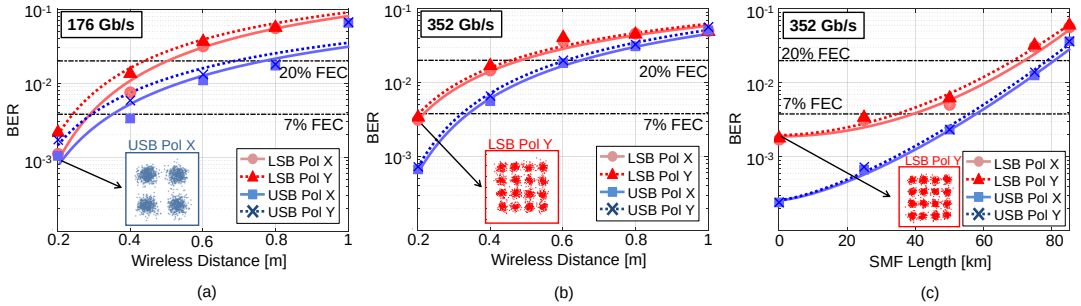

Fig 4. (a) 176 Gb/s transmission BER versus wireless distance, (b) 352 Gb/s transmission BER versus wireless distance, and (c) 352 Gb/s transmission BER versus SMF length.

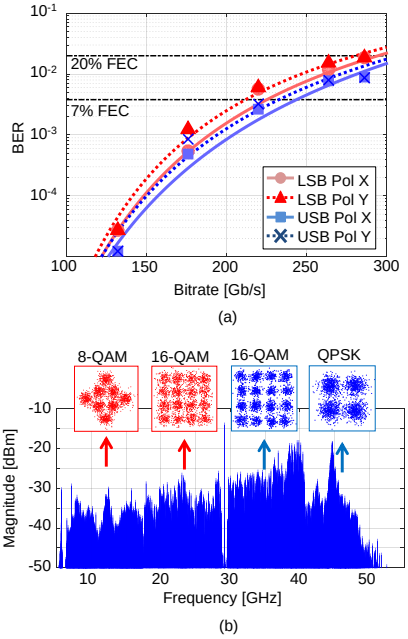

Fig. 5. (a) BER versus aggregated bitrate transmissions, (b) 286 Gb/s transmission IF signal electrical spectrum and received symbol constellations for X polarization.

band, for a fixed SMF length of 25 km and a fixed wireless distance of 20 cm. As it can be observed, up to 176 Gb/s is achieved with a BER below 7% FEC, whereas up to 286 Gb/s is achieved below 20% FEC threshold. As a sample case, in Fig. 5(b) is shown the 286 Gb/s transmission IF signal spectrum and the received symbol constellations for X polarization. The independence of each sideband can be clearly noted, as well as the uneven gain due the D-band EAs.

V. Discussion

We described the generation of ISB modulation signals and its experimental validation through fiber-wireless 2×2 MU-MIMO transmissions with total bitrates up to 352 Gb/s in the wireless D-band. These results were achieved by means of spectrally efficient modulation, PDM, and SPM, i.e. MU-MIMO. The main transmission impairments were the uneven gain of the D-band EAs producing different performances of both sidebands, the high FSPLs, and the optical I/Q imbalance, i.e. power and phase mismatch. Due the scarce and the experimental stage of mmWave D-band amplifiers, the wireless distance is limited up to 1 m. On the other hand, polarization and wireless crosstalk were not an issue as confirmed by the measured results. The BER of each sideband in both polarizations is practically the same, due to high polarization isolation (>25 dB) and the use of high directional HAs.

In our transmissions, the I/Q imbalance decreased the ISB modulation performance since the Hilbert transform requires,

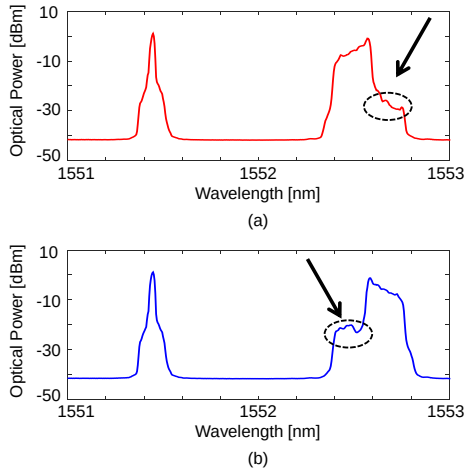

Fig. 6. (a) LSB imaging crosstalk and (b) USB imaging crosstalk due optical I/Q imbalance in 352 Gb/s transmission.

ideally, a perfect phase shift of $\pi/2$ between the I and Q components. Experimentally, this condition is difficult to always fulfill, therefore imaging crosstalk between the sidebands is eventually produced [23]. In Fig. 6 is shown the imaging effect in our 352 Gb/s transmission. By increasing the DFE number of feedback taps to 525, the I/Q imbalance was compensated and a BER below FEC threshold was achieved. This noticeable improvement is due I/Q correlation as reported in [27]. In the particular case of our 352 Gb/s transmission, although intentional decorrelation of the symbol sequences of each sideband was done during its generation and transmission, these signals are still correlated. This is due, first the PRBSs used for each side band were generated based on the same polynomial generator [27], and because the same symbol constellation is used in both sidebands. In Fig. 7(a) is shown a

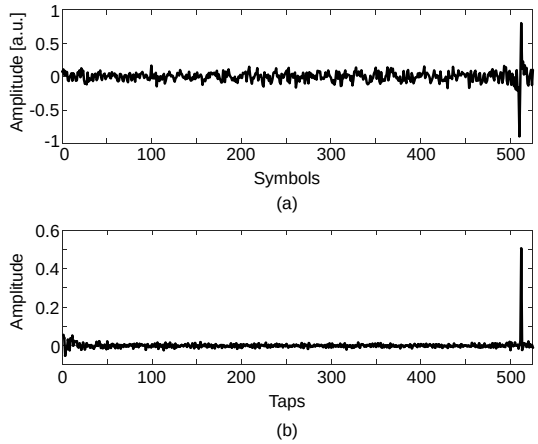

Fig. 7. 352 Gb/s transmission: (a) Cross-correlation of the received symbol sequences of each sideband, (b) real-part of DFE feedback T-spaced complex taps.

segment of the cross-correlation of the received symbol sequences of each sideband, where is visible a strong correlation just above 500 symbols. In Fig. 7(b) is shown the real-part of the DFE feedback complex taps. As expected, with 525 feedback taps was possible to compensate the imaging crosstalk due to I/Q correlation.

By means of proper I/Q imbalance compensation the equalization complexity can be greatly relaxed. In [9] we report W-band wireless transmissions, in which I/Q imbalance is reduced significantly to the extent that only 11 feedforward and 21 feedback DFE T-spaced complex taps are required to achieve BER below 7% FEC threshold. A net bitrate of 56.08 Gb/s over a wireless distance of 50 m is experimentally demonstrated.

VI. Conclusions

We experimentally demonstrated ultra-high capacity photonically-enabled D-band wireless transmissions up to 352 Gb/s. We proposed a scheme that by applying ISB modulation, the benefits of multiband modulation schemes can be maintained while achieving the same spectral efficiency of traditional single carrier QAM modulation. This experiment effectively bridges fiber-like capacity in the air using an untapped wireless frequency band. Furthermore, we show the flexibility and potential of mmWave communications systems, as a suitable solution for next generation small cell dense networks.

Although large tap count was necessary to achieve our results due I/Q correlation that is not present in real transmissions, further experiments show the feasibility of minimizing the imaging crosstalk and achieving high capacity transmissions, while relaxing the number of equalization taps to few tens [9].

References

[1] Cisco, "Cisco Visual Networking Index: Global Mobile Data Traffic Forecast Update, 2016–2021 White Paper," February 2017.

[2] J. G. Andrews, S. Buzzi, W. Choi, S. V Hanly, A. Lozano, A. C. K. Soong, and J. C. Zhang, "What Will 5G Be?," *IEEE J. Sel. Areas Commun.*, vol. 32, no. 6, pp. 1065–1082, 2014.

[3] A. Osseiran, F. Boccardi, V. Braun, K. Kusume, P. Marsch, M. Maternia, O. Queseth, M. Schellmann, H. Schotten, H. Taoka, H. Tullberg, M. A. Uusitalo, B. Timus, and M. Fallgren, "Scenarios for 5G mobile and wireless communications: the vision of the METIS project," *IEEE Commun. Mag.*, vol. 52, no. 5, pp. 26–35, 2014.

[4] F. Boccardi, R. W. Heath, A. Lozano, T. L. Marzetta, and P. P. Aalborg, "Five disruptive technology directions for 5G," *IEEE Commun. Mag*, pp. 74–80, 2014.

[5] P. Demestichas, A. Georgakopoulos, D. Karvounas, K. Tsagkaris, V. Stavroulaki, J. Lu, C. Xiong, and J. Yao, "5G on the Horizon: Key Challenges for the Radio-Access Network," *IEEE Veh. Technol. Mag.*, vol. 8, no. 3, pp. 47–53, Sep. 2013.

[6] R. Baldemair, T. Irnich, K. Balachandran, E. Dahlman, G. Mildh, Y. Selén, S. Parkvall, M. Meyer, and A. Osseiran, "Ultra-dense networks in millimeter-wave frequencies," *IEEE Commun. Mag.*, vol. 53, no. 1, pp. 202–208, 2015.

[7] N. Bhushan, J. Li, D. Malladi, R. Gilmore, D. Brenner, A. Damnjanovic, R. T. Sukhavasi, C. Patel, and S. Geirhofer, "Network densification: the dominant theme for wireless evolution into 5G," *IEEE Commun. Mag.*, vol. 52, no. 2, pp. 82–89, 2014.

[8] X. Li, J. Yu, K. Wang, Y. Xu, L. Chen, L. Zhao, and W. Zhou, "Bidirectional delivery of 54-Gbps 8QAM W-band signal and 32-Gbps 16QAM K-band signal over 20-km SMF-28 and 2500-m wireless distance," in *2017 Optical Fiber Communications Conference and Exhibition (OFC)*, 2017, pp. 1–3.

[9] R. Puerta, S. Rommel, J. J. V. Olmos, and I. T. Monroy, "Optically Generated Single Side-Band Radio-over-Fiber Transmission of 60Gbit/s over 50m at W-Band," in *Optical Fiber Communication Conference*, 2017, p. M3E.4.

[10] J. Xiao, J. Yu, X. Li, Y. Xu, Z. Zhang, and L. Chen, "20-Gb/s PDM-QPSK Signal Delivery over 1.7-km Wireless Distance at W-Band," in *Optical Fiber Communication Conference*, 2015, p. W4G.4.

[11] S. Rommel, S. Rodriguez, L. Chorchos, E. P. Grakhova, A. K. Sultanov, J. P. Turkiewicz, J. J. V Olmos, and I. T. Monroy, "225m Outdoor W-band radio-over-fiber link using an optical SFP+ module," in *2016 Optical Fiber Communications Conference and Exhibition (OFC)*, 2016, pp. 1–3.

[12] R. G. Stephen and R. Zhang, "Joint Millimeter-Wave Fronthaul and OFDMA Resource Allocation in Ultra-Dense CRAN," *IEEE Trans. Commun.*, vol. 65, no. 3, pp. 1411–1423, 2017.

[13] W. Roh, J. Y. Seol, J. Park, B. Lee, J. Lee, Y. Kim, J. Cho, K. Cheun, and F. Aryanfar, "Millimeter-wave beamforming as an enabling technology for 5G cellular communications: theoretical feasibility and prototype results," *IEEE Commun. Mag.*, vol. 52, no. 2, pp. 106–113, 2014.

[14] X. Pang, A. Caballero, A. Dogadaev, V. Arlunno, R. Borkowski, J. S. Pedersen, L. Deng, F. Karinou, F. Roubeau, D. Zibar, X. Yu, and I. T. Monroy, "100 Gbit/s hybrid optical fiber-wireless link in the W-band (75–110 GHz)," *Opt. Express*, vol. 19, no. 25, pp. 24944–24949, Dec. 2011.

[15] A. Stohr, B. Shih, S. Abraha, A. Steffan, and A. Ng'oma, "High Spectral-Efficient 512-QAM-OFDM 60 GHz CRoF System using a Coherent Photonic Mixer (CPX) and an RF Envelope Detector," in *Optical Fiber Communication Conference*, 2016, p. Tu3B.4.

[16] S. Rommel, R. Puerta, J. J. V. Olmos, and I. T. Monroy, "Capacity Enhancement for Hybrid Fiber-Wireless Channels with 46.8Gbit/s Wireless Multi-CAP Transmission over 50m at W-Band," in *Optical Fiber Communication Conference*, 2017, p. M3E.5.

[17] A. Batra, J. Balakrishnan, G. R. Aiello, J. R. Foerster, and A. Dabak, "Design of a multiband OFDM system for realistic UWB channel environments," *IEEE Trans. Microw. Theory Tech.*, vol. 52, no. 9, pp. 2123–2138, Sep. 2004.

[18] R. Puerta, S. Rommel, J. J. V Olmos, and I. T. Monroy, "Up to 35 Gbps ultra-wideband wireless data transmission links," in *2016 IEEE 27th Annual International Symposium on Personal, Indoor, and Mobile Radio Communications (PIMRC)*, 2016, pp. 1–5.

[19] M. I. Olmedo, T. Zuo, J. B. Jensen, Q. Zhong, X. Xu, S. Popov, and I. T. Monroy, "Multiband Carrierless Amplitude Phase Modulation for High Capacity Optical Data Links," *Light. Technol. J.*, vol. 32, no. 4, pp. 798–804, Feb. 2014.

[20] R. Puerta, M. Agustin, L. Chorchos, J. Tonski, J. R. Kropp, N. Ledentsov, V. A. Shchukin, N. N. Ledentsov, R. Henker, I. T. Monroy, J. J. V Olmos, and J. P. Turkiewicz, "Effective 100 Gb/s IM/DD 850-nm Multi- and Single-Mode VCSEL Transmission Through OM4 MMF," *J. Light. Technol.*, vol. 35, no. 3, pp. 423–429, Feb. 2017.

[21] Cisco, "802.11ac: The Fifth Generation of Wi-Fi, Technical White Paper," March 2014.

[22] J. Wei, Q. Cheng, D. G. Cunningham, R. V Penty, and I. H. White, "100-Gb/s Hybrid Multiband CAP/QAM Signal Transmission Over a Single Wavelength," *J. Light. Technol.*, vol. 33, no. 2, pp. 415–423, Jan. 2015.

[23] Y. Wang, J. Yu, H. C. Chien, X. Li, and N. Chi, "Transmission and Direct Detection of 300-Gbps DFT-S OFDM Signals Based on O-ISB Modulation with Joint Image-cancellation and Nonlinearity-mitigation," in *ECOC 2016; 42nd European Conference on Optical Communication*, 2016, pp. 1–3.

[24] L. Zhang, T. Zuo, Y. Mao, Q. Zhang, E. Zhou, G. N. Liu, and X. Xu, "Beyond 100-Gb/s Transmission Over 80-km SMF Using Direct-Detection SSB-DMT at C-Band," *J. Light. Technol.*, vol. 34, no. 2, pp. 723–729, Jan. 2016.

[25] C.-H. Ho, C.-T. Lin, Y.-H. Cheng, H.-T. Huang, C.-C. Wei, and S. Chi, "High spectral efficient W-band optical/wireless system employing Single-Sideband Single-Carrier Modulation," *Opt. Express*, vol. 22, no. 4, pp. 3911–3917, Feb. 2014.

[26] R. Puerta, J. Yu, X. Li, Y. Xu, J. J. V. Olmos, and I. T. Monroy, "Demonstration of 352 Gbit/s Photonically-enabled D-Band Wireless Delivery in one 2x2 MIMO System," in *Optical Fiber Communication Conference*, 2017, p. Tu3B.3.

[27] X. Zhou, L. E. Nelson, P. Magill, R. Isaac, B. Zhu, D. W. Peckham, P. I. Borel, and K. Carlson, "High Spectral Efficiency 400 Gb/s Transmission Using PDM Time-Domain Hybrid 32-64 QAM and Training-Assisted Carrier Recovery," *J. Light. Technol.*, vol. 31, no. 7, pp. 999–1005, Apr. 2013.

[28] S. Haykin and M. Moher, *Communications Systems*, 4th ed. New York: John Wiley & Sons Ltd, 2001.

[29] J. P. Costas, "Synchronous Communications," *Proc. IRE*, vol. 44, no. 12, pp. 1713–1718, Dec. 1956.

[30] Y. Wu, X. Wang, R. Citta, B. Ledoux, S. Lafleche, and B. Caron, "An ATSC DTV receiver with improved robustness to multipath and distributed transmission environments," IEEE Trans. Broadcast., vol. 50, no. 1, pp. 32–41, 2004.

[31] J. R. Treichler, I. Fijalkow, and C. R. Johnson, "Fractionally spaced equalizers," IEEE Signal Process. Mag., vol. 13, no. 3, pp. 65–81, 1996.

Paper 6: Optically Generated Single Side-Band Radio-over-Fiber Transmission of 60 Gbit/s over 50 m at W-Band

R. Puerta, S. Rommel, J. J. V. Olmos, and I. T. Monroy, "Optically Generated Single Side-Band Radio-over-Fiber Transmission of 60Gbit/s over 50m at W-Band," in *Optical Fiber Communication Conference*, 2017, p. M3E.4.

DOI: 10.1364/OFC.2017.M3E.4

Optically Generated Single Side-Band Radio-over-Fiber Transmission of 60Gbit/s over 50m at W-Band

Rafael Puerta[1*], Simon Rommel[1], Juan José Vegas Olmos[1], Idelfonso Tafur Monroy[1,2]

[1]*Department of Photonics Engineering, Technical University of Denmark, 2800 Kgs. Lyngby, Denmark*
[2]*ITMO University, St. Petersburg 197101, Russia*

[*]*rapur@fotonik.dtu.dk*

Abstract: 60 Gbit/s single side-band multi-band CAP radio-over-fiber transmission at W-band is demonstrated. A spectral efficiency of 3.8 bit/s/Hz and bit error rates below 3.8×10^{-3} are achieved after 50 m wireless transmission.

OCIS codes: (060.5625) Radio frequency photonics, (060.4080) Modulation, (060.4510) Optical communications.

1. Introduction

High-speed wide-band wireless communication systems have become a requirement in order to support the higher data rates required in wireless access and mobile front- and backhaul. This is driven by the rapid increase of data demands from cloud computing, multimedia applications on portable devices, and the internet of things (IoT). To cope with these demands, millimeter-wave (mm-wave) frequencies (30–300 GHz) offer the bandwidth available for appealing new broadband solutions [1]. Additionally, through mm-wave technology, wireless transmission can match speeds and bandwidths of fiber optic links, enabling integration with current optical networks [2–4].

In order to efficiently exploit the bandwidth available of mm-wave photonics-enabled links, advanced modulation schemes and digital signal processing (DSP) are required. Recently, carrierless amplitude phase modulation (CAP) and its multi-band approach (multi-CAP), have shown high spectral efficiency and flexibility to adjust to impairments from fiber optic and wireless links [4–6]. Further, by means of DSP, single side-band (SSB) modulation can be enabled, considerably increasing spectral efficiency. SSB W-band wireless links have been demonstrated up to 2 m [7, 8], relaxing hardware requirements compared to double side-band (DSB) transmissions of comparable spectral efficiency [9, 10].

In this paper we propose and experimentally demonstrate a 60 Gbit/s W-band wireless transmission employing multi-CAP modulation and the Hilbert transform to achieve SSB operation and effectively doubling spectral efficiency. Transmission was performed over 10 km standard single mode fiber (SMF) and 50 m wireless distance. With a multi-CAP signal of three bands and an overall width of 15.7 GHz, a spectral efficiency of 3.8 Bit/Hz and bit error rates (BER) below the limit for a commercial forward error correction (FEC) with 7 % overhead (OH) of 3.8×10^{-3} are achieved.

2. Experimental Setup

Figure 1 shows the experimental setup used for optical SSB signal generation, wireless transmission, and signal recovery. The output of a free running external cavity laser (ECL) at 1550 nm is used as input to a Mach-Zehnder modulator (MZM). By driving the modulator with a pure sinusoidal tone at 44 GHz, generated by a vector signal generator (VSG), the second harmonic of this tone is obtained at the output of the MZM. Thus, the generation of two optical signals with a separation of 88 GHz is achieved. An erbium doped fiber amplifier (EDFA) is used to amplify the signal, and an arrayed waveguide grating (AWGG) separates the two optical lines to enable the modulation of one thereof.

The data signal is generated by an arbitrary waveform generator (AWG) at a sampling rate of 60 GSa/s. Optical SSB modulation is achieved by means of a single optical I/Q modulator. By applying the Hilbert transform to the original multi-CAP signal, the in-phase (I) and quadrature (Q) components to drive the modulator are generated, removing the upper side-band (USB) as shown in the inset of Fig. 1. The I and Q components are amplified with driver amplifiers to obtain suitable voltage magnitudes to drive the I/Q modulator. A variable optical attenuator (VOA) is used to set equal power in both the unmodulated and modulated optical signals and an optical coupler combines the two. A second EDFA and a second VOA are employed to set the launch power into the 10 km SMF. After fiber transmission, a high speed photodiode (PD) converts the optical signal to the electrical domain, where the signal is boosted by a 10 dB medium power amplifier (MPA) before wireless transmission over 50 m.

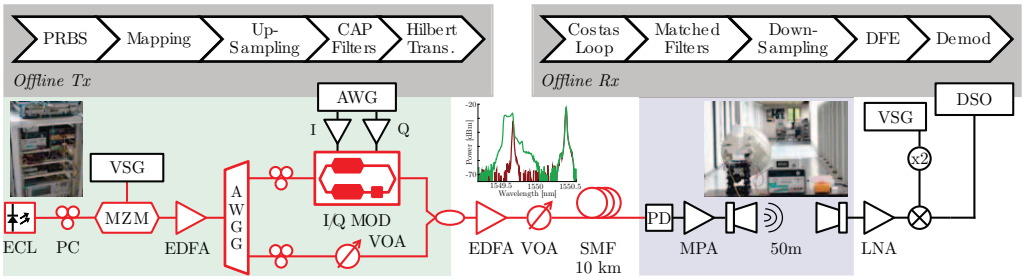

Fig. 1. Schematic of the experimental setup and offline DSP at the transmitter and receiver; photographs of optical signal generation and radio transmission setups; inset: SSB optical spectrum.

Table 1. Multi-CAP signal parameters for transmission of 60 Gbit/s in three bands.

Band	1	2	3
Symbol rate [GBd]	5	5	5
Constellation	16-QAM	16-QAM	16-QAM
Bit rate [Gbit/s]	20	20	20
Power loading [dB]	0	1	3

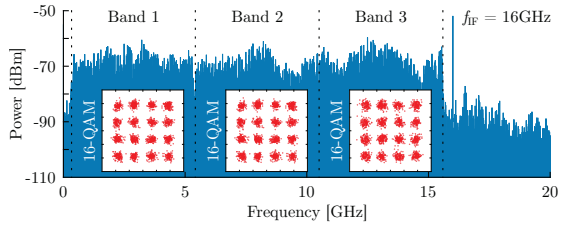

Fig. 2. Signal spectrum after downconversion to f_{IF} and received constellations after equalization for $P_{opt} = 3$ dBm.

A pair of parabolic antennas, with 48 dBi gain each, is used for wireless transmission. At the receiver, the transmitted signal is amplified by a 20 dB low noise amplifier (LNA). Heterodyne downconversion is performed by a balanced mixer to an intermediate frequency (IF) of 16 GHz. The mixer is driven by a 72 GHz local oscillator (LO) generated by a passive frequency doubler with a pure sinusoid of 36 GHz from a second VSG. The IF signal was recorded on a digital storage oscilloscope (DSO) at a sampling rate of 80 GSa/s for offline DSP.

3. Single-Sideband Multi-CAP Signal Generation and Processing

In order to mitigate channel unevenness and maximize data rate, a multi-CAP signal with three bands, each with a baudrate of 5 Gbaud, is generated offline. For each band, pseudo-random bit sequences (PRBSs) of length 2^{11}-1 are mapped into 16-QAM symbol sequences, which are up-sampled and filtered by the corresponding orthogonal CAP filters. By means of power loading a BER below FEC threshold is ensured for each band. The Hilbert transform is applied to the generated multi-CAP signal for SSB operation, doubling transmission spectral efficiency. The offline transmitter is shown in Fig. 1 alongside the corresponding offline receiver, while Table 1 gives the multi-CAP parameters.

The IF signal that was recovered from the DSO is resampled, before carrier recovery and donconversion with a Costas loop. Orthogonal CAP matched filters retrieve the symbol sequences of each band and a decision feedback equalizer (DFE) with 11 feed forward and 21 feed back tap mitigates impairments from the transmission channel and device imperfections. After demodulation, error vector magnitude (EVM) and BER are estimated separately for each band by error counting with at least 0.23 Mbit analyzed per band.

4. Transmission Results and Discussion

Performance evaluation of the optically generated 60 Gbit/s SSB multi-CAP RoF transmission is performed after 50 m W-band wireless and downconversion to IF. The received spectrum is shown in Fig. 2, clearly confirming successful SSB transmission and showing the IF carrier at 16 GHz; insets show recovered constellations after equalization.

Observed BER after transmission is shown in Fig. 3 for optical powers on the PD of –0.5–6.5 dBm, showing a minimum around 3 dBm; Table 2 gives corresponding BER and EVM. Despite the use of power loading, significant differences in BER are observed between the bands, with the second band showing worst performance. Nevertheless, all bands achieve a BER below the limit of 3.8×10^{-3} for a standard commercial FEC with only 7 % overhead.

The BER performance of the system clearly suggests a power limited regime at the lower powers, while at higher

Table 2. BER and EVM for the 60 Gbit/s SSB multi-CAP signal after 50 m wireless transmission with $P_{opt} = 3$ dBm.

Band	1	2	3
BER	8.9×10^{-4}	3.5×10^{-3}	1.9×10^{-3}
EVM	13.6 %	14.9 %	14.9 %

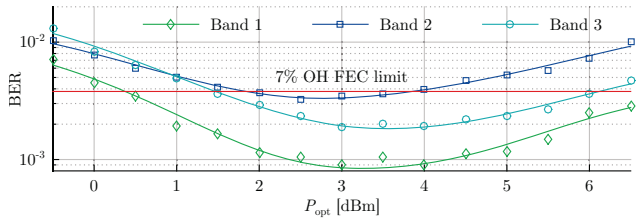

Fig. 3. BER over optical power on the PD after 50 m W-band transmission of 60 Gbit/s SSB multi-CAP.

powers BER performance is degraded due to saturation of the receiving LNA. The availability of an additional 3.5 dB optical power beyond the optimum observed, together with receiver amplifier saturation, suggests a significant extension of transmission distance to as much as 100 m to be possible [2]; this could however not be tested due to laboratory space restrictions.

From the IF spectrum in Fig. 2 the spectral efficiency of the system is easily calculated. With a symbol rate of 5 GBd in each multi-CAP band and guard bands of only 2 %, the signal occupies only 15.3 GHz of spectrum and thus—with an additional gap of 400 MHz to the carrier—the overall system requires only 15.7 GHz of RF bandwidth. This results in a spectral efficiency of 3.8 bit/Hz for a single polarization, single carrier and single input single output system. To the best of the authors' knowledge this is the first time SSB transmission at W-band has been demonstrated over distances beyond 2 m, outperforming previous demonstrations in both data rate and wireless distance [7, 8].

5. Conclusions

Transmission of a 60 Gbit/s SSB multi-CAP signal over 10 km SMF and a wireless distance of 50 m is successfully demonstrated with a BER below the limit for a FEC with 7 % overhead. Optical SSB generation by means of the Hilbert transform and a single I/Q modulator is exploited to achieve a spectral efficiency of 3.8 Bit/Hz in both the optical and wireless transmission. To the best of the authors' knowledge, this the first demonstration of SSB transmission in W-band over significant wireless distances.

Acknowledgments

R. Puerta thanks the Colombian Administrative Department of Science, Technology and Innovation (COLCIENCIAS) for partly funding his research. This work was partly funded by the DFF FTP mmW-SPRAWL project. The authors thank Keysight Technologies for providing access to the AWG.

References

[1] C. Dehos *et al.*, "Millimeter-Wave Access and Backhauling: The Solution to the Exponential Data Traffic Increase in 5G Mobile Communications Systems?," IEEE Commun. Mag. **52**, pp. 88–95 (2014).
[2] S. Rommel *et al.*, "Outdoor W-Band Hybrid Photonic Wireless Link Based on an Optical SFP+ Module," IEEE Photon. Technol. Lett. **28**, pp. 2303–2306 (2016).
[3] L. Cavalcante *et al.*, "On the capacity of radio-over-fiber links at the W-band," Opt. Quant. Electron. **48** (2016).
[4] J. Zhang *et al.*, "Experimental demonstration of 24-Gb/s CAP-64QAM radio-over-fiber system over 40-GHz mm-wave fiber-wireless transmission," Opt. Express **21**, pp. 26888–26895 (2013).
[5] R. Puerta *et al.*, "Up to 35 Gbps Ultra-Wideband Wireless Data Transmission Links," in *Proc. PIMRC 2016*, paper WeD7.2 (2016).
[6] R. Puerta *et al.*, "107.5 Gb/s 850 nm multi- and single-mode VCSEL transmission over 10 and 100 m of multimode fiber," in *Proc. OFC 2016*, paper Th5B.5 (2016).
[7] X. Li, Y. Xu and J. Yu, "Single-sideband W-band photonic vector millimeter-wave signal generation by one single I/Q modulator," Opt. Lett. **41**, pp. 4165–4165 (2016).
[8] C. Ho *et al.*, "High spectral efficient W-band optical/wireless system employing Single-Sideband Single-Carrier Modulation," Opt. Express **22**, pp. 3911–3917 (2016).
[9] A. Stöhr *et al.*, "High Spectral-Efficient 512-QAM-OFDM 60 GHz CRoF System using a Coherent Photonic Mixer (CPX) and an RF Envelope Detector," in *Proc. OFC 2016*, paper Tu3B.4 (2016).
[10] M. Xu *et al.*, "Multiband OQAM CAP modulation in MMW RoF systems with enhanced spectral and computational efficiency," in *Proc. OFC 2016*, paper Tu3B.3 (2016).

Paper 7: Demonstration of 352 Gbit/s Photonically-enabled D-Band Wireless Delivery in one 2×2 MIMO System

R. Puerta, J. Yu, X. Li, Y. Xu, J. J. V. Olmos, and I. T. Monroy, "Demonstration of 352 Gbit/s Photonically-enabled D-Band Wireless Delivery in one 2×2 MIMO System," in *Optical Fiber Communication Conference*, 2017, p. Tu3B.3.

DOI: 10.1364/OFC.2017.Tu3B.3

Demonstration of 352 Gbit/s Photonically-enabled D-Band Wireless Delivery in one 2x2 MIMO System

Rafael Puerta[1,*], Jianjun Yu[2,3], Xinying Li[2,3], Yuming Xu[3], J.J. Vegas Olmos[1] and I. Tafur Monroy[1,4]
[1]*Dpt. Photonics Engineering, Technical University of Denmark (DTU), Akademivej Building 358, 2800 Kgs. Lyngby, Denmark*
[2]*ZTE (TX) Inc., NJ 07960, USA*
[3]*MoE, Fudan University, Shanghai 200433, China*
[4]*ITMO University, St. Petersburg 197101, Russia*
*E-mail: *rapur@fotonik.dtu.dk, yu.jianjun@ztetx.com*

Abstract: First demonstration of photonically-enabled independent side-bands D-Band wireless transmission up to 352 Gbit/s with a BER below $3.8x10^{-3}$. These results were achieved by means of advanced DSP and antenna polarization multiplexing (2x2 MIMO).
OCIS codes: (060.4510) Optical communications; (060.5625) Radio frequency photonics

1. Introduction

Broadband wireless communications systems are essential as higher transmission speeds are needed in access, local area and in-building networks. Furthermore, novel low-latency high capacity scenarios require wireless systems seamlessly integrated with fiber-like capacity [1–4] (e.g. high-performance computing, short reach wireless rack-to-rack interconnections, and mobile fronthaul).

Millimeter-wave (mm-wave) communications systems (30–300 GHz) can provide larger bandwidths, unlike conventional narrow frequency bands which are overcrowded with current radio services. Furthermore, mm-wave bands offer enough bandwidth able to support fiber-like capacity and integration with upcoming 400 Gbit/s systems. Recently, enabled by the rapid development of electronics and radio-over-fiber (RoF) technology, vast research on mm-wave wireless systems has been made. To increase wireless data rates, very complex multi-carrier MIMO systems, combining the bandwidth available from the K_a-band to the W-band (26.5–110 GHz), have been proposed [1,2]. By employing spatial multiplexing 2x2 MIMO, maximum bitrates up to 224 Gbit/s have been reported. Research efforts are now moving to colonize even higher frequency bands: work in the D-band (110–170 GHz) achieving bitrates up to 60Gbit/s over a wireless distance of 0.4 m have been reported [3,4]. Also, the first demonstration of a D-band 2x2 MIMO optical-wireless system, with a bitrate up to 32 Gbit/s, was presented recently [4]. However, these demonstrations fall short on exploiting the large bandwidth of the D-band.

Only through the use of photonic technologies, advanced modulation formats and digital signal processing (DSP) from optics, the bandwidth available in wireless bands can be exploited. In this experiment, we employed carrierless amplitude phase (CAP) modulation and its multi-band approach (MultiCAP) in order to use the bandwidth efficiently and to be able to mitigate the unevenness of the channel frequency response [5]. Additionally, through DSP we applied the Hilbert transform to the transmitted signal, and by using an optical I/Q modulator, we enabled the independent operation of the side-bands of the optical carrier and consequently double the spectral efficiency [6].

In this paper, we propose and experimentally validate an optical independent side-bands (O-ISB) RoF system, with optical up-conversion to the D-Band with a resulting carrier frequency of 141 GHz and a bitrate up to 352 Gbit/s in the air. To the best of our knowledge, this is the photonics-aided wireless transmission with the highest bitrate ever achieved with a single carrier and dual polarization (2x2 MIMO) in any mm-wave wireless frequency band (e.g. V-, W-, and D-Band).

2. Experimental Setup and DSP

Fig. 1(a) shows the procedure to generate the transmitted signal: pseudo-random binary sequences (PRBSs) of length 2^{11}-1 were mapped into the corresponding symbol constellations. Resulting symbol sequences were up-sampled and CAP modulation in-phase (I) and quadrature (Q) components were generated by means of its signature orthogonal filters. Next, by applying the Hilbert transform, the resulting lower side-band (LSB) and upper side-band (USB) were made independent from each other when modulating the optical carrier. The laser source used was a free-running external cavity laser (ECL1), with a linewidth <100kHz and 13 dBm output power, which was modulated with an optical I/Q modulator. An 88 GSa/s digital to analog converter (DAC), with 22 GHz electrical bandwidth, was loaded with the independent side-bands signal and was used to drive the I/Q modulator. The generated O-ISB signal was amplified with an erbium-doped fiber amplifier (EDFA). After amplification, polarization division multiplexing (PDM) stage was done by splitting the output of the I/Q amplifier with a polarization-maintaining optical coupler (OC), adding a delay line to decorrelate each polarization, and combining

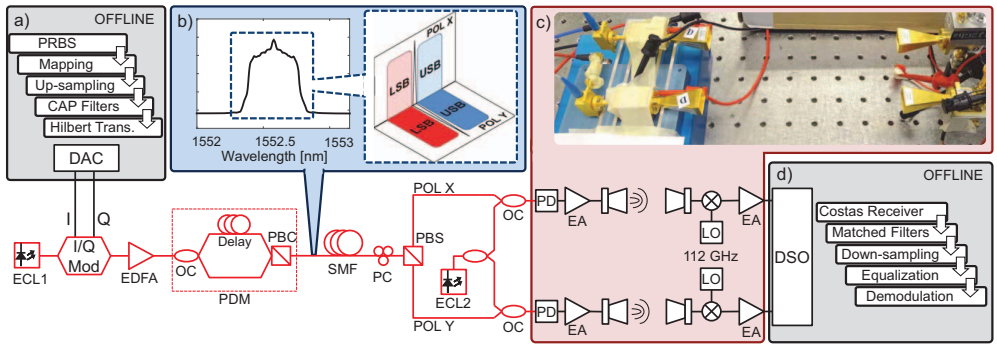

Fig. 1. O-ISB RoF system experimental setup.

both polarizations again with a polarization beam combiner (PBC). After PDM stage, the optical signal was transmitted over 25 km of standard single-mode fiber (SMF). Fig. 1(b) illustrates each polarization with its corresponding independent side-bands. Prior to wireless generation, each polarization was retrieved by a polarization beam splitter (PBS). A second ECL2 was used as optical local oscillator, with 141 GHz frequency spacing relatively to the ECL1 transmitted signal, thus generating a D-Band mm-wave wireless carrier through heterodyning at the photodiodes (PDs). In Fig. 2(a) is shown the comparison of the optical spectra of a signal with 22 Gbaud per side-band, when transmitting only the LSB, when transmitting only the USB, and when transmitting both side bands, respectively.

The generated mm-wave signals from each polarization, were first amplified by 15 dB gain D-Band electrical amplifiers (EAs) and then transmitted wirelessly by a pair of 25 dBi gain horn antennas (HAs). In Fig 1(c) the 2x2 MIMO antenna setup is shown. After wireless transmission, the received signals were down-converted to an intermediate-frequency (IF) of 29 GHz by means of two parallel balanced mixers and two 112 GHz local oscillators. The down-converted signals were amplified and stored with a 65 GHz digital storage oscilloscope (DSO) at a sampling rate of 160 GSa/s for further offline DSP, which included (Fig. 1(d)): carrier and phase recovery by a Costas loop, CAP matched filters, down sampling to construct the symbol constellations, and decision feed-back equalization (DFE).

3. Experimental Results

Since O-ISB makes each side-band independent from each other, in this section we present four sets of results: bit error rates (BERs) of the LSB and USB for each polarization (X and Y). We first investigated the transmission system based on low number of taps of the equalizer (176 Gbit/s). Then the transmission data rate is maximized by increasing the number of taps (352 Gbit/s).

Fig. 2(b) shows the measured BER versus wireless distance for a 176 Gbit/s transmission with a fixed SMF length of 25 km (i.e. QPSK at 22 Gbaud per side-band in each polarization). At 20 cm the BER was below the 7% forward error correction (FEC) threshold of $3.8\text{x}10^{-3}$, and up to 80 cm (only the USB) the BER was below the 20% FEC threshold of $2\text{x}10^{-2}$. Fig. 2(c) shows the measured BER versus the aggregated bitrate, for a fixed SMF length of

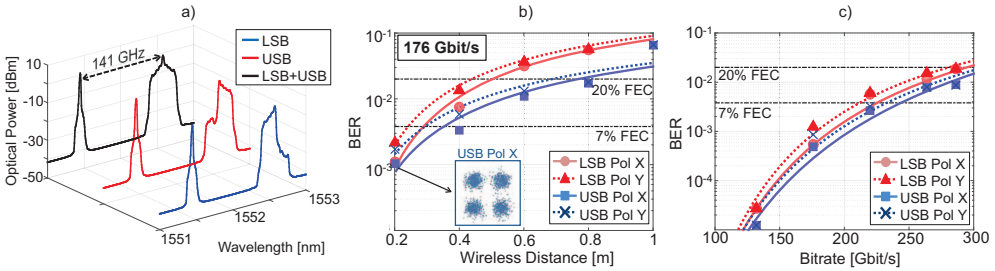

Fig. 2. a) Comparison of optical spectra for a transmission of 22 Gbaud per side-band, b) 176 Gbit/s transmission BER versus wireless distance, and c) BER versus bitrate.

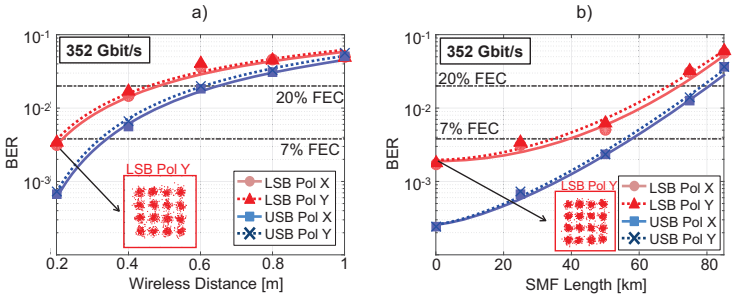

Fig. 3. a) 352 Gbit/s transmission BER versus wireless distance, and b) 352 Gbit/s transmission BER versus SMF length.

25 km and fixed wireless distance of 20 cm. As it can be observed, up to 176 Gbit/s is achieved with BER below 7% FEC, whereas up to 286 Gbit/s is achieved below 20% FEC threshold.

In order to increase the robustness of the system, the number of taps in the DFE was increased. This enabled transmissions up to 352 Gbit/s below FEC thresholds (i.e. 16-CAP at 22 Gbaud per side-band in each polarization). Fig. 3(a) shows the BER versus the wireless distance for the 352 Gbit/s transmission by using a long-tap equalizer. At 20 cm the BER was below the 7% FEC threshold. Up to 60 cm, only the USB BER (for both polarizations) was below the 20% FEC threshold. In Fig. 3(b) is shown the measured BER versus the SMF length for affixed wireless distance of 20 cm. For all SMF lengths, the received optical power of the PDs was kept to 9 dBm by increasing the EDFA gain. Up to 50 km the BERs were below FEC thresholds, but for longer lengths, the EDFA was already in its saturated range worsening the performance of the system.

4. Discussion

We described the first demonstration of 352 Gbit/s operating entirely in the D-band (i.e. carrier frequency 141 GHz) using a 2x2 MIMO system enabled by photonic technologies. These results were achieved by means of MultiCAP modulation. The main transmission impairments were the uneven gain of both side-bands of the wireless carrier and the imbalance characteristics of the I/Q modulator (i.e. power and time delay). Polarization and wireless crosstalk were not noticeable as shown in the measured results, where both polarizations practically have the same BER results (i.e. polarization isolation >25 dB and high directional antennas were used). The system performance was limited by free-space losses, which can be overcome by increasing the power budget through amplification. To increase the capacity, we used large tap counts at the DFE [1,7]. Thus, we obtained BERs below FEC performance at 176 Gbit/s and 352 Gbit/s (i.e. QPSK and 16 CAP, respectively).

5. Conclusion

We experimentally demonstrated the highest photonically-enabled wireless transmission in the D-band. For the first time, only with two transmitter antennas, single-carrier, and dual polarization a bitrate up to 352 Gbit/s was transmitted and recovered below FEC threshold. This experiment effectively bridges fiber-like capacity in the air using an untapped wireless frequency band.

6. Acknowledgements

R. Puerta thanks the Colombian Department of Science, Technology and Innovation for supporting his research.

7. References

[1] J. Yu *et al.*, "432-Gb/s PDM-16QAM signal wireless delivery at W-band using optical and antenna polarization multiplexing," Proc. ECOC 2014, Cannes, France, We.3.6.6.

[2] X. Li *et al.*, "A 400G optical wireless integration delivery system," *Opt. Express*, **21**(16), 18812–18819 (2013).

[3] I. Ando *et al.*, "Wireless D-band communication up to 60 Gbit/s with 64QAM using GaAs HEMT technology," *IEEE Radio and Wireless Symposium (RWS) 2016*, 193–195.

[4] X. Li *et al.*, "A 2×2 MIMO optical wireless system at D-band," *Proc. OFC 2015*, Los Angeles, CA, Th4A.7.

[5] R. Puerta *et al.*, "107.5 Gb/s 850 nm multi- and single-mode VCSEL transmission over 10 and 100 m of multi-mode fiber," *Proc. OFC 2016*, Anaheim, CA, PDP Th5B.5.

[6] H.-C. Chien *et al.*, "Optical independent-sideband modulation for bandwidth-economic coherent transmission," *Opt. Express.*, **22**(8), 9465–9470 (2014).

[7] X. Zhou *et al.*, "High Spectral Efficiency 400 Gb/s Transmission Using PDM Time-Domain Hybrid 32 64 QAM and Training-Assisted Carrier Recovery," *J. Light. Technol.*, **31**(7), 999–1005 (2013).

Paper 8: Ultra Wideband Technology Comeback: Prospective Solution for 5G Next Generation Networks

R. Puerta, S. Rommel, J. J. V. Olmos, and I. T. Monroy, "Ultra Wideband Technology Comeback: Prospective Solution for 5G Next Generation Networks," submitted to *IEEE Commun. Mag.*, Apr. 2017.

DOI: -

Ultra Wideband Technology Comeback: Prospective Solution for 5G Next Generation Networks

Rafael Puerta, Simon Rommel, Juan José Vegas Olmos, and Idelfonso Tafur Monroy

***Abstract*—Extensive research is being performed to establish the technologies and standards for the upcoming fifth generation (5G) of wireless communication systems. Some of the most challenging requirements of 5G systems, compared to its predecessor, are to increase the spectral efficiency by a factor of 10 and to increase the capacity by a factor of 1000 of current systems. The rapid evolution of internet of things (IoT) applications and devices has triggered a drastic increase in its number and variety. New technologies must offer an adequate framework for the IoT, which will enable higher capacities and the flexibility to adapt to dynamic scenarios. In order to cope with these challenging demands, a compelling approach is to exploit the current radio services bands by means of spectrum sharing and cooperation techniques, which alleviate the bandwidth requirements of next generation communication systems. In addition, advanced modulation schemes have a fundamental role in ensuring the best usage of the spectrum available in bandlimited systems. In this article, we present ultra wideband (UWB) technology as a prospective solution for upcoming 5G networks. Its main feature is its capability to operate simultaneously, without introducing interference, with current radio services on an unlicensed basis. We report experimental results reaching data rates up to 35 Gbit/s using the multiband approach of carrierless amplitude phase (MB-CAP) modulation. To validate the versatility of the proposed system, our experimental tests were performed under the UWB regulations established by the United States Federal Communications Commission (FCC), the European Electronic Communications Committee (ECC), and the Russian State Committee for Radio Frequencies (SCRF). The regulations chosen provide diversity enough to demonstrate the capacity of MB-CAP modulation to comply with worldwide regulations.**

***Index Terms*—5G communication systems, ultra wideband technology, multiband carrierless amplitude phase modulation.**

I. Introduction

Global mobile data traffic has increased 4000-fold over the last decade, and is forecast to continue growing, with nearly a sevenfold increase predicted between 2016 and 2021 [1]. The increasing demands for ubiquitous access to information and entertainment at higher data rates is one of the main challenges of future 5G communication systems. Users are expecting wireless communications to reach the capacity of wired communications. Therefore, flexible wireless systems reaching multi-gigabit data rates are fundamental for next generation communication systems.

Manuscript received April xx, 2017; revised xx; accepted xx. R. Puerta would like to express his gratitude to the Colombian Administrative Department of Science, Technology and Innovation (COLCIENCIAS) for supporting his research. This work was partly funded by the DFF FTP mmW-SPRAWL project.

R. Puerta, S. Rommel, J. J. Vegas Olmos, and I. Tafur Monroy are with the Department of Photonics Engineering, Technical University of Denmark, 2800 Kgs. Lyngby, Denmark, e-mail: rapur@fotonik.dtu.dk.

The accelerated growth of mobile and cloud applications, the fast development of the internet of things (IoT) and machine-to-machine (M2M) technologies, the massive adoption of mobile connectivity by end users, and the need for an optimal management of the bandwidth available are driving the development of new technologies and approaches to cope with these new demands [1]–[4]. An attractive and straightforward approach to effectively increase the network capacity is to decrease the size of the network cells, e.g. by introducing pico- and femtocells, establishing more active nodes and thus increasing the spectral efficiency per unit area [4]. This approach is consistent with current trends which are focusing on implementing a suitable framework for the IoT.

Offload traffic, which is generated when users switches from cellular networks to Wi-Fi or small cell networks, is growing considerably. For the first time in 2015, mobile offload traffic exceeded cellular traffic [1]. This is due to a great part of the mobile data activity taking place indoors within users' homes, offices and the like, i.e. while connected to Wi-Fi access points or operator-owned femtocells and picocells. As a consequence, traffic generated by mobile and portable devices is offloaded from mobile networks, which demands denser networks with more fixed access nodes [1].

In this context of small cells and short range wireless communications, ultra-wideband (UWB) technology is a promising alternative which can exploit large bandwidths and has the potential of achieving high-capacity wireless transmissions. It can enable from diverse IoT services to high-speed wireless personal area networks (WPANs), where conventional computing and portable devices exchange large amounts of data. The main features of UWB technology are its capacity to allow unlicensed operation if regulatory conditions are fulfilled [5]–[7], provision of very large bandwidths, and its ability to coexist with current narrowband wireless communications systems, e.g. Wi-Fi, WiMAX [8]. Another appealing alternative for 5G networks is millimeter-Wave (mmWave) technology which provides a larger bandwidth, i.e. 30–300 GHz, and therefore the potential of higher capacities. Although extensive research is being performed on mmWave wireless systems, the complexity and cost of these systems are still high compared to conventional microwave solutions. This is mainly due the scarce and expensive electronics operating at these frequencies, and the strong propagation impairments of millimeter waves such as high free-space path loss (FSPL), atmospheric and rain absorptions, and poor penetration through objects [3], [4]. In addition, mobile communications using this spectrum range are still under standardization.

Although large bandwidths are needed to achieve high data

rates, advanced modulation schemes are essential to optimize the usage of these bandwidths by increasing the spectral efficiency. New solutions are highly likely to replace classic spectrally inefficient pulse-based systems by more advanced and flexible modulation schemes. In addition, to optimize the management of large bandwidths, multiband schemes provide the flexibility to split these bandwidths into several bands and adjust them independently. Thus, depending on the number of bands, the modulation scheme and baud rate of each band, as well as the forward error correction (FEC) used, a wide range of data rates can be achieved under diverse and varying channel conditions.

Multiband orthogonal frequency division multiplexing (MB-OFDM) is the most popular multiband scheme for UWB communications systems. First, it was adopted by the WiMedia Alliance (no longer operating) as a standard, and then adopted by the Wireless USB Promoter Group to support high-speed wireless connections, ensuring USB-like user experience. Following FCC regulations, WiMedia's last physical layer (PHY) specification [9], specified the usage of the frequency range between 3.1 GHz and 10.6 GHz reaching date rates up to 1024 Mbit/s, supporting transmissions of 480 Mbit/s over distances up to 3 m and 110 Mbit/s up to 10 m. The MB-OFDM scheme is suitable for wireless communications since it can alleviate the effects of multipath propagation, however MB-OFDM implementation faces some challenges which increase its complexity. The most notorious are the distortion generated due the high peak-to-average power ratio (PAPR) which stresses the limited linear range of power amplifiers, and the time and frequency synchronization relying on the addition of pilot tones or pilot symbols to the signal [10].

Carrierless amplitude phase (CAP) modulation is a variation of quadrature amplitude modulation (QAM) modulation, in which, instead of modulating the amplitude of a sine and a cosine carrier of the same frequency, modulation and demodulation is achieved by means of two orthogonal filters. In complexity terms, both QAM and CAP are similar, however CAP modulation provides higher spectral efficiencies by using special pulse shaping functions, and as a result of the accelerated development of high-speed electronics, CAP modulation implementation can be completely digital, reducing its complexity. Given the advantages of CAP modulation, its multiband approach (MB-CAP) was developed and first introduced for fiber-optic links [11], demonstrating its flexibility to adapt to the large bandwidths of optical links, while achieving record data rates. In addition, MB-CAP modulation has better features than MB-OFDM, such as a lower PAPR, alleviating the restrictions on the operation range of electrical amplifiers, and a lower computational complexity in its implementation [11]. Thus, the flexible nature of MB-CAP modulation is highly suitable for UWB wireless communications systems, allowing to adjust the power and bandwidth used to comply with a variety of current regulatory UWB standards [5]–[7].

In this article, we propose the inherently low power UWB technology as a prospective solution for 5G next generation networks, which is able to provide ultra high-speed links and large bandwidths suitable for small cell wireless communications and future IoT applications and devices. We use, for the first time, MB-CAP modulation for wireless transmissions exploiting the large bandwidths defined by UWB regulations, supporting data rates from multiple gigabits per second to hundreds of megabits per second. We experimentally validate the capacity of the proposed solution. Wireless transmissions with a total data rate of 10 Gbit/s were performed in compliance with the regulations established by the United States FCC, the European ECC, and the Russian SCRF. The maximum wireless distances achieved were 3.5 m, 2 m, and 1.3 m, respectively [12]. In further experiments, for a set of wireless distances ranging from 0.5 m to 9 m, we experimentally demonstrate transmission data rates up to 35.1 Gbit/s and 21.6 Gbit/s complying with the FCC and ECC regulations, respectively [13]. In all cases, the mentioned bit rates were achieved with bit error rates (BERs) below the commercial 7% overhead forward error correction (FEC) limit of 3.8×10^{-3}.

This article is structured as follows: section II discusses UWB technology regulations worldwide, regarding maximum power and bandwidth values permitted, and the principle of operation of MB-CAP modulation. Section III describes the experimental setup and the digital signal processing (DSP) used for validation of the proposed solution, while section IV shows the obtained experimental results. Finally section V summarizes and concludes the paper with remarks regarding current challenges and future work.

II. Framework

This section provides a short discussion of current UWB regulations and a brief description of MB-CAP modulation.

A. Ultra Wide-Band Regulations

The part of the spectrum allocated for current microwave radio services such as cellular and Wi-Fi networks, fixed and mobile-satellite services, global positioning systems, among others, is saturated and requires expensive licenses to access. To maximize the capacity of the bandwidth used by these services, worldwide regulatory agencies established regulations enabling to share a wide range of frequency bands of this bandwidth on an unlicensed basis. To avoid adding interference to current services, these regulations impose strict limits on the radiated power spectral density over a set of frequency bands. Thus, traditional narrowband receivers perceive UWB emissions as ordinary noise [14].

The United States FCC was the first agency to establish an UWB spectral emission mask for indoors applications. It consists of a single flat window with a permitted average effective isotropic radiated power (EIRP) of, at most, -41.3 dBm/MHz for the frequency range between 3.1 GHz and 10.6 GHz [5]. For Europe, the ECC established a spectral emission mask with the same maximum permitted EIRP, but, unlike the FCC regulation, a gap in the mask defines two main windows with frequency ranges between 3.1–4.8 GHz and 6–9 GHz [6]. For Russia, the SCRF established an even more stringent regulation by defining three main windows segmented as follows: 3.950–4.425 GHz, 4.425–5.470 GHz, 6.000–8.100 GHz, 8.625–9.150 GHz, and 9.150–10.600 GHz, with maximum EIRP values of -54.5, -50.0, -47.0, -47.0, and

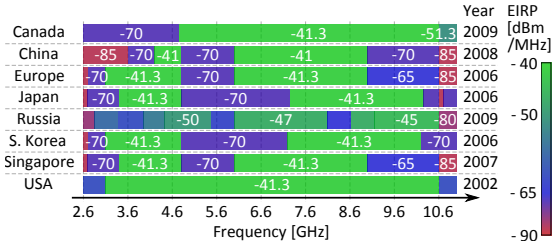

Fig. 1. Comparison of main UWB regulations worldwide.

-45.0 dBm/MHz, respectively [7]. The segmentation of the European and Russian regulations imposes a much greater challenge on the generation of UWB signals to achieve high data rates. The definition of these regulations makes UWB technology inherently a low-power solution. Assuming the usage of the whole bandwidth at maximum radiated power defined by the FCC regulation, which is the most generous regulation in terms of power and bandwidth, the total radiated power is only 0.55 mW [14].

The FCC regulation allows UWB devices to operate simultaneously with licensed users as long as the EIRP levels are within the permitted values. In Europe, the ECC regulation is more conservative to further mitigate potential interference. For some bands, additional protection mechanisms are required such as detect and avoid (DAA) and low duty cycle (LDC) [6]. The main goal of our work is to show the full potential of UWB communications systems in terms of capacity. Therefore, these protection mechanisms are outside of the scope of our tests and are left to further research.

To corroborate the potential of UWB technology to operate worldwide, Fig. 1 shows worldwide regulations with their corresponding values of maximum EIRP permitted within different bands, alongside the year in which they were established.

B. Multi-Band Carrierless Amplitude Phase Modulation

CAP is a scheme that, like quadrature amplitude modulation (QAM), transmits two streams of data separately by means of two orthogonal signals, namely the in-phase (I) and quadrature (Q) components. A distinctive feature of CAP modulation is the use of a pulse shaping function to significantly improve the spectral efficiency. Unlike QAM, the generation of the CAP signal is not achieved by modulating two orthogonal carriers with the same frequency, i.e. sine and cosine complementary signals. Instead, two orthogonal filters are used to generate the two components of the signal. These filters are the result of the time-domain multiplication of a pulse shaping function and two orthogonal carriers. The root raised cosine (RRC) pulse shaping function is a convenient choice to generate the filters, since at the receiver a pair of matched filters with the same shape are used to retrieve the signal. Therefore, by combining both filters at the transmitter and the receiver, the complete response of the system has the characteristics of a raised cosine (RC) function, which minimizes intersymbol interference (ISI).

CAP modulation, as many others modulation schemes, requires a flat frequency response of the transmission link to ensure a reliable performance. To mitigate this impairment, MB-CAP has been proposed for wireless and optical links, achieving high spectral efficiencies over large bandwidths [11]–[13]. By splitting the spectrum into sub-bands, MB-CAP modulation enables the use of bit- and power-loading techniques for each band independently [11], according to the signal to noise ratio (SNR) and channel conditions over the frequency range of each band. Thus, with an adequate number of bands, non-flat frequency responses, e.g. uneven antenna gain, non-flat frequency response of devices, can be alleviated to maximize spectral efficiency.

To generate MB-CAP signalling, binary sequences are mapped into the symbol constellations determined by the modulation scheme and order of each band, i.e. bit-loading. The mapped symbol sequences are filtered using the pair of orthogonal CAP filters of each band to generate its corresponding I and Q components. These filters are implemented as finite impulse response (FIR) filters, guaranteeing output stability and allowing simple implementation. To compensate the unevenness of the frequency response of the link, power loading technique is applied by assigning different magnitude weights to each band. Thus, it is ensured that the BER performance of all bands is homogeneous. To transmit the MB-CAP signal, the I and Q components of all bands are added together into a single signal. At the receiver side, pairs of matched filters, i.e. matched to the CAP filters at the transmitter, are used to retrieve the I and Q components of each band. Finally, the resulting symbol sequences are synchronized and down-sampled to construct the corresponding symbol constellations.

III. Experimental Validation

This section describes the experimental setup used to validate UWB wireless transmissions, the digital signal processing required for MB-CAP modulation signal generation and demodulation, and the experimental results.

A. Experimental Setup

The MB-CAP electrical signal was generated using a high-speed arbitrary waveform generator (AWG). Before feeding the transmitter antenna, a set of attenuators ensured that the antenna EIRP was within the permitted levels established by the UWB regulations. After wireless transmission, the received signal was filtered by a pass-band filter and amplified by two low noise amplifiers (LNAs) with a gain of 26 dB each and a typical noise figure of 3 dB. For offline DSP, the signal was recorded with a high-speed digital storage oscilloscope (DSO). The experiments were performed using identical bow-tie type antennas at the transmitter and receiver, with an antenna gain as shown in Fig. 2(f).

B. Signal Generation and Digital Signal Processing

Future 5G systems must reach peak data rates of 10 Gbit/s. Therefore, a first set of transmissions are aimed to reach maximum wireless distances while achieving data rates of

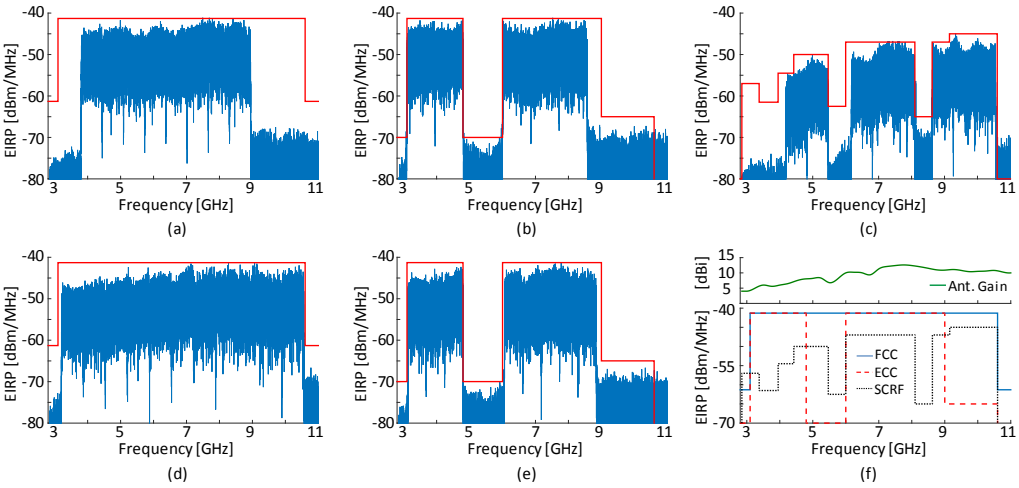

Fig. 2. Spectra of transmitted 10 Gbit/s signals under (a) FCC, (b) ECC, and (c) SCRF regulations, and maximum bit rates signals under (d) FCC, and (e) ECC regulations. (f) Comparison of FCC, ECC and SCRF spectral masks, and antenna gain.

10 Gbit/s under the FCC, ECC, and SCRF regulations. To maximize wireless distances, an appropriate trade-off between modulation order and bandwidth requirements is fundamental. For low power UWB radiation, low order modulation is preferable since it exhibits more robustness against low SNR, however, it requires more bandwidth due its low spectral efficiency.

UWB technology is inherently suitable for short-range wireless transmissions, including largely indoor communication links in environments characterized by dense multipath propagation. Indoor multipath channels can generate delays varying from tens of nanoseconds to hundreds of nanoseconds, which leads to ISI degrading the quality of the transmitted signal. However, by means of narrow pulse formats (i.e. symbol time duration comparable to multipath delays) and decision-feedback equalizers (DFEs), it is possible to accurately identify and mitigate the received multipath components [15].

To comply with the FCC regulation and mitigate channel impairments, 8 bands with a baud rate of 0.625 Gbaud each were used. Although power loading technique is applied, the unevenness of the antenna gain can not be fully compensated. Thus, over the frequency range in which the antenna gain is the lowest, i.e. 3–4 GHz, and over the high frequency range which has the highest FSPL, no bands were allocated (Fig. 2(a)). Since FCC regulation offers a large bandwidth, quadrature phase shift keying (QPSK) modulation scheme was selected for all bands. For the ECC regulation however, since less bandwidth is available, only 5 bands with a baud rate of 0.833 Gbaud each were used, covering almost all bandwidth available (Fig. 2(b)). Binary phase shift keying (BPSK) was selected in the first band to compensate the low antenna gain, and 8-QAM modulation scheme was used in the high frequency window bands to increase the overall spectral efficiency, ensuring a data rate of 10 Gbit/s. The

TABLE I
PARAMETERS OF 10 GBIT/S TRANSMISSIONS

	Band	Baud Rate [GBaud]	Modulation Scheme	Bit Rate [Gbit/s]	Central Frequency [GHz]	Power Loading [dB]
FCC	1	0.625	QPSK	1.250	4.1219	3.0
	2	0.625	QPSK	1.250	4.7656	2.0
	3	0.625	QPSK	1.250	5.4094	2.0
	4	0.625	QPSK	1.250	6.0531	1.0
	5	0.625	QPSK	1.250	6.6969	0.5
	6	0.625	QPSK	1.250	7.3406	0.0
	7	0.625	QPSK	1.250	7.9844	0.5
	8	0.625	QPSK	1.250	8.6281	1.5
ECC	1	0.833	BPSK	0.833	3.5225	5.1
	2	0.833	QPSK	1.667	4.3808	4.5
	3	0.833	8QAM	2.500	6.4292	1.1
	4	0.833	8QAM	2.500	7.2875	0.0
	5	0.833	8QAM	2.500	8.1458	0.8
SCRF	1	0.625	BPSK	0.625	4.5044	0.0
	2	0.625	QPSK	1.250	5.1481	2.5
	3	0.625	QPSK	1.250	6.4906	2.0
	4	0.625	8QAM	1.875	7.1344	3.0
	5	0.625	8QAM	1.875	7.7781	2.0
	6	0.625	QPSK	1.250	8.9469	4.0
	7	0.625	QPSK	1.250	9.5906	5.0
	8	0.625	BPSK	0.625	10.2344	5.5

SCRF regulation in terms of bandwidth is similar to the ECC regulation, but due its more stringent segmentation and EIRP constraints it is more challenging to achieve high data rates. Therefore, a higher segmentation than the ECC case is required and 8 bands with a baud rate of 0.625 Gbaud each were used (Fig. 2(c)). Again, a combination of modulation schemes ranging from BSPK to 8-QAM were selected to compensate the uneven gain of the SCRF spectral mask, maintaining a 10 Gbit/s bit rate. Table I summarizes the main parameters of the MB-CAP signalling for all three spectral masks.

To evaluate the maximum capacity of the link, further experiments were performed using the whole bandwidth per-

mitted by the regulations. Only FCC and ECC regulations are considered since the lower EIRP restrictions of the SCRF regulation leave small margin for further improvements above 10 Gbit/s. The link was tested with wireless distances spanning from 0.5 m to 9 m. To cover the largest amount of bandwidth permitted by the FCC and ECC regulations, eleven bands with a baud rate of 0.65 Gbaud each were used (Fig. 2(d)), and 8 bands with a baud rate of 0.5417 Gbaud each were used (Fig. 2(e)) respectively. For each wireless distance a combination of modulation schemes ranging from BPSK to 64-QAM were assigned to the bands. Thus, the inherently non-flat channel gain was compensated while maximizing the total data rate. For both regulations, the modulation schemes of all bands at each wireless distance are presented in Table II.

It is to be noted that the spectra of the generated signals were measured using an electrical spectrum analyzer (ESA) with the FCC and ECC given settings for UWB compliance testing, i.e. 1 MHz root mean square (RMS) average power measurement with 1 ms time averaging [5], [6]. The antenna gain magnitude was added to the measured spectra, and the resulting effective spectra were checked for compliance.

For both experiments, to generate the signal for each band, decorrelated pseudo-random binary sequences (PRBSs) of $2^{11}-1$ length were mapped into the corresponding symbol constellations. The symbol sequences were up-sampled to the number of samples per symbol determined by the baud rate of the bands and the sampling frequency of the AWG. The resulting sequences were filtered by the pair of CAP orthogonal filters corresponding to each band. For all bands, these FIR filters have a length of 45 symbols and a sharp RRC roll-off factor of 0.03. At the receiver, the corresponding match filters of each were applied. After filtering, the retrieved symbol sequence of each band was down-sampled to construct the symbol constellations, from which the symbols were demodulated with a DFE with 23 feed-forward and feed-back taps.

C. Experimental Results

For the transmissions with a fixed data rate of 10 Gbits/s compliant with the FCC, ECC, and SCRF regulations, Fig. 3 shows the BER versus wireless distance curves for each MB-CAP band. Successful 10 Gbit/s transmission with a BER below the commercial 7% overhead FEC limit of 3.8×10^{-3} was achieved over distances up to 3.5 m, 2 m, and 1.3 m under FCC, ECC, and SCRF spectral mask restrictions respectively. Shorter distances were reached for the ECC and SCRF masks for two main reasons: first, since the bandwidth available is considerably less than the FCC mask, for some of the bands high order modulation schemes were used to increase the spectral efficiency, which are less tolerant to low SNR than QPSK; secondly, for the ECC spectral mask case, it was necessary to transmit one of the bands close to the lower limit of the mask at 3.1 GHz where the antenna gain is the lowest, and for the SCRF spectral mask case, due to its lower EIRP allowed in all frequency bands.

Under the FCC and ECC spectral mask restrictions, Fig.4(a) shows the maximum bit rates achieved with a measured BER

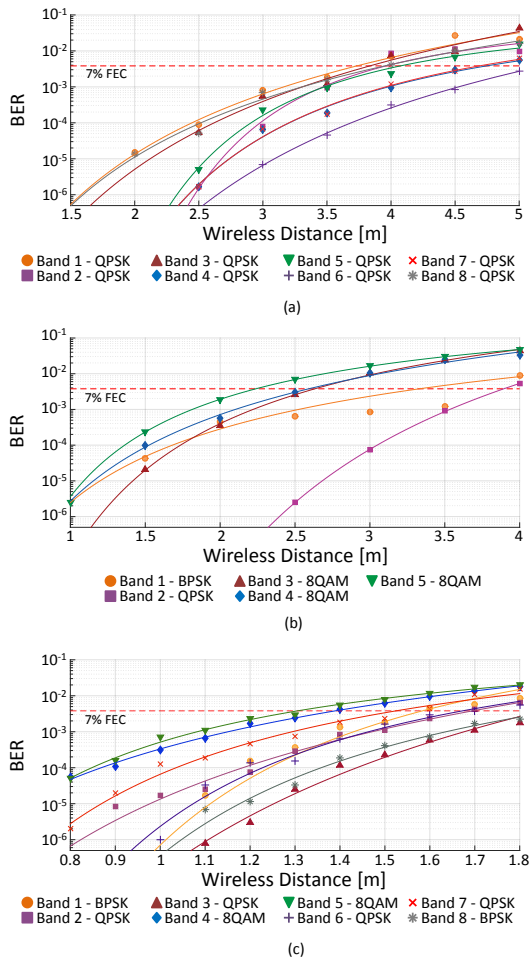

Fig. 3. BER versus wireless distance curves for 10 Gbit/s transmissions under (a) FCC, (b) ECC, and (c) SCRF regulations.

below the commercial 7% overhead FEC limit of 3.8×10^{-3}, over the wireless distance range of 0.5 m to 9 m. Table II summarizes the modulation scheme of each band, the total bit rate, and the average spectral efficiency at each distance. As an example, Fig.4(b) and Fig.4(c) show the symbol constellations and error vector magnitudes (EVMs) of all bands for the transmissions with the highest bit rates achieved, i.e. 35.1 Gbit/s and 20.6 Gbit/s under FCC and ECC regulations respectively, over a wireless distance of 0.5 m. As the distance is incremented, the signal to noise ratio (SNR) of the signal worsens, thus the modulation order of each band must be decreased accordingly to ensure a BER below FEC limit. The power loading gains presented in Table I were slightly changed over the set of wireless distances. As a result, it was possible to emphasize the bands that are more resilient to low SNR and consequently longer distances of transmission were

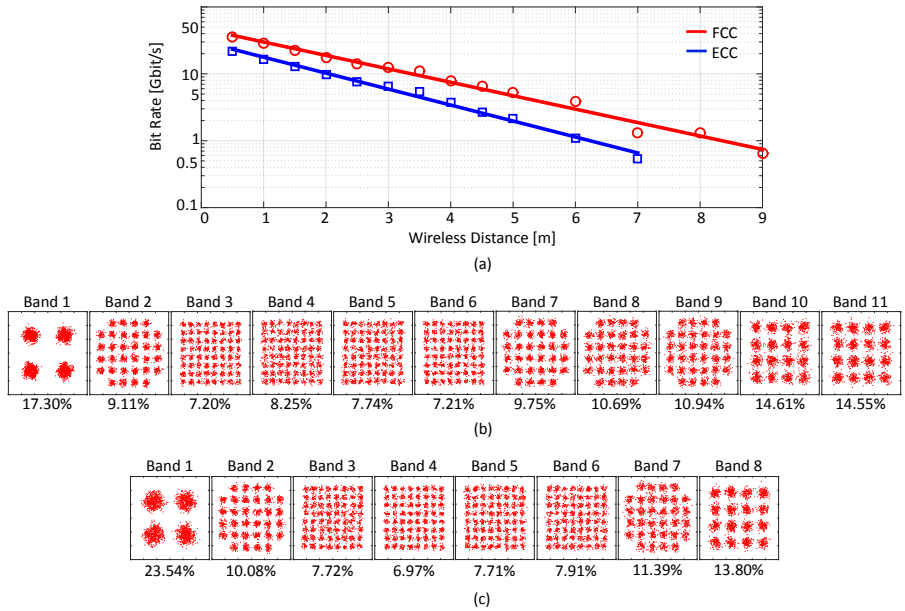

Fig. 4. (a) Maximum bit rates versus wireless distance under FCC and ECC regulations. Band constellations and EVMs of highest bit rates transmissions under (b) FCC, and (c) ECC regulations.

reached. The total bit rates presented in Table II are calculated by adding the individual bit rate of each band at each distance. Due to low SNRs, for some specific bands at given distances, transmission BER below FEC limit was not achieved even with BPSK. Consequently, the bit rate of these bands are not taken into account to calculate the total bit rate. For transmissions under the FCC mask, Band 4 (5.22–5.87 GHz) is the most resilient to low SNRs, being able to maintain a BER below FEC limit up to 9 m, which is the frequency band with the best trade-off between free-space path losses and the antenna gain with our experimental setup. In contrast, under the ECC regulation, it was not possible to use this frequency band and the frequency bands above 9 GHz, thus shorter distances and lower bit rates were attained. Through offline DSP, the number of symbols processed in each band was 61440 and 51200 for the FCC and ECC masks, respectively. Thus, for example, for the FCC case, 368640 bits were processed for the band with the highest modulation order, namely 64-QAM, and 61440 bits for the band with lowest modulation order, namely BPSK.

It is to be noted that the results obtained may be sub-optimal and extra methods, e.g. bit and power loading adaptive algorithms used in OFDM-based systems, can be applied to optimize the assignment of the different parameters of MB-CAP modulation signalling.

IV. Conclusions and Future Work

By means of a single input single output (SISO) wireless link, we experimentally validated the capabilities of UWB technology and MB-CAP modulation to adapt to different scenarios, i.e. different worldwide regulations, while achieving record data rates over distances up to 9 m. To our knowledge, the presented results are the highest bit rates ever achieved under the FCC, ECC, and SCRF UWB indoor regulations by means of a SISO wireless link. High-speed UWB communication systems represent a flexible solution that can be adjusted to comply with current and future regulatory standards for upcoming 5G short range communications, and a prospective solution for upcoming IEEE 802.11 and IEEE 802.15 high data rate systems standardization.

UWB wireless communication systems are suitable for ultra-dense networks which can improve the spectral efficiency per unit area. By applying current MIMO technology to our proposed solution, i.e. beamforming techniques, intra- and intercell interference can be minimized [3], [4]. In addition, to provide a robust and reliable connectivity, further research is necessary to establish optimal techniques for mobility management, i.e. user mobility from one microcell to another [2]. Furthermore, data rates can be increased drastically by exploiting spatial diversity multiplexing (SDM), more specifically multi-user multiple input multiple output (MU-MIMO) technology, used in current commercial 802.11ac Wi-Fi standard compliant products.

The MB-CAP modulation scheme increases data rates significantly at the expense of increasing the complexity of the transceivers. Future work will be devoted to realize a feasible real-time implementations. By means of current low cost off the shelf devices such as digital to analog converters (DACs) and analog to digital converters (ADCs), which are available with sampling rates up to 2 GSa/s, MB-CAP baseband signals of each band can be generated and captured. Through fre-

TABLE II
PARAMETERS AND SPECTRAL EFFICIENCIES OF MAXIMUM BIT RATES TRANSMISSIONS

Distance [m]		Modulation											Total Bit Rate [Gbit/s]	Spectral Efficiency [bit/s/Hz]
		Band 1	Band 2	Band 3	Band 4	Band 5	Band 6	Band 7	Band 8	Band 9	Band 10	Band 11		
FCC	0.5	QPSK	32QAM	64QAM	64QAM	64QAM	64QAM	32QAM	32QAM	32QAM	16QAM	16QAM	35.10	4.77
	1.0	QPSK	16QAM	32QAM	32QAM	32QAM	16QAM	32QAM	16QAM	16QAM	8QAM	8QAM	28.60	3.88
	1.5	QPSK	8QAM	16QAM	16QAM	16QAM	8QAM	16QAM	8QAM	8QAM	QPSK	QPSK	22.10	3
	2.0	BPSK	QPSK	8QAM	8QAM	16QAM	8QAM	8QAM	8QAM	QPSK	QPSK	BPSK	17.55	2.38
	2.5	BPSK	QPSK	8QAM	QPSK	8QAM	QPSK	8QAM	QPSK	QPSK	BPSK	BPSK	14.30	1.94
	3.0	BPSK	BPSK	QPSK	QPSK	8QAM	QPSK	QPSK	QPSK	QPSK	BPSK	BPSK	12.35	1.68
	3.5	BPSK	BPSK	QPSK	QPSK	QPSK	QPSK	QPSK	QPSK	QPSK	BPSK	–	11.05	1.65
	4.0	–	BPSK	BPSK	QPSK	QPSK	BPSK	QPSK	QPSK	BPSK	–	–	7.80	1.46
	4.5	–	BPSK	BPSK	BPSK	QPSK	BPSK	QPSK	BPSK	BPSK	–	–	6.50	1.21
	5.0	–	BPSK	BPSK	BPSK	QPSK	BPSK	BPSK	BPSK	–	–	–	5.20	1.11
	6.0	–	BPSK	–	BPSK	QPSK	BPSK	BPSK	–	–	–	–	3.90	1.17
	7.0	–	–	–	BPSK	BPSK	–	–	–	–	–	–	1.30	0.97
	8.0	–	–	–	BPSK	BPSK	–	–	–	–	–	–	1.30	0.97
	9.0	–	–	–	BPSK	–	–	–	–	–	–	–	0.65	0.97
ECC	0.5	QPSK	32QAM	64QAM	64QAM	64QAM	64QAM	32QAM	16QAM				21.6667	4.85
	1.0	BPSK	16QAM	16QAM	32QAM	32QAM	16QAM	16QAM	16QAM				16.2500	3.64
	1.5	–	8QAM	16QAM	16QAM	16QAM	16QAM	8QAM	QPSK				13.0000	3.33
	2.0	–	QPSK	8QAM	8QAM	8QAM	8QAM	QPSK	QPSK				9.7500	2.50
	2.5	–	QPSK	QPSK	8QAM	QPSK	QPSK	QPSK	BPSK				7.5833	1.94
	3.0	–	BPSK	QPSK	QPSK	QPSK	QPSK	QPSK	BPSK				6.5000	1.66
	3.5	–	BPSK	QPSK	QPSK	QPSK	QPSK	BPSK	–				5.4167	1.62
	4.0	–	BPSK	BPSK	QPSK	BPSK	BPSK	BPSK	–				3.7917	1.13
	4.5	–	BPSK	BPSK	BPSK	BPSK	BPSK	–	–				2.7083	0.97
	5.0	–	–	BPSK	BPSK	BPSK	BPSK	–	–				2.1667	0.97
	6.0	–	–	BPSK	BPSK	–	–	–	–				1.0833	0.97
	7.0	–	–	–	BPSK	–	–	–	–				0.5417	0.97

quency multipliers and mixers each band can be up-converted to its corresponding frequency band for transmission, and down-converted to baseband at the receiver. In addition, by optimizing MB-CAP modulation, signalling parameters and further mitigation of channel impairments, demodulation computational complexity can be relaxed by decreasing the number of arithmetic operations necessary, e.g. fewer taps required for equalization.

REFERENCES

[1] Cisco, "Cisco Visual Networking Index: Global Mobile Data Traffic Forecast Update, 2016–2021 White Paper," February 2017.

[2] A. Osseiran *et al.*, "Scenarios for 5G mobile and wireless communications: the vision of the METIS project," *IEEE Communications Magazine*, vol. 52, no. 5, pp. 26–35, May 2014.

[3] F. Boccardi *et al.*, "Five disruptive technology directions for 5G," *IEEE Communications Magazine*, vol. 52, no. 2, pp. 74–80, February 2014.

[4] J. G. Andrews *et al.*, "What Will 5G Be?" *IEEE Journal on Selected Areas in Communications*, vol. 32, no. 6, pp. 1065–1082, June 2014.

[5] Federal Communications Commission, "Ultra-wideband operation," in *Title 47 Chapter I Part 15.F.*, 2005.

[6] Electronic Communications Committee, "The harmonised conditions for devices using ultra-wideband (UWB) technology in bands below 10.6 GHz," in *ECC Decision (06)04*, 2006.

[7] State Commission for Radio Frequencies, "Ultrawideband Wireless Devices," in *Annex to SCRF No. 09-05-02*, 2009.

[8] M. Chiani and A. Giorgetti, "Coexistence between uwb and narrow-band wireless communication systems," *Proceedings of the IEEE*, vol. 97, no. 2, pp. 231–254, Feb 2009.

[9] W. Alliance, "MultiBand OFDM Physical Layer Specification," August 2009.

[10] T. Keller and L. Hanzo, "Adaptive multicarrier modulation: a convenient framework for time-frequency processing in wireless communications," *Proceedings of the IEEE*, vol. 88, no. 5, pp. 611–640, May 2000.

[11] M. I. Olmedo *et al.*, "Multiband Carrierless Amplitude Phase Modulation for High Capacity Optical Data Links," *J. Lightw. Technol.*, vol. 32, no. 4, pp. 798–804, 2014.

[12] R. Puerta, S. Rommel, J. J. Vegas Olmos, and I. Tafur Monroy, "10Gb/s ultra-wideband wireless transmission based on multi-band carrierless amplitude phase modulation," in *2016 IEEE 17th Annual Wireless and Microwave Technology Conference (WAMICON)*, April 2016, pp. 1–4.

[13] R. Puerta, S. Rommel, J. J. Vegas Olmos and I. Tafur Monroy, "Up to 35 Gbps ultra-wideband wireless data transmission links ," in *2016 IEEE 27th Annual International Symposium on Personal, Indoor, and Mobile Radio Communications (PIMRC)*, Sept 2016, pp. 1–5.

[14] D. Porcino and W. Hirt, "Ultra-wideband radio technology: potential and challenges ahead," *IEEE Communications Magazine*, vol. 41, no. 7, pp. 66–74, July 2003.

[15] I. J. Fevrier, S. B. Gelfand, and M. P. Fitz, "Reduced complexity decision feedback equalization for multipath channels with large delay spreads," *IEEE Transactions on Communications*, vol. 47, no. 6, pp. 927–937, Jun 1999.

Paper 9: Up to 35 Gbps ultra-wideband wireless data transmission links

R. Puerta, S. Rommel, J. J. V Olmos, and I. T. Monroy, "Up to 35 Gbps ultra-wideband wireless data transmission links," in *2016 IEEE 27th Annual International Symposium on Personal, Indoor, and Mobile Radio Communications*, 2016, pp. 1–5.

DOI: 10.1109/PIMRC.2016.7794775

2016 IEEE 27th Annual IEEE International Symposium on Personal, Indoor and Mobile Radio Communications - (PIMRC): Fundamentals and PHY

Up to 35 Gbps Ultra-Wideband Wireless Data Transmission Links

Rafael Puerta, Simon Rommel, Juan José Vegas Olmos, Idelfonso Tafur Monroy
Department of Photonics Engineering
Technical University of Denmark
Kgs. Lyngby, 2800, Denmark
{rapur,sirem,jjvo,idtm}@fotonik.dtu.dk

***Abstract*—For the first time Ultra-Wideband record data transmission rates up to 35.1 Gbps and 21.6 Gbps are achieved, compliant with the restrictions on the effective radiated power established by both the United States Federal Communications Commission and the European Electronic Communications Committee, respectively. To achieve these record bit rates, the multi-band approach of Carrierless Amplitude Phase modulation scheme was employed. Wireless transmissions were achieved with a BER below the 7% overhead FEC threshold of $3.8 \cdot 10^{-3}$.**

Keywords—Ultra-wideband, effective isotropic radiated power, carrierless amplitude phase modulation

I. Introduction

The accelerated development of electronics and portable devices, aimed mainly for multimedia applications, is increasing exponentially the data demands per user. In this context, for low-power high-speed wireless communications over short distances, Ultra-wideband (UWB) technology is one of the most appealing alternatives suitable for indoor scenarios such as Wireless Personal Area Networks (WPANs), where conventional computing and communicating devices are able to exchange large amounts of data [1], [2]. Furthermore, UWB systems do not require a license if regulatory conditions are fulfilled [3], [4], and are able work in parallel with existing narrowband wireless systems since receivers of this kind perceives UWB emissions as ordinary noise [5].

To cope with these new data demands in limited bandwidth systems, new approaches must be applied evolving from classic spectral inefficient pulse-based systems [6]–[8] to more advanced and flexible modulation schemes such as Multi-band Orthogonal Frequency Division Multiplexing (MB-OFDM) [9], [10], and Multi-band Carrierless Amplitude Phase (MultiCAP) modulation [11]. Under dynamically changing conditions MB-OFDM has been shown to provide the flexibility to adapt to channel conditions and to comply with current and future regulatory UWB standards worldwide. Recently, MultiCAP modulation, with the advantages of a multi-band approach, has shown remarkable results for UWB wireless transmissions [12], [13]. Furthermore, the overall CAP system architecture has been demonstrated to be less complex than OFDM scheme architecture [14].

To the best of our knowledge the current state of the art of an UWB wireless transmission, compliant with the regulations of the FCC and the European Electronic Communications Committee (ECC), is 10 Gbps over a distance of 3.5 m and 2 m, respectively [13]. These records were obtained using MultiCAP modulation scheme with bit error rates (BERs) below the commercial 7% overhead forward error correction (FEC) limit of $3.8 \cdot 10^{-3}$.

In this paper, we present the highest bit rates achieved by means of MultiCAP modulation, for a set of wireless distances spanning from 0.5 m to 9 m. We experimentally demonstrate record transmission bit rates up to 35.1 Gbps and 21.6 Gbps, under the regulations established by both the FCC and the ECC, respectively. To the best of our knowledge the achieved data rates and distances establish new records for both considered UWB regulations.

This paper is organized as follows: In section II a brief description of MultiCAP modulation scheme and UWB regulations are described. In section III the experimental setup is described and in section IV the experimental results are presented. Finally, in section V conclusions are presented.

II. Framework

A. Multi-band Carrierless Amplitude Phase Modulation

Carrierless amplitude phase modulation (CAP) is a multilevel and multidimensional modulation scheme [11], [15], similar to high order phase shift keying (PSK) and quadrature amplitude modulation (QAM) in transmitting two channels of data separately – i.e. in-phase (I) and quadrature (Q) channels. It does however not rely on a pure sinusoidal tone to generate the orthogonal I and Q components and the two channels of the CAP signal rather are generated with two orthogonal pass-band filters from the time-domain multiplication between the pulse shaping function – here a root raised cosine (RRC) – and a cosine/sine for I and Q components respectively:

$$p_i(t) = g(t)\cos(2\pi f_c t) \quad (1)$$

$$p_q(t) = g(t)\sin(2\pi f_c t) \quad (2)$$

The main parameters of the CAP filters are: i. the cosine/sine frequency determining the central frequency of the transmitted band; ii. the roll off factor α of the RRC which determines the excess bandwidth consumed (i.e. with an RRC pulse shape the total pass-band bandwidth of a CAP signal is $(1+\alpha)$ times the baud rate); iii. the filter length in the number of

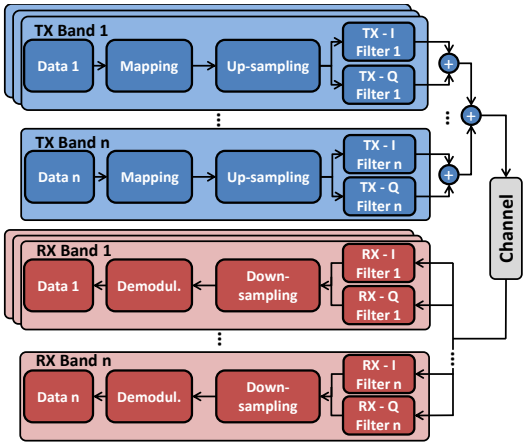

Fig. 1. Block diagram of MultiCAP transmitter and receiver.

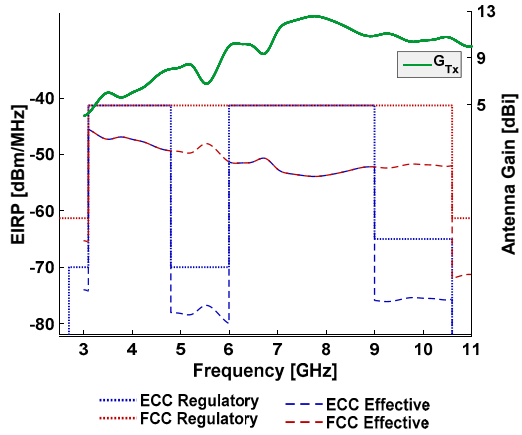

Fig. 2. Comparison of the regulatory spectral emission masks set by the ECC and FCC and the resulting effective masks when antenna gain is taken into account.

samples which affects both performance and complexity of the system. For short lengths the overall system is simpler, but performance decreases significantly [11].

A CAP signal is generated by mapping the original binary sequence with an M-ary QAM or M-ary PSK encoder, the mapped symbols are up-sampled – i.e. zeros are inserted between the symbols – in order to perform a time-domain convolution with the CAP filters. After filtering, the signals from the I and Q channels are added and transmitted. At the receiver, to separate the two channels, two filters matched to the pass-band filters described in Eq. (1) and Eq. (2) are employed [16]. Then the two channels are separately down-sampled and the data decoded.

MultiCAP modulation relies on simultaneous transmission of several CAP signals assigned to different frequency bands, ensuring bands are non-overlapping. This is achieved by using not only one pair of orthogonal filters, but several pairs with different cosine/sine frequencies assigned to each frequency band. Fig. 1 shows the block diagrams of a MultiCAP transmitter and receiver.

The flexibility offered by MultiCAP allows to independently choose the modulation format scheme, order, and signal power – i.e. allows power loading – in each band, alleviating the need for a flat frequency response of the channel which is required for reliable transmission of conventional CAP and QAM signals. The combination of power loading and use of a different signal constellations in each band makes MultiCAP a prime candidate for wireless links where frequency selectivity of the channel and uneven antenna gain over the operating frequency range cause significant degradations.

B. UWB Regulation

To avoid interference with (possibly licensed) radio services – such as mobile and WiFi networks, as well as the global positioning system (GPS) – the power spectral density of unlicensed UWB system signals must be limited to a level where within its own bandwidth a traditional narrowband receiver will perceive the UWB emissions as ordinary noise. The FCC has established a spectral emission mask for indoor applications, consisting of a single flat window with a permitted average effective isotropic radiated power (EIRP) of at most -41.3dBm/MHz between 3.1 GHz and 10.6 GHz [4]. For Europe the ECC has established regulations specifying a spectral emission mask with the same maximum permitted EIRP, but unlike in the FCC case a gap in the mask defines two usable windows with frequency ranges of 3.1–4.8 GHz and 6–9 GHz [3]. Due to this segmentation attaining high data rates under the ECC mask poses a greater challenge when compared to the FCC mask. Fig. 2 shows the FCC and ECC EIRP masks for indoors applications and compares them to the resulting effective masks for the transmitted signal, when the gain of the transmitting antenna is taken into account; antenna gain over frequency is also shown in Fig. 2.

The flexibility provided by MultiCAP modulation allows to assign a set of bands with its own modulation schemes/orders, baud rates, and power values, thus enabling to fit and achieve high data rates under both spectral emission masks. Taking into account the variation of the antenna gain over frequency, the parameters of a set of well-defined MultiCAP signals were determined for transmission under the FCC and ECC masks. With the evenness provided by the FCC mask, using practically all bandwidth available was achieved by using eleven bands with a baud rate of 0.65 GBauds/s each one. Under the ECC mask however, since the restrictions are more stringent and less bandwidth is available only eight bands, each one with a baud rate of 0.5417 GBauds/s, were allocated.

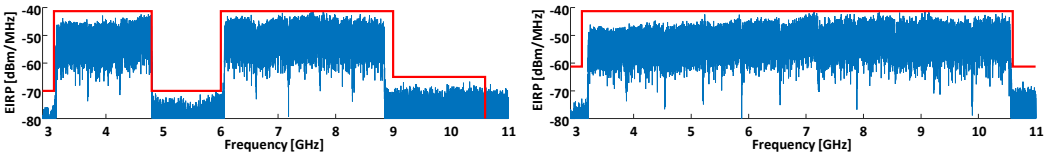

Fig. 3. Effective spectra of MutiCAP signals fitting ECC and FCC masks . These spectra correspond to the 0.5 m transmissions.

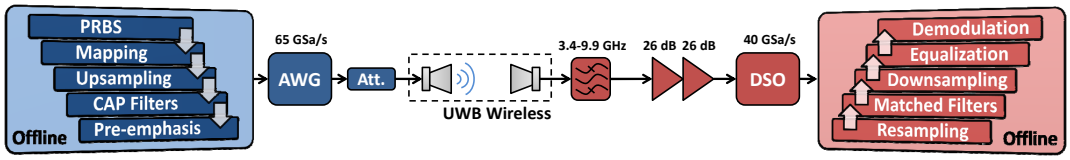

Fig 4. Block diagram of experimental setup. PRBS: pseudo-random binary sequence, AWG: arbitrary waveform generator, Att: attenuator, DSO: digital storage oscilloscope

The spectrum of the generated signal is measured using an electrical spectrum analyzer (ESA) with the ECC and FCC prescribed settings for UWB compliance testing – i.e. 1 MHz root mean square (RMS) average power measurement with 1 ms time averaging [3], [4]. The measured frequency spectra are combined with the magnitude of the antenna gain over frequency and the resulting effective spectra are checked for compliance with the ECC and FCC spectral emission masks as shown in Fig. 3, where these spectra correspond to the wireless transmissions over 0.5 m.

III. Experimental Setup

MultiCAP electrical signal was generated using an arbitrary waveform generator (AWG) with a sampling rate 65 GSa/s and a vertical resolution with an effective number of bits (ENOB) of 5. A set of attenuators – along with the power loading technique – ensured that the antenna EIRP was within the permitted levels. After wireless transmission, the received signal was filtered by a pass-band filter (3.4 – 9.9 GHz) and amplified by two low noise amplifiers (LNAs) with a gain of 26 dB each and a typical noise figure of 3 dB. For offline digital signal processing (DSP), the signal was recorded with a digital storage oscilloscope (DSO) at a sampling rate of 40 Gbps and with 8 bits of vertical resolution. The experiments were performed using a set of bow-tie type antennas for both the transmitter and receiver. Fig. 4 shows the block diagram of both the offline signal processing part and the system setup, and Fig. 5 shows the laboratory setup.

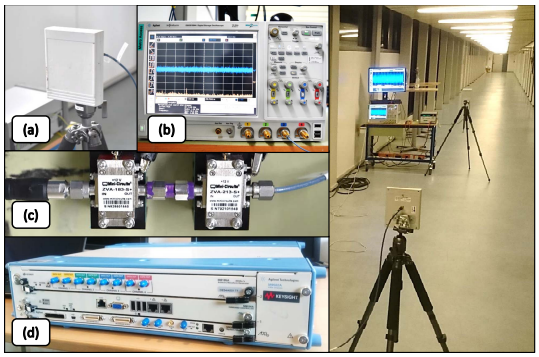

Fig. 5. Experimental setup, (a) bow-tie type antena, (b) 40 GSa/s DSO, (c) 26 dB LNAs, and (d) 65 GSa/s AWG.

IV. Experiments Results

In Fig. 6 is shown the maximum bit rates achieved versus wireless distance for both the ECC and FCC regulations. Successful transmissions, with a measured BER below the 7% overhead FEC limit of $3.8 \cdot 10^{-3}$, were achieved for distances over the range of 0.5 m to 9 m. It is to be noted that, for all distances, the individual BER of each band was below the FEC limit. Through offline DSP, the number of symbols processed in each band was 51200 and 61440 for the ECC mask and the FCC mask transmissions, respectively. Thus, for example, for the FCC case, 368640 bits were processed for the band with the highest modulation order, namely 64-QAM, and 61440 bits were processed for the band with lowest modulation order,

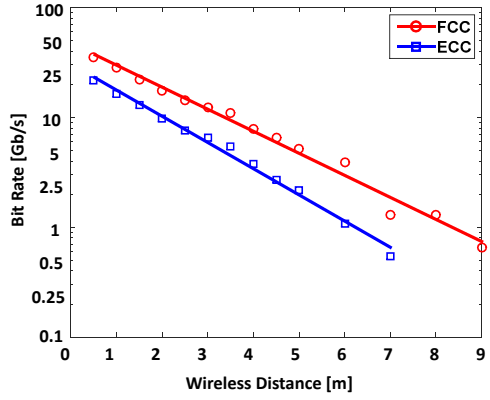

Fig. 6. Measured bit rates versus wireless distance.

TABLE I
PARAMETERS FOR ECC TRANSMISSIONS AND SPECTRAL EFFICIENCIES

Distance [m]	Modulation								Total Bit Rate [Gbps]	Spectral Efficiency [bit/s/Hz]
	Band 1	Band 2	Band 3	Band 4	Band 5	Band 6	Band 7	Band 8		
0.5	QPSK	32-QAM	64-QAM	64-QAM	64-QAM	64-QAM	32-QAM	16-QAM	21.6667	4.85
1.0	BPSK	16-QAM	16-QAM	32-QAM	32-QAM	16-QAM	16-QAM	16-QAM	16.2500	3.64
1.5	–	8-QAM	16-QAM	16-QAM	16-QAM	16-QAM	8-QAM	QPSK	13.0000	3.33
2.0	–	QPSK	8-QAM	8-QAM	8-QAM	8-QAM	QPSK	QPSK	9.7500	2.50
2.5	–	QPSK	QPSK	8-QAM	QPSK	QPSK	QPSK	BPSK	7.5833	1.94
3.0	–	BPSK	QPSK	QPSK	QPSK	QPSK	QPSK	BPSK	6.5000	1.66
3.5	–	BPSK	QPSK	QPSK	QPSK	QPSK	BPSK	–	5.4167	1.62
4.0	–	BPSK	BPSK	QPSK	BPSK	BPSK	BPSK	–	3.7917	1.13
4.5	–	BPSK	BPSK	BPSK	BPSK	BPSK	–	–	2.7083	0.97
5.0	–	–	BPSK	BPSK	BPSK	BPSK	–	–	2.1667	0.97
6.0	–	–	BPSK	BPSK	–	–	–	–	1.0833	0.97
7.0	–	–	–	BPSK	–	–	–	–	0.5417	0.97

TABLE II
PARAMETERS FOR FCC TRANSMISSIONS AND SPECTRAL EFFICIENCIES

Dist. [m]	Modulation											Total Bit Rate [Gbps]	Spectral Efficiency [bit/s/Hz]
	Band 1	Band 2	Band 3	Band 4	Band 5	Band 6	Band 7	Band 8	Band 9	Band 10	Band 11		
0.5	QPSK	32-QAM	64-QAM	64-QAM	64-QAM	64-QAM	32-QAM	32-QAM	32-QAM	16-QAM	16-QAM	35.10	4.77
1.0	QPSK	16-QAM	32-QAM	32-QAM	32-QAM	16-QAM	32-QAM	16-QAM	16-QAM	8-QAM	8-QAM	28.60	3.88
1.5	QPSK	8-QAM	16-QAM	16-QAM	16-QAM	8-QAM	16-QAM	8-QAM	8-QAM	QPSK	QPSK	22.10	3
2.0	BPSK	QPSK	8-QAM	8-QAM	16-QAM	8-QAM	8-QAM	8-QAM	QPSK	QPSK	BPSK	17.55	2.38
2.5	BPSK	QPSK	8-QAM	QPSK	8-QAM	QPSK	8-QAM	QPSK	QPSK	BPSK	BPSK	14.30	1.94
3.0	BPSK	BPSK	QPSK	QPSK	8-QAM	QPSK	QPSK	QPSK	QPSK	BPSK	BPSK	12.35	1.68
3.5	BPSK	BPSK	QPSK	QPSK	QPSK	QPSK	QPSK	QPSK	QPSK	BPSK	–	11.05	1.65
4.0	–	BPSK	BPSK	QPSK	QPSK	BPSK	QPSK	QPSK	BPSK	–	–	7.80	1.46
4.5	–	BPSK	BPSK	BPSK	QPSK	BPSK	QPSK	BPSK	BPSK	–	–	6.50	1.21
5.0	–	BPSK	BPSK	BPSK	QPSK	BPSK	BPSK	BPSK	–	–	–	5.20	1.11
6.0	–	BPSK	–	BPSK	QPSK	BPSK	BPSK	–	–	–	–	3.90	1.17
7.0	–	–	–	BPSK	BPSK	–	–	–	–	–	–	1.30	0.97
8.0	–	–	–	BPSK	BPSK	–	–	–	–	–	–	1.30	0.97
9.0	–	–	–	BPSK	–	–	–	–	–	–	–	0.65	0.97

namely Bipolar Phase Shift Keying (BPSK). In Tables I and II a summary of all distances, modulations schemes/orders of all bands, and spectral efficiencies (SEs) are presented for the ECC and FCC masks, respectively. As the distance is incremented, the signal to noise ratio (SNR) of the signal worsens, thus the modulation order of each band must decrease accordingly in order to ensure a BER below 7% overhead FEC limit.

In Tables I and II, total bit rates were calculated by adding the individual bit rate achieved by each band. Furthermore, due low SNRs dashes indicate that, for a specific band at a given distance, not even with BPSK modulation a BER below FEC limit was achieved. Consequently, the bitrate of these bands were not taken into account to calculate the total bit rate. Likewise, spectral efficiencies were calculated only considering the bands with a BER above FEC limit. For transmissions under the FCC mask, Band 4 (5.22–5.87 GHz) is the more resilient to low SNRs being able to maintain a BER below FEC limit up to 9 meters, which is the frequency band with the best tradeoff between free-space path losses and the antenna gain with our setup. On the other hand, under the ECC regulation, it was not possible to use this frequency band and the frequency bands over 9 GHz, therefore shorter distances and lower bit rates were attained. Since UWB communications relies on the availability of a wide bandwidth, it is to be noted that spectral efficiency is not as relevant as total capacity.

The experimental results validate the capabilities of MultiCAP based transmissions to adapt to different scenarios, while achieving record data rates for UWB applications.

V. CONCLUSIONS

MultiCAP based wireless data transmissions links for high-speed UWB communication systems over short distances represents a flexible solution that can be easily adapted to comply with current and future regulatory UWB standards. To the best of our knowledge the presented results are the highest bit rates achieved over distances up to 9 m under the ECC and FCC spectral emission masks.

ACKNOWLEDGMENT

R. Puerta would like to express his gratitude to the Colombian Administrative Department of Science, Technology and Innovation (COLCIENCIAS) for supporting his research. This work was partly funded by the DFF FTP mmW-SPRAWL. Keysight Technologies is acknowledged for providing the AWG for the experiments.

REFERENCES

[1] D. Porcino and W. Hirt, "Ultra-wideband radio technology: Potential and challenges ahead," *IEEE Commun. Mag*., vol. 41, no. 7, pp. 66–74, 2003.

[2] S. Emami, *UWB Communication Systems: Conventional and 60 GHz*. New York: Springer, 2013.

[3] Electronic Communications Committee, "The harmonised conditions for devices using ultra-wideband (UWB) technology in bands below 10.6 GHz," in *ECC Decision (06)04*. Copenhagen: ECO, 2006.

[4] Federal Communications Commission, "Ultra-wideband operation," in *Title 47 Chapter I Part 15.F*. Washington D.C.: GPO, 2005, pp. 849–858.

[5] T. K. K. Tsang and M. N. El-Gamal, "Ultra-wideband (UWB) communications systems: An overview," in *Proc. NEWCAS 2005*. Québec: IEEE, 2005, pp. 381–386.

[6] J. B. Jensen, R. Rodes, A. Caballero, X. Yu, T. B. Gibbon, and I. Tafur Monroy, "4 Gbps impulse radio (IR) ultra-wideband (UWB) transmission over 100 meters multi mode fiber with 4 meters wireless transmission," *Opt. Express*, vol. 17, no. 19, pp. 16 898–16 903, sep 2009.

[7] J. B. Jensen, T. B. Gibbon, X. Yu, R. Rodes, and I. Tafur Monroy, "Bidirectional 3.125 Gbps downstream / 2 Gbps upstream impulse radio ultrawide-band (UWB) over combined fiber and wireless link," in *Proc. OFC 2010*. San Diego: OSA, 2010, paper OThO5.

[8] J. B. Jensen, R. Rodes, M. Beltran, and I. Tafur Monroy, "Shared medium 2 Gbps baseband & 2 Gbps UWB in-building converged optical/wireless network with multimode fiber and wireless transmission," in *Proc. ECOC 2016*. Torino: IEEE, 2010, paper We.7.B.4.

[9] M. Magani, L. Guo, X. Chen, Y. Alfadhl, and A. Alomainy, "Evaluation of MB OFDM UWB for high data rate applications," in *Proc. LAPC 2012*. Loughborough: IEEE, 2012.

[10] V. Sipal, J. Gelabert, C. J. Stevens, B. Allen, and D. J. Edwards, "Adaptive OFDM for wireless interconnect in confined enclosures," *IEEE Wireless Commun. Lett*., vol. 2, no. 5, pp. 507–510, 2013.

[11] M. I. Olmedo, T. Zuo, J. B. Jensen, Q. Zhong, X. Xu, S. Popov, and I. T. Monroy, "Multiband Carrierless Amplitude Phase Modulation for High Capacity Optical Data Links," *Light. Technol. J.*, vol. 32, no. 4, pp. 798–804, Feb. 2014.

[12] R. Puerta, S. Rommel, J. A. Altabas, L. Pyndt, R. Idrissa, A. K. Sultanov, J. J. Vegas Olmos, and I. Tafur Monroy, "Multiband carrierless amplitude/phase modulation for ultrawideband high data rate wireless communications," *Microw. Opt. Technol. Lett.*, vol. 58, no. 7, pp. 1603–1607, 2016.

[13] R. Puerta, S. Rommel, J. J. V Olmos, and I. T. Monroy, "10Gb/s ultra-wideband wireless transmission based on multi-band carrierless amplitude phase modulation," in *2016 IEEE 17th Annual Wireless and Microwave Technology Conference (WAMICON)*, 2016, pp. 1–4.

[14] J. L. Wei, J. D. Ingham, D. G. Cunningham, R. V Penty, and I. H. White, "Performance and Power Dissipation Comparisons Between 28 Gb/s NRZ, PAM, CAP and Optical OFDM Systems for Data Communication Applications," *J. Light. Technol.*, vol. 30, no. 20, pp. 3273–3280, 2012.

[15] J. D. Ingham, R. Penty, I. White, and D. Cunningham, "40 Gbps carrierless amplitude and phase modulation for low-cost optical datacommunication links," in *Proc. OFC 2011*. Los Angeles: OSA, 2011, paper OThZ3.

[16] S. Haykin and M. Moher, *Communication Systems*, 4th ed. New York: John Wiley & Sons Ltd, 2001.

Paper 10: Flexible MultiCAP Modulation and its Application to 850 nm VCSEL-MMF Links

R. Puerta, J. J. V Olmos, I. T. Monroy, N. N. Ledentsov, and J. P. Turkiewicz, "Flexible MultiCAP Modulation and its Application to 850 nm VCSEL-MMF Links," *J. Light. Technol.*, vol. 35, no. 15, pp. 3168–3173, Aug. 2017.

DOI: 10.1109/JLT.2017.2701887

Flexible MultiCAP Modulation and its Application to 850 nm VCSEL-MMF Links

Rafael Puerta, *Student Member, IEEE*, Juan José Vegas Olmos, *Senior Member, IEEE*, Idelfonso Tafur Monroy, *Senior Member, IEEE*, Nikolay N. Ledentsov, and Jarosław P. Turkiewicz, *Senior Member, IEEE*

***Abstract*—In this paper, we introduce a flexible scheme for the multiband approach of carrierless amplitude phase (flexible MultiCAP) modulation. The proposed modulation scheme can adapt to different data traffic demands and transmission link conditions, with advantages of variable bit rate and, therefore, power consumption adaptivity. First, simulations results are presented to show the capacity of the proposed scheme under different bandwidth restrictions, and then, as a proof of concept, its feasibility is experimentally demonstrated in 850 nm vertical-cavity surface-emitting laser based transmissions over 100 m of OM4 multimode fiber. Data rates up to 40.6 Gb/s with spectral efficiencies up to 4 bit/s/Hz are achieved. All measured bit error rates were below the 7% overhead forward error correction threshold of 3.8×10^{-3}.**

***Index Terms*—Multi-band carrierless amplitude phase modulation, optical fiber communication, vertical cavity surface emitting lasers.**

I. Introduction

CURRENTLY, research efforts on the optical transmission do not only concentrate on higher transmission and switching rates, but also on the energy efficiency of the proposed solutions [1]–[5]. Application of the energy efficient technologies reduces the carbon footprint and operating cost. Energy efficiency and overall cost reduction is particularly important for systems with massive deployments like fiber to the home (FTTH) systems and data interconnects, with the latter applied to data transmissions in the inter- and intra-rack level. Additionally, due the accelerated growth of data traffic demands, FTTH systems and data interconnects are developing towards data rates >25 Gb/s per lane [6]–[9].

Manuscript received September 15, 2016; revised December 12, 2016, March 17, 2017, and April 26, 2017; accepted May 1, 2017. Date of publication May 7, 2017; date of current version June 24, 2017. This work was supported in part by the European Commission under the FP7 Grant 619197 ADDAPT "Adaptive Data and Power Aware Transceivers for Optical Communications" and in part by the science funds for years 2014–2017 Granted for International Project Execution. The work of R. Puerta was partly supported by the Colombian Administrative Department of Science, Technology and Innovation (COLCIENCIAS). *(Corresponding author: Rafael Puerta.)*

R. Puerta, J. J. Vegas Olmos, and I. Tafur Monroy are with the Technical University of Denmark, Kongens Lyngby 2800, Denmark (e-mail: rapur@fotonik.dtu.dk; jjvo@fotonik.dtu.dk; idtm@fotonik.dtu.dk).

N. N. Ledentsov is with the VI-Systems GmbH, Berlin 10623, Germany (e-mail: nikolay.ledentsov@v-i-systems.com).

J. P. Turkiewicz is with the Warsaw University of Technology, Warsaw 00-665, Poland (e-mail: jturkiew@tele.pw.edu.pl).

Color versions of one or more of the figures in this paper are available online at http://ieeexplore.ieee.org.

Digital Object Identifier 10.1109/JLT.2017.2701887

It is known that the data traffic varies in the milliseconds and hour time scale [10]. Therefore, a way to reduce energy consumption can be attained by means of variable transmission techniques that can adjust to the varying demand. While the variations in the micro scale are challenging to be exploited, due to the required system reaction time, the variations in the macro scale can form the basis for the energy consumption reduction. Several approaches on the topic have been proposed [11], [12] which include variable modulation formats, variable symbol rates, and sleep modes, e.g. optical link deactivation.

Carrierless amplitude phase (CAP) modulation has shown high energy efficiency and advantages over orthogonal frequency-division multiplexing (OFDM) and pulse amplitude modulation (PAM) with respect to power dissipation as shown in [13]. However, CAP modulation, as others modulation schemes, needs a flat frequency response of the transmission link to ensure a reliable performance. To mitigate this impairment, the multiband approach of carrierless amplitude phase (MultiCAP) has been proposed for optical and wireless links, achieving high spectral efficiencies over large bandwidths [14]–[16]. MultiCAP modulation allows to independently choose the modulation scheme, order, baud rate, and signal power for each of its bands, achieving, with limited bandwidth components, high spectral efficiency and good performance even with a non-flat channel frequency response. In [17] a transmission technique employing MultiCAP modulation is presented, where the bandwidth of each band can be dynamically adjusted according to the requirements of optical network units (ONUs). However, only the concept is stated without any demonstration or validation of its dynamicity.

Here, we introduce and validate a flexible MultiCAP modulation that allows adjustment of the data rate to the current needs [18]. By activating and deactivating the MultiCAP sub-bands, the total bit rate of the transmission system can be adjusted for different traffic demands. Further, the modulation scheme within a given band can be also adjusted, and unlike traditional MultiCAP modulation, each band may have a different baud rate. The proposed system can not only adjust to the varying traffic demand but also to the transmission link conditions, e.g. lower baud rates have higher tolerance to the transmission impairments such as chromatic dispersion, therefore longer transmission links can be bridged. Data rate flexibility can be translated into energy savings since each transmission band can be supplied by a separate transmitter and receiver sub-blocks. Therefore an

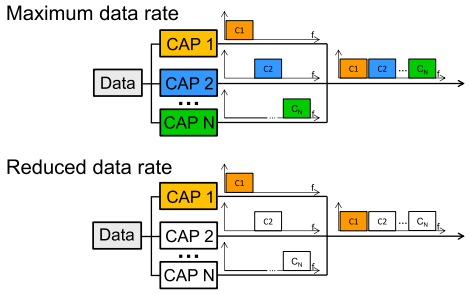

Fig. 1. Flexible multiCAP modulation principle of operation.

adaptive transmission link is achieved, where by switching off bands, when the traffic demand is low, the energy consumption of the system is reduced. In Fig. 1 the principle of the flexible MultiCAP modulation operation is depicted. Additional energy savings can be achieved due to the fact that low data rates transmissions require lower signal power. Therefore, the transmitter launch power can be decreased.

In this paper, we introduce a flexible MultiCAP modulation concept and its application to the data interconnects. The successful performance of this flexible scheme is experimentally demonstrated for 850 nm vertical-cavity surface-emitting laser (VCSEL) based transmissions up to 40.6 Gb/s over 100 m of multi-mode fiber (MMF). Furthermore, we demonstrate that for low data rates the VCSEL bias current can be decreased contributing to the additional energy savings.

II. Experimental Setup and Digital Signal Processing

Fig. 2 shows the block diagram of the experimental setup used to validate the flexibility of the proposed scheme for data interconnect applications. The transmitter consists of a 24 GSa/s arbitrary waveform generator (AWG) (Tektronix AWG7122C) with a vertical resolution of 10 bits and a 3-dB bandwidth of 5.6 GHz, a Bias-T, a DC current source, and a commercially available directly modulated 850 nm VCSEL [19]. The transmitter digital signal processing (DSP) is done offline and the generated signal samples are loaded to the AWG after quantization. After transmission through 100 m of OM4 multi-mode fiber (MMF), which has a bandwidth of 4700 MHz·km, the optical signal is converted into the electrical domain by a 22 GHz PIN photodiode (PD) with a conversion gain of 80 V/W. After conversion, the electrical signal is captured with a 33 GHz digital storage oscilloscope (DSO) at a sampling rate of 100 GSa/s and 8 bits of vertical resolution for further offline DSP. Bit error rates (BERs) are computed offline, for each band separately, from the actual received data stored with the DSO.

Fig. 3(a) shows the frequency response of the back-to-back (B2B) and 100 m OM4 transmission links, measured with a 50 GHz network analyzer. These frequency responses were measured from the input of the Bias-T to the output of the PD. It is to be noted that these frequency responses are considerably flat up to 10 GHz. As a result, the AWG used in the experiments was the limiting factor of the transmissions, since it has a lower bandwidth than the end-to-end system frequency response (Fig. 3(b)).

A. Simulations and Offline Processing

The flexible MultiCAP signal is generated to make the best usage of the available bandwidth as well as assure adaptive operation. To generate the signal for each band, decorrelated pseudo-random binary sequences (PRBSs) of $2^{11}-1$ bits of length are mapped into its corresponding quadrature amplitude modulation (QAM) and phase shift keying (PSK) symbol constellations, i.e. bit loading. The obtained symbol sequences are up-sampled to the number of samples per symbol determined by the baud rate of each band and filtered by the pair of CAP orthogonal filters corresponding to each band. Power loading is employed by assigning different signal amplitude weights to each band of the MultiCAP signal to mitigate the impairments due to the non-flat frequency response, e.g. frequency response of the AWG. At the receiver, after signal resampling, the in-phase (I) and quadrature (Q) channels of each MultiCAP band are retrieved by filtering with filters matched to the CAP filters at the transmitter. Finally, each channel is down-sampled to construct the corresponding symbol constellations, from which the binary sequences are demodulated by means of a decision-feedback equalizer (DFE) with 30 feed-forward taps and 30 feed-back taps, and the k-means algorithm. It is to be noted that after the pre-emphasis stage at the transmitter and before the resampling stage at the receiver, the signals are quantized in accordance to the vertical resolutions of the AWG and DSO, respectively.

The main limiting factor to achieve high data rates is the frequency response of the AWG, which is considerably lower than the end-to-end frequency response of the link as can be seen in Fig. 3(b). To include these frequency responses in the simulations, linear-phase finite impulse response (FIR) filters are designed to match them. In Fig. 3(b) is shown the comparison

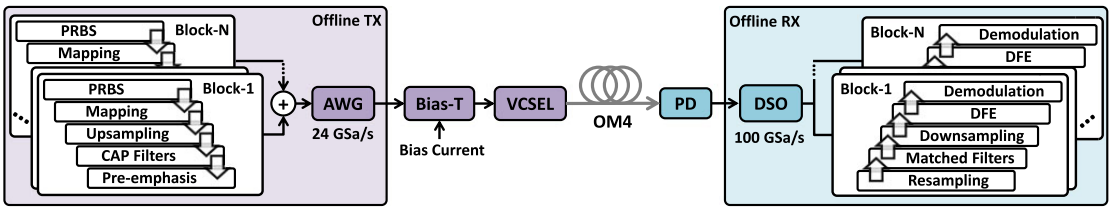

Fig. 2. Block diagram of experimental setup. PRBS: pseudo-random binary sequence, AWG: arbitrary waveform generator, VCSEL: vertical cavity surface emitting laser, PD: photodiode, DSO: digital storage oscilloscope.

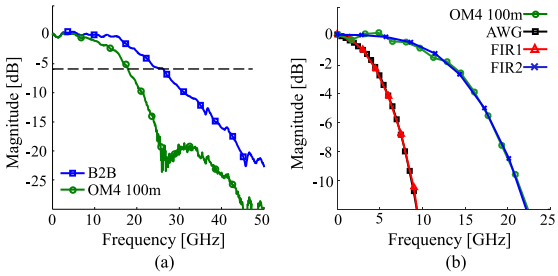

Fig. 3. (a) End-to-end frequency responses of B2B and 100 m OM4 links, and (b) comparison of frequency responses of the AWG, 100 m OM4 link, and its corresponding FIR filters used in simulations.

of the frequency responses of the AWG, the 100 m OM4 link, and the designed FIR filters. To show the full capacity of MultiCAP modulation, first simulations are performed only considering the frequency response of the end-to-end 100 m OM4 link, and then, to simulate the conditions of the real experimental setup, further simulations are performed including the AWG frequency response.

In simulations, the generated MultiCAP signals are filtered by the FIR filters in order to determine suitable parameters for the MultiCAP signaling. First simulations are focused on showing the potential high bit rates that can be achieved by means of MultiCAP modulation, while showing its flexibility to adjust the modulation schemes and baud rates of each band. Assuming a generator with the same sampling frequency as the DSO used in the experiments, i.e. 100 GSa/s, and the frequency response of the 100 m OM4 link, a bit rate over 100 Gb/s is achieved with a BER below the commercial 7% overhead forward error correction (FEC) threshold of 3.8×10^{-3}. In Fig. 4 is shown the spectrum of the transmitted signal including the link frequency response, the power loading applied to the bands, and the symbol constellations of all bands as insets. Table I summarizes the main parameters of the 102.75 Gb/s generated signal. Seven bands are allocated using a total bandwidth of 23.1 GHz. It is to be noted that, as the frequency increases the signal-to-noise ratio (SNR) worsens due to the roll-off of the link frequency response. As consequence, for low frequencies where the frequency response is fairly flat and the gain is higher, high modulation orders can be employed, e.g. 128-QAM, and for high frequencies where the bandwidth constraints are more noticeable, low-order modulation schemes must be employed to ensure a good performance of the link, e.g. QPSK. To avoid the crosstalk between adjacent bands, a guard band corresponding to the sum of the 1% of the adjacent bands baud rate is left between the bands, e.g. the guard band between band 1 and band 2 is $0.01 \times 1.25 + 0.01 \times 2 = 0.02325$ GHz.

To simulate the real experimental setup conditions, i.e. a 3-dB bandwidth of 5.6 GHz and required bit rate and modulation adjustability, an adequate tradeoff between performance and the number of bands is achieved with 5 bands. Table II shows the parameters found for each band which maximizes the bit rate. As in previous simulations, to avoid the crosstalk between adjacent bands the same percentage is used to determine the guard bands, and the modulation orders of the bands are decreased in accordance to the frequency response of the link. Furthermore, with the selected baud rates for each band, bit rates between 6 Gb/s and 10 Gb/s were achieved. By switching on and off the appropriate bands 6, 15, 28.6, and 40.6 Gb/s total data rates can be achieved. Fig. 5 shows the simulation signal spectrum at the transmitter when all bands are active, including power loading and as insets the symbol constellations of all bands with which the BERs of each band were below the commercial 7% overhead FEC threshold. It can be noticed the

TABLE I
102.75 GB/S SIGNAL PARAMETERS

Band	Baud Rate [Gbaud]	Modulation Scheme	Bit Rate [Gb/s]	Central Frequency [GHz]	Weight (Amplitude)
1	1.25	128-QAM	8.75	0.6375	$\sqrt{2}$
2	2	64-QAM	12	2.2950	1
3	2	64-QAM	12	4.3350	1
4	2.5	64-QAM	15	6.6300	$\sqrt{1.2}$
5	5	32-QAM	25	10.4550	$\sqrt{1.2}$
6	5	16-QAM	20	15.5550	$\sqrt{1.2}$
7	5	QPSK	10	20.6550	1

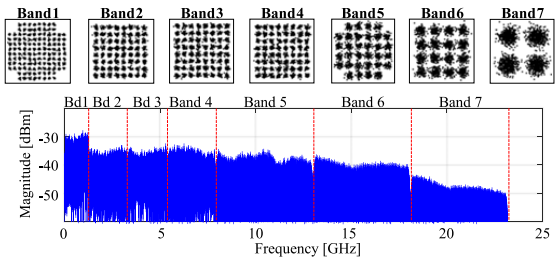

Fig. 4. MultiCAP 102.75 Gb/s signal electrical spectrum at the transmitter and symbol constellations.

TABLE II
40.6 GB/S SIGNAL PARAMETERS

Band	Baud Rate [Gbaud]	Modulation Scheme	Bit Rate [Gb/s]	Central Frequency [GHz]	Weight (Amplitude)
1	1	64-QAM	6	0.5100	1
2	1.5	64-QAM	9	1.7850	$\sqrt{2}$
3	2	32-QAM	10	3.5700	$\sqrt{2}$
4	2.4	16-QAM	9.6	5.8140	$\sqrt{3}$
5	3	QPSK	6	8.5680	$\sqrt{2}$

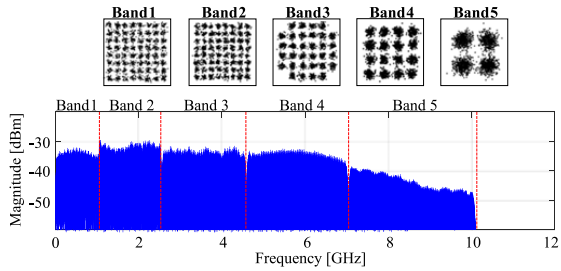

Fig. 5. MultiCAP 40.6 Gb/s signal electrical spectrum at the transmitter and symbol constellations.

TABLE III
FLEXIBLE MULTICAP MODULATION PARAMETERS IN FIXED MODULATION SCENARIO

Band	Baud rate [Gbaud]	Modulation Order [M-QAM]				Bit Rate [Gb/s]			
		Case 1	Case 2	Case 3	Case 4	Case 1	Case 2	Case 3	Case 4
1	1	64		64	64	6		6	6
2	1.5	64	64	64		9	9	9	
3	2	32	32			10	10		
4	2.4	16	16			9.6	9.6		
5	3	4				6			
TOTAL						40.6	28.6	15	6

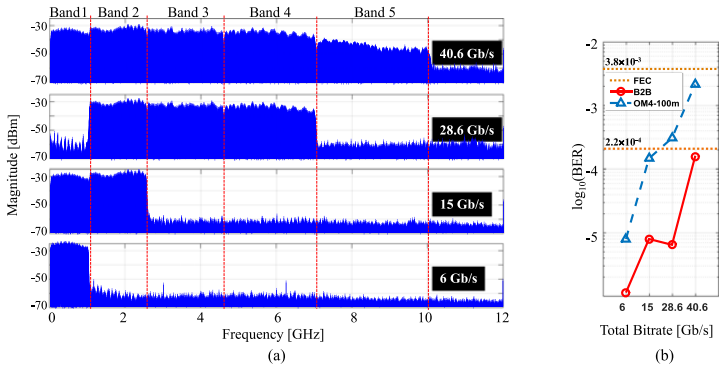

Fig. 6. Fixed modulation scenario, (a) received spectra, and (b) measured BER versus total bit rate.

different bandwidth occupied by each band and the different value of power of each band due to power loading technique. For the highest bit rate case, the total signal bandwidth is 10.1 GHz, with a spectral efficiency of 4 bit/s/Hz.

By increasing considerably the number of taps of the DFE, it is possible to further decrease the BER below more recent FEC threshold standards such as 2.2×10^{-4} (e.g. 400GBase-DR4). However, the complexity of the system increases at a rapid pace with the number of taps, therefore a DFE with a low number of taps is used to compute the BER results in the experiments.

III. TRANSMISSION EXPERIMENTS

The operation of the proposed scheme was investigated in two different scenarios. The first scenario was examined by activating and deactivating bands, while maintaining the modulation orders of the bands unchanged. Four different cases were implemented with bit rates of 40.6, 28.6, 15 and 6 Gb/s, respectively. In all cases, the VCSEL bias current was 4 mA and the driving voltage was 0.7 V_{pp}. In Table III a summary of the main parameters for each case is presented. The shades in the table indicate when a band is inactive for a particular case. In Fig. 6 the received signal spectra generated from the DSO captured data and the BER results are shown for the four different cases. In Fig. 6(a) activation and deactivation of the bands is clearly visible. It can be seen in Fig. 6(b) that, in all cases, the average BER of all bands is below the 7% FEC limit, proving excellent operation of the proposed concept.

In the second scenario, not only the selected bands were activated and deactivated, but also the modulation order for a given band as well as the VCSEL bias current were adjusted. Since low-order modulation schemes can tolerate a lower SNR, lower signal powers can be provided to the receiver and still achieve a successful transmission. Therefore the VCSEL bias current can be reduced, which contributes to the further transmission system energy savings. In this scenario, four different cases were studied. In Table IV a summary of the main parameters for each case is presented, and Fig. 7 shows the received electrical spectra. Activation and deactivation of the appropriate bands is visible. Fig. 8(a) shows the measured BER as function of the received optical power, and Fig. 8(b) as a function of the bias current. It is to be noted that the received optical power was adjusted only by adjusting the VCSEL bias current, thus the power values in

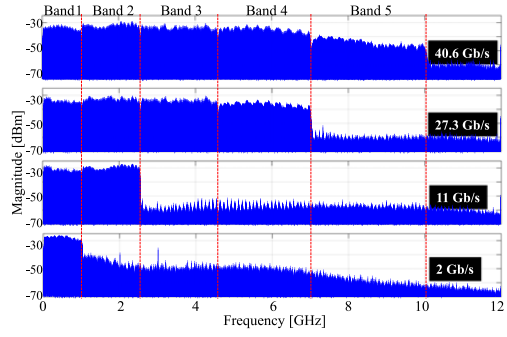

Fig. 7. Spectra for different cases in the variable modulation order scenario.

TABLE IV
FLEXIBLE MULTICAP MODULATION PARAMETERS WITH VARIABLE MODULATION

Band	Baud rate [Gbaud]	Modulation Order [M-QAM]				Bit Rate [Gb/s]			
		Case 1	Case 2	Case 3	Case 4	Case 1	Case 2	Case 3	Case 4
1	1	64	32	32	4	6	5	5	2
2	1.5	64	32	16		9	7.5	6	
3	2	32	32			10	10		
4	2.4	16	4			9.6	4.8		
5	3	4				6			
TOTAL						40.6	27.3	11	2

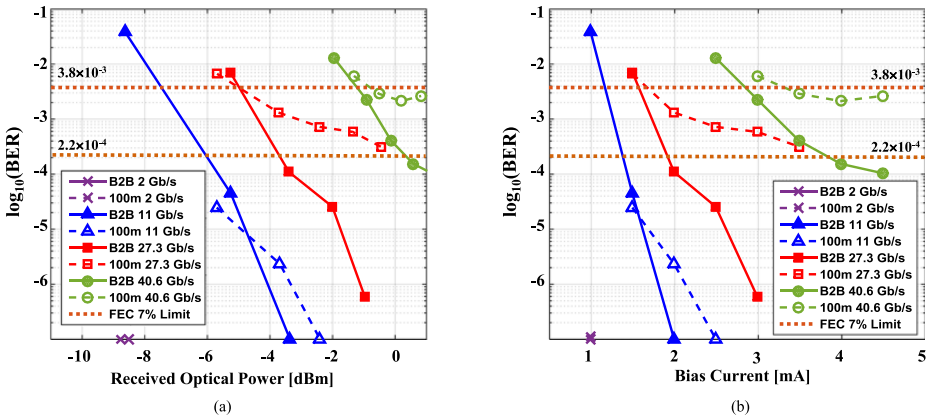

Fig. 8. (a) BER versus received optical power, and (b) BER versus bias current for different bit rates and MMF lengths.

Fig. 8(a) correspond to the bias current values in Fig. 8(b). In all transmission cases, i.e. with different bit rates as well as the B2B and 100 m MMF length, operation below the 7% FEC limit was observed proving excellent operation of the system.

IV. DISCUSSION

For both scenarios, the performance of our proposal was validated with BERs below the commercial 7% overhead FEC threshold of 3.8×10^{-3}. For more stringent FEC thresholds of recent standards, e.g. 2.2×10^{-4}, only B2B transmissions and lower bit rates transmissions over 100 m of MMF are compliant. The performance of the transmissions can be further improved at the cost of increasing the complexity of the receiver, e.g. increasing the number of equalization taps.

For the first scenario, it was noted that the guard band that was left between the first and the second band is not enough to ensure the best performance for high modulation orders, i.e. 64-QAM. As can be noted in the B2B results (Fig. 6(a)), in the 28.6 Gb/s transmission only one band with 64-QAM modulation is active, i.e. second band, while in the 15 Gb/s transmission two consecutive bands with 64-QAM modulation are active, i.e. first and second band. Therefore, the performance of this last transmission is worst even if the bit rate is lower. Contrary to the B2B case, after 100 m of OM4 MMF, the impairments of the transmission, e.g. inter-modal dispersion, are more dominant than the crosstalk effects within the bands. Therefore, for 100 m OM4 MMF transmissions the performance of the 15 Gb/s transmission is better than the 28 Gb/s transmission.

In the second scenario, in the second set of measurements (Fig. 8(b)), for a given transmission case, the VCSEL bias current was adjusted (decreased) to reach operation in proximity to the FEC limit. As can be noticed, for each transmission case, the bias current could be significantly reduced, while preserving operation below FEC threshold, e.g. for the 40.6 Gb/s 100 m transmission the current could be reduced from 4.5 to 3.5 mA, and for the 11 Gb/s 100 m transmission from 2.5 to 1.5 mA. Fig. 9 hows the actual and the normalized (to 3.5 mA) VCSEL bias current versus the bit rate for the 100 m link, for which the BER is still below 7% FEC limit. By having as reference the 40.6 Gb/s transmission, when transmitting 27.3, 11, and 2 Gb/s

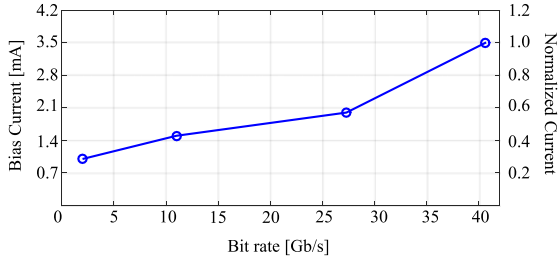

Fig. 9. Actual and normalized VCSEL bias current versus bit rate.

the bias current of the VCSEL was reduced 1.75, 2.33, and 3.5 times (57.14%, 42.85%, and 28.57%), respectively. Thus, the optical received power was reduced by 3.22, 5.18, and 8.28 dB, respectively. The lowest transmission rates allow higher current reduction. Therefore, in this scenario the energy savings can not only come from activation and deactivation of the modulation/demodulation sub-blocks but also from the adjustment of the VCSEL bias current. It is to be noted that, the BERs of the 27.3 and 40.6 Gb/s transmissions over 100 m of MMF, get worse faster than the low bit rate cases since high modulation orders, i.e. 64-, 32-QAM, require a higher SNR to achieve a good performance. As well that, when the bias current of the VCSEL is close to its threshold current, i.e. <1 mA, the dominant link impairment is the VCSEL itself, since its operation point is far from the optimal one. Therefore, it was not possible to decrease the VCSEL bias current below 1 mA.

For all transmissions, the different symbol constellations were scaled, i.e. the distance between the symbols in the constellations, in order to make all of them have the same average energy. Thus, the power consumption of the bands due the modulation order is always the same. Additionally, assuming that the electronics of each sub-block are the same, and given that the VCSEL output power is linear with respect to its bias current in our range of operation [19], it is possible to approximate that the energy savings behaves linearly with respect to the number of active bands (sub-blocks).

V. Conclusion

In this paper, we propose and validate experimentally a novel flexible scheme for MultiCAP modulation. The proposed scheme offers high spectral efficiency, adjustable bit rate as well as reduced energy consumption. Simulations results validate the feasibility of the proposed scheme with bit rates over 100 Gb/s by using state-of-the-art electronics, e.g. super high-speed digital to analog converters (DACs) [20], [21]. As a proof of concept, we validate its operation in 850 nm VCSEL based data interconnect up to 40 Gb/s, showing all its key advantages. Results prove the proposed flexible MultiCAP as a prospective solution, which can be successfully applied in transmission systems that require bit rate adaptivity and energy consumption reduction.

Similarly to the study presented in [13], further research is aimed to perform a thorough comparison of the most common modulation schemes, i.e. NRZ, PAM, and OFDM, regarding bit rate adjustment and the resulting energy savings for 850 nm data interconnects.

Acknowledgment

Laboratory equipment was provided through the Polish Innovative Economy Program POIG.02.01.00-14-197/09 FOTEH Project.

References

[1] C. Gray, R. Ayre, K. Hinton, and R. S. Tucker, "Power consumption of IoT access network technologies," in *Proc. 2015 IEEE Int. Conf. Commun. Workshop*, 2015, pp. 2818–2823.

[2] A. Liu and D. Bimberg, "Vertical-cavity surface-emitting lasers with nanostructures for optical interconnects," *Frontiers Optoelectron.*, vol. 9, no. 2, pp. 249–258, 2016.

[3] H. Li *et al.*, "Energy-efficient and temperature-stable oxide-confined 980 nm VCSELs operating error-free at 38 Gbit/s at 85°C," *Electron. Lett.*, vol. 50, no. 2, pp. 103–105, 2014.

[4] J. Baliga, R. Ayre, K. Hinton, W. V Sorin, and R. S. Tucker, "Energy consumption in optical IP networks," *J. Lightw. Technol.*, vol. 27, no. 13, pp. 2391–2403, Jul. 2009.

[5] R. S. Tucker, "Green optical communications—Part II: Energy limitations in networks," *IEEE J. Sel. Topics Quantum Electron.*, vol. 17, no. 2, pp. 261–274, Mar./Apr. 2011.

[6] K. Szczerba, T. Lengyel, M. Karlsson, P. Andrekson, and A. Larsson, "94 Gbps 4-PAM using an 850 nm VCSEL, pre-emphasis and receiver equalization," *IEEE Photon. Technol. Lett.*, vol. 28, no. 22, pp. 2519–2521, Nov. 2016.

[7] J. Wei *et al.*, "Demonstration of the first real-time end-to-end 40-Gb/s PAM-4 for next-generation access applications using 10-Gb/s transmitter," *J. Lightw. Technol.*, vol. 34, no. 7, pp. 1628–1635, Apr. 2016.

[8] G. Stepniak *et al.*, "54 Gbit/s OOK transmission using single-mode VCSEL up to 2.2 km MMF," *Electron. Lett.*, vol. 52, no. 8, pp. 633–635, 2016.

[9] J. P. Turkiewicz, J. R. Kropp, N. N. Ledentsov, V. A. Shchukin, and G. Schafer, "High speed optical data transmission with compact 850 nm TO-Can Assemblies," *IEEE J. Quantum Electron.*, vol. 50, no. 4, pp. 281–286, Apr. 2014.

[10] T. Benson, A. Akella, and D. A. Maltz, "Network traffic characteristics of data centers in the wild," in *Proc. 10th ACM SIGCOMM Conf. Internet Meas.*, 2010, pp. 267–280.

[11] A. Morea, O. Rival, N. Brochier, and E. Le Rouzic, "Datarate adaptation for night-time energy savings in core networks," *J. Lightw. Technol.*, vol. 31, no. 5, pp. 779–785, Mar. 2013.

[12] A. Dixit, S. Lambert, B. Lannoo, D. Colle, M. Pickavet, and P. Demeester, "Towards energy efficiency in optical access networks [Invited]," in *Proc. 2013 IEEE Int. Conf. Adv. Netw. Telecommun. Syst.*, 2013, pp. 1–6.

[13] J. L. Wei, J. D. Ingham, D. G. Cunningham, R. V Penty, and I. H. White, "Performance and power dissipation comparisons between 28 Gb/s NRZ, PAM, CAP and optical OFDM systems for data communication applications," *J. Lightw. Technol.*, vol. 30, no. 20, pp. 3273–3280, Oct. 2012.

[14] R. Puerta, S. Rommel, J. J. V Olmos, and I. T. Monroy, "Up to 35 Gbps ultra-wideband wireless data transmission links," in *Proc. 2016 IEEE 27th Annu. Int. Symp. Pers., Indoor, Mobile Radio Commun.*, 2016, pp. 1–5.

[15] R. Puerta, S. Rommel, J. J. V. Olmos, and I. T. Monroy, "Optically generated single side-band radio-over-fiber transmission of 60 Gbit/s over 50 m at W-Band," in *Proc. Opt. Fiber Commun. Conf.*, 2017, Art. no. M3E.4.

[16] M. I. Olmedo *et al.*, "Multiband carrierless amplitude phase modulation for high capacity optical data links," *J. Lightw. Technol.*, vol. 32, no. 4, pp. 798–804, Feb. 2014.

[17] L. Zhang, B. Liu, X. Xin, and Y. Wang, "10 $\times$ 70.4-Gb/s dynamic FBMB/CAP PON based on remote energy supply," *Opt. Express*, vol. 22, no. 22, pp. 26985–26990, Nov. 2014.

[18] R. Puerta, J. J. V. Olmos, I. T. Monroy, J. P. Turkiewicz, and S. Echeverri-Chacón, "Adaptive MultiCAP modulation for short range VCSEL based transmissions," in *Proc. Latin Amer. Opt. Photon. Conf.*, 2016, Paper LW4C.3.

[19] VI Systems, "V40-850M multi mode fiber coupled VCSEL transmitter module datasheet," 2012. [Online]. Available: http://www.hikari-trading.com/visystems/file/VIS_Data027.pdf

[20] R. Puerta *et al.*, "Effective 100 Gb/s IM/DD 850-nm multi- and single-mode VCSEL transmission through OM4 MMF," *J. Lightw. Technol.*, vol. 35, no. 3, pp. 423–429, Feb. 2017.

[21] R. Puerta, J. Yu, X. Li, Y. Xu, J. J. V. Olmos, and I. T. Monroy, "Demonstration of 352 Gbit/s photonically-enabled D-band wireless delivery in one 2 $\times$ 2 MIMO System," in *Proc. Opt. Fiber Commun. Conf.*, 2017, Paper Tu3B.3.

Authors' biographies not available at the time of publication.

Bibliography

[1] Cisco, "The Zettabyte Era: Trends and Analysis, White Paper," June 2017.

[2] Cisco, "Cisco Global Cloud Index: Forecast and Methodology, 2015–2020, White Paper," 2016.

[3] Cisco, "Cisco Visual Networking Index: Global Mobile Data Traffic Forecast Update, 2016–2021, White Paper," February 2017.

[4] Finisar, "Introduction to EDFA Technology, White Paper," June 2009.

[5] Finisar, "Introduction to Optical Amplifiers, White Paper," June 2010.

[6] C. Kachris and I. Tomkos, "A roadmap on optical interconnects in data centre networks," in *2015 17th International Conference on Transparent Optical Networks (ICTON)*, 2015, pp. 1–3.

[7] C. F. Lam, H. Liu, and R. Urata, "What devices do data centers need?," in *Optical Fiber Communication Conference*, 2014, p. M2K.5.

[8] R. Puerta, M. Agustin, L. Chorchos, J. Tonski, J.-R. Kropp, N. Ledentsov, V. A. Shchukin, N. N. Ledentsov, R. Henker, I. T. Monroy, J. J. V. Olmos, and J. P. Turkiewicz, "Short-range links beyond 100 Gb/s with vertical-cavity surface-emitting lasers," *SPIE Newsroom*, p. 1–3, 2017.

[9] J. P. Turkiewicz, L. Chorchos, R. Puerta, J. J. V. Olmos, and N. Ledentsov, "On high speed transmission with the 850nm VCSELs," *Proc. SPIE*, vol. 10031. p. 100311B–100311B–6, 2016.

[10] J. A. Tatum, D. Gazula, L. A. Graham, J. K. Guenter, R. H. Johnson, J. King, C. Kocot, G. D. Landry, I. Lyubomirsky, A. N. MacInnes, E. M. Shaw, K. Balemarthy, R. Shubochkin, D. Vaidya, M. Yan, and F. Tang, "VCSEL-Based Interconnects for Current and Future Data Centers,"*J. Light. Technol.*, vol. 33, no. 4, pp. 727–732, Feb. 2015.

[11] R. Michalzik and K. J. Ebeling, "Operating Principles of VCSELs," in *Vertical-Cavity Surface-Emitting Laser Devices*, H. E. Li and K. Iga, Eds. Berlin, Heidelberg: Springer Berlin Heidelberg, 2003, pp. 53–98.

[12] C. Caspar, J. R. Kropp, V. A. Shchukin, N. N. Ledentsov, V. Jungnickel, and R. Freund, "High speed transmission over Multimode Fiber with direct modulated single-mode VCSEL," in *Broadband Coverage in Germany. 9th ITG Symposium. Proceedings*, 2015, pp. 1–4.

[13] G. Stepniak, A. Lewandowski, J. R. Kropp, N. N. Ledentsov, V. A. Shchukin, N. Ledentsov, G. Schaefer, M. Agustin, and J. P. Turkiewicz, "54 Gbit/s OOK transmission using single-mode VCSEL up to 2.2 km MMF," *Electron. Lett.*, vol. 52, no. 8, pp. 633–635, 2016.

[14] D. Coleman. (2012). Optical Trends in the Data Center [Online]. Available: https://www.bicsi.org/uploadedfiles/bicsi_conferences/canada/2012/presentations/concses_2a.pdf.

[15] M. Kuschnerov, F. N. Hauske, K. Piyawanno, B. Spinnler, M. S. Alfiad, A. Napoli, and B. Lankl, "DSP for Coherent Single-Carrier Receivers," *J. Light. Technol.*, vol. 27, no. 16, pp. 3614–3622, Aug. 2009.

[16] S. J. Savory, "Digital Coherent Optical Receivers: Algorithms and Subsystems," *IEEE J. Sel. Top. Quantum Electron.*, vol. 16, no. 5, pp. 1164–1179, Sep. 2010.

[17] F. N. Hauske, *The Importance of Digital Signal Processing in High Speed Optical Receivers: Equalization, Impairment Compensation and Performance Monitoring*, 1st ed. Verlag Dr. Koster, 2013.

[18] K. Kikuchi, "Fundamentals of Coherent Optical Fiber Communications," *J. Light. Technol.*, vol. 34, no. 1, pp. 157–179, Jan. 2016.

[19] M. S. Faruk and S. J. Savory, "Digital Signal Processing for Coherent Transceivers Employing Multilevel Formats," *J. Light. Technol.*, vol. 35, no. 5, pp. 1125–1141, 2017.

[20] R. Rios-Muller, J. Renaudier, P. Brindel, A. Ghazisaeidi, I. Fernandez, P. Tran, C. Simonneau, L. Schmalen, and G. Charlet, "Spectrally-Efficient 400-Gb/s Single Carrier Transport Over 7 200 km," *J. Light. Technol.*, vol. 33, no. 7, pp. 1402–1407, Apr. 2015.

[21] H.-C. Chien, J. Zhang, J. Yu, and Y. Cai, "Single-Carrier 400G PM-256QAM Generation at 34 GBaud Trading off Bandwidth Con-

straints and Coding Overheads," in *Optical Fiber Communication Conference*, 2017, p. W1J.3.

[22] J. Zhang, J. Yu, B. Zhu, F. Li, H.-C. Chien, Z. Jia, Y. Cai, X. Li, X. Xiao, Y. Fang, and Y. Wang, "Transmission of single-carrier 400G signals (515.2-Gb/s) based on 128.8-GBaud PDM QPSK over 10,130- and 6,078 km terrestrial fiber links," *Opt. Express*, vol. 23, no. 13, pp. 16540–16545, Jun. 2015.

[23] D. van den Borne, *Robust optical transmission systems: modulation and equalization*, Technische Universiteit Eindhoven, 2008.

[24] K. Kikuchi, "Coherent Optical Communications: Historical Perspectives and Future Directions," in *High Spectral Density Optical Communication Technologies*, 1st ed. Springer-Verlag Berlin Heidelberg, 2010, ch. 2.

[25] F. Adachi, "Wireless past and future-evolving mobile communications systems," *IEICE Trans. Fundam.*, vol. 84, no. 1, pp. 55–60, 2001.

[26] J. G. Andrews, S. Buzzi, W. Choi, S. V Hanly, A. Lozano, A. C. K. Soong, and J. C. Zhang, "What Will 5G Be?," *IEEE J. Sel. Areas Commun.*, vol. 32, no. 6, pp. 1065–1082, 2014.

[27] A. Osseiran, F. Boccardi, V. Braun, K. Kusume, P. Marsch, M. Maternia, O. Queseth, M. Schellmann, H. Schotten, H. Taoka, H. Tullberg, M. A. Uusitalo, B. Timus, and M. Fallgren, "Scenarios for 5G mobile and wireless communications: the vision of the METIS project," *IEEE Commun. Mag.*, vol. 52, no. 5, pp. 26–35, 2014.

[28] F. Boccardi, R. W. Heath, A. Lozano, T. L. Marzetta, and P. P. Aalborg, "Five disruptive technology directions for 5G," *IEEE Commun. Mag*, pp. 74–80, 2014.

[29] P. Demestichas, A. Georgakopoulos, D. Karvounas, K. Tsagkaris, V. Stavroulaki, J. Lu, C. Xiong, and J. Yao, "5G on the Horizon: Key Challenges for the Radio-Access Network," *IEEE Veh. Technol. Mag.*, vol. 8, no. 3, pp. 47–53, Sep. 2013.

[30] R. Baldemair, T. Irnich, K. Balachandran, E. Dahlman, G. Mildh, Y. Selen, S. Parkvall, M. Meyer, and A. Osseiran, "Ultra-dense networks in millimeter-wave frequencies," *IEEE Commun. Mag.*, vol. 53, no. 1, pp. 202–208, 2015.

[31] N. Bhushan, J. Li, D. Malladi, R. Gilmore, D. Brenner, A. Damnjanovic, R. T. Sukhavasi, C. Patel, and S. Geirhofer, "Network den-

sification: the dominant theme for wireless evolution into 5G," *IEEE Commun. Mag.*, vol. 52, no. 2, pp. 82–89, 2014.

[32] H. Kaji, S. Kumagai, K. Temma, and F. Adachi, "Spectrum-Energy Efficiency Tradeoff of Distributed Antenna Network," *2014 IEEE 11th Vehicular Technology Society Asia Pacific Wireless Communications Symposium*, Ping Tung, Taiwan, Aug. 2014.

[33] F. Adachi, W. Peng, T. Obara, T. Yamamoto, R. Matsukawa, and M. Nakada, "Distributed antenna network for gigabit wireless access," *AEU - Int. J. Electron. Commun.*, vol. 66, no. 8, pp. 605–612, 2012.

[34] X. Li, J. Yu, K. Wang, Y. Xu, L. Chen, L. Zhao, and W. Zhou, "Bidirectional delivery of 54-Gbps 8QAM W-band signal and 32-Gbps 16QAM K-band signal over 20-km SMF-28 and 2500-m wireless distance," in *2017 Optical Fiber Communications Conference and Exhibition (OFC)*, 2017, pp. 1–3.

[35] R. Puerta, S. Rommel, J. J. V. Olmos, and I. T. Monroy, "Optically Generated Single Side-Band Radio-over-Fiber Transmission of 60Gbit/s over 50m at W-Band," in *Optical Fiber Communication Conference*, 2017, p. M3E.4.

[36] J. Xiao, J. Yu, X. Li, Y. Xu, Z. Zhang, and L. Chen, "20-Gb/s PDM-QPSK Signal Delivery over 1.7-km Wireless Distance at W-Band," in *Optical Fiber Communication Conference*, 2015, p. W4G.4.

[37] S. Rommel, S. Rodriguez, L. Chorchos, E. P. Grakhova, A. K. Sultanov, J. P. Turkiewicz, J. J. V Olmos, and I. T. Monroy, "225m Outdoor W-band radio-over-fiber link using an optical SFP+ module," in *2016 Optical Fiber Communications Conference and Exhibition (OFC)*, 2016, pp. 1–3.

[38] R. G. Stephen and R. Zhang, "Joint Millimeter-Wave Fronthaul and OFDMA Resource Allocation in Ultra-Dense CRAN," *IEEE Trans. Commun.*, vol. 65, no. 3, pp. 1411–1423, 2017.

[39] J. Wells, "Faster than fiber: The future of multi-G/s wireless," *IEEE Microw. Mag.*, vol. 10, no. 3, pp. 104–112, 2009.

[40] W. Roh, J. Y. Seol, J. Park, B. Lee, J. Lee, Y. Kim, J. Cho, K. Cheun, and F. Aryanfar, "Millimeter-wave beamforming as an enabling technology for 5G cellular communications: theoretical feasibility and prototype results," *IEEE Commun. Mag.*, vol. 52, no. 2, pp. 106–113, 2014.

[41] D. Porcino and W. Hirt, "Ultra-wideband radio technology: potential and challenges ahead," *IEEE Communications Magazine*, vol. 41, no. 7, pp. 66–74, July 2003.

[42] Federal Communications Commission, "Ultra-wideband operation," in *Title 47 Chapter I Part 15.F.*, 2005.

[43] Electronic Communications Committee, "The harmonised conditions for devices using ultra-wideband (UWB) technology in bands below 10.6 GHz," in *ECC Decision (06)04*, 2006.

[44] State Commission for Radio Frequencies, "Ultrawideband Wireless Devices," in *Annex to SCRF No. 09-05-02*, 2009.

[45] M. Chiani and A. Giorgetti, "Coexistence between UWB and narrowband wireless communication systems," *Proceedings of the IEEE*, vol. 97, no. 2, pp. 231–254, Feb 2009.

[46] S. Emami, *UWB Communication Systems: Conventional and 60 GHz*. New York: Springer, 2013.

[47] S. Haykin, *Communication Systems*, 4th ed. Wiley Publishing, 2001.

[48] J. G. Proakis, *Digital Communications*, 4th ed. McGraw-Hill, 2001.

[49] M. I. Olmedo, T. Zuo, J. B. Jensen, Q. Zhong, X. Xu, S. Popov, and I. T. Monroy, "Multiband Carrierless Amplitude Phase Modulation for High Capacity Optical Data Links," *Light. Technol. J.*, vol. 32, no. 4, pp. 798–804, Feb. 2014.

[50] T. Zuo, A. Tatarczak, M. Iglesias, J. Estaran, J. B. Jensen, Q. Zhong, X. Xu, and I. Tafur, "O-band 400 Gbit/s Client Side Optical Transmission Link," in *Optical Fiber Communication Conference*, 2014, p. M2E.4.

[51] P. A. Haigh, S. T. Le, S. Zvanovec, Z. Ghassemlooy, P. Luo, T. Xu, P. Chvojka, T. Kanesan, E. Giacoumidis, P. Canyelles-Pericas, H. L. Minh, W. Popoola, S. Rajbhandari, I. Papakonstantinou, and I. Darwazeh, "Multi-band carrier-less amplitude and phase modulation for bandlimited visible light communications systems," *IEEE Wirel. Commun.*, vol. 22, no. 2, pp. 46–53, Apr. 2015.

[52] C. Xie, P. Dong, S. Randel, D. Pilori, P. Winzer, S. Spiga, B. Kogel, C. Neumeyr, and M. C. Amann, "Single-VCSEL 100-Gb/s short-reach system using discrete multi-tone modulation and direct detection," in *Optical Fiber Communications Conference and Exhibition (OFC)*, 2015, 2015, pp. 1â"3.

[53] I. C. Lu, C. C. Wei, H. Y. Chen, K. Z. Chen, C. H. Huang, K. L. Chi, J. W. Shi, F. I. Lai, D. H. Hsieh, H. C. Kuo, W. Lin, S. W. Chiu, and J. Chen, "Very High Bit-Rate Distance Product Using High-Power Single-Mode 850-nm VCSEL With Discrete Multitone Modulation Formats Through OM4 Multimode Fiber," *IEEE J. Sel. Top. Quantum Electron.*, vol. 21, no. 6, pp. 444–452, Nov. 2015.

[54] R. Puerta, J. J. V. Olmos, I. T. Monroy, J. P. Turkiewicz, "Adaptive MultiCAP modulation for short range VCSEL based transmissions," in *Latin America Optics and Photonics Conference*, 2016, p. LW4C.3.

[55] R. Puerta, J. J. V Olmos, I. T. Monroy, N. N. Ledentsov, and J. P. Turkiewicz, "Flexible MultiCAP Modulation and its Application to 850 nm VCSEL-MMF Links," *J. Light. Technol.*, vol. 35, no. 15, pp. 3168–3173, Aug. 2017.

[56] A. C. Singer, N. R. Shanbhag, and H. m. Bae, "Electronic dispersion compensation," *IEEE Signal Process. Mag.*, vol. 25, no. 6, pp. 110–130, Nov. 2008.

[57] RP Photonics. Ultrashort Pulses and Signals in Fibers [Online]. Available: https://www.rp-photonics.com/passive_fiber_optics12.html.

[58] G. P. Agrawal, *Fiber-Optic Communication Systems*, 4th ed. John Wiley Sons, 2010

[59] J. P. Costas, "Synchronous Communications," *Proc. IRE*, vol. 44, no. 12, pp. 1713–1718, Dec. 1956.

[60] Y. Wu, X. Wang, R. Citta, B. Ledoux, S. Lafleche, and B. Caron, "An ATSC DTV receiver with improved robustness to multipath and distributed transmission environments," *IEEE Trans. Broadcast.*, vol. 50, no. 1, pp. 32–41, 2004.

[61] C. A. Belfiore and J. H. Park, "Decision feedback equalization," *Proc. IEEE*, vol. 67, no. 8, pp. 1143–1156, Aug. 1979.

[62] C. Xia and W. Rosenkranz, "Nonlinear Electrical Equalization for Different Modulation Formats With Optical Filtering," *J. Light. Technol.*, vol. 25, no. 4, pp. 996–1001, Apr. 2007.

[63] R. Puerta, M. Agustin, L. Chorchos, J. Tonski, J. R. Kropp, N. Ledentsov, V. A. Shchukin, N. N. Ledentsov, R. Henker, I. T. Monroy, J. J. V Olmos, and J. P. Turkiewicz, "Effective 100 Gb/s IM/DD 850-nm Multi- and Single-Mode VCSEL Transmission Through OM4 MMF," *J. Light. Technol.*, vol. 35, no. 3, pp. 423–429, Feb. 2017.

[64] B. Wu, X. Zhou, Y. Ma, J. Luo, K. Zhong, S. Qiu, Z. Feng, Y. Luo, M. Agustin, N. Ledentsov, J. Kropp, V. Shchukin, N. N. Ledentsov, I. Eddie, and L. Chao, "Close to 100 Gbps discrete multitone transmission over 100m of multimode fiber using a single transverse mode 850nm VCSEL," *Proc. SPIE*, vol. 9766. p. 97660K–97660K–7, 2016.

[65] K. L. Chi, Y. X. Shi, X. N. Chen, J. J. Chen, Y. J. Yang, J. R. Kropp, N. Ledentsov, M. Agustin, N. N. Ledentsov, G. Stepniak, J. P. Turkiewicz, and J. W. Shi, "Single-Mode 850-nm VCSELs for 54-Gb/s ON-OFF Keying Transmission Over 1-km Multi-Mode Fiber," *IEEE Photonics Technol. Lett.*, vol. 28, no. 12, pp. 1367–1370, 2016.

[66] D. M. Kuchta, A. V Rylyakov, F. E. Doany, C. L. Schow, J. E. Proesel, C. W. Baks, P. Westbergh, J. S. Gustavsson, and A. Larsson, "A 71-Gb/s NRZ Modulated 850-nm VCSEL-Based Optical Link," *IEEE Photonics Technol. Lett.*, vol. 27, no. 6, pp. 577–580, 2015.

[67] R. Puerta, M. Agustin, L. Chorchos, J. Tonski, J.-R. Kropp, N. Ledentsov, V. A. Shchukin, N. N. Ledentsov, R. Henker, I. T. Monroy, J. J. V. Olmos, and J. P. Turkiewicz, "107.5 Gb/s 850 nm multi- and single-mode VCSEL transmission over 10 and 100 m of multi-mode fiber," in *Optical Fiber Communication Conference Postdeadline Papers*, 2016, p. Th5B.5.

[68] J. Prat, A. Napoli, J. M. Gene, M. Omella, P. Poggiolini, and V. Curri, "Square root strategy: A novel method to linearize an optical communication system with electronic equalizers," in *Eur. Conf. Optical Commun.*, Glasgow, U.K., 2005, Paper We4.P.106.

[69] A. J. Lowery and J. Armstrong, "Orthogonal-frequency-division multiplexing for dispersion compensation of long-haul optical systems," *Opt. Express*, vol. 14, no. 6, pp. 2079–2084, Mar. 2006.

[70] S. Randel, D. Pilori, S. Chandrasekhar, G. Raybon, and P. Winzer, "100-Gb/s discrete-multitone transmission over 80-km SSMF using single-sideband modulation with novel interference-cancellation scheme," in *2015 European Conference on Optical Communication (ECOC)*, 2015, pp. 1–3.

[71] Z. Li, M. S. Erkilinc, L. Galdino, K. Shi, B. C. Thomsen, P. Bayvel, and R. I. Killey, "Comparison of digital signal-signal beat interference compensation techniques in direct-detection subcarrier modulation systems," *Opt. Express*, vol. 24, no. 25, pp. 29176–29189, Dec. 2016.

[72] Z. Li, M. S. Erkilinc, K. Shi, E. Sillekens, L. Galdino, B. C. Thomsen, P. Bayvel, and R. I. Killey, "SSBI Mitigation and the Kramers–Kronig Scheme in Single-Sideband Direct-Detection Transmission With Receiver-Based Electronic Dispersion Compensation," *J. Light. Technol.*, vol. 35, no. 10, pp. 1887–1893, 2017.

[73] A. Mecozzi, C. Antonelli, and M. Shtaif, "Kramers-Kronig coherent receiver," *Optica*, vol. 3, no. 11, pp. 1220–1227, Nov. 2016.

[74] X. Chen, C. Antonelli, S. Chandrasekhar, G. Raybon, J. Sinsky, A. Mecozzi, M. Shtaif, and P. Winzer, "218-Gb/s single-wavelength, single-polarization, single-photodiode transmission over 125-km of standard singlemode fiber using Kramers-Kronig detection," in *2017 Optical Fiber Communications Conference and Exhibition (OFC)*, 2017, pp. 1–3.

[75] R. Puerta and I. T. Monroy, "Single Photodiode 60 Gb/s 16-QAM and QPSK Coherent Transmission," submitted to *IEEE Photonics Technol. Lett.*, Aug. 2017.

[76] R. Puerta, T. Yamauchi, T. Tanimura, Y. Akiyama, T. Takahara, I. T. Monroy, and T. Hoshida, "Single-Wavelength, Single-Photodiode per Polarization 276 Gb/s PDM 8-QAM over 100 km of SSMF," submitted to *Optical Fiber Communication Conference*, Oct. 2017.

[77] J. Yu, X. Li, J. Zhang, and J. Xiao, "432-Gb/s PDM-16QAM signal wireless delivery at W-band using optical and antenna polarization multiplexing," in *2014 The European Conference on Optical Communication (ECOC)*, 2014, pp. 1–3.

[78] X. Li, J. Yu, J. Zhang, Z. Dong, F. Li, and N. Chi, "A 400G optical wireless integration delivery system," *Opt. Express*, vol. 21, no. 16, pp. 18812–18819, Aug. 2013.

[79] I. Ando, M. Tanio, M. Ito, T. Kuwabara, T. Marumoto, and K. Kunihiro, "Wireless D-band communication up to 60 Gbit/s with 64QAM using GaAs HEMT technology," in *2016 IEEE Radio and Wireless Symposium (RWS)*, 2016, pp. 193–195.

[80] X. Li, Y. Xu, J. Xiao, and J. Yu, "A 2×2 MIMO Optical Wireless System at D-Band," in *Optical Fiber Communication Conference*, 2016, p. Th4A.7.

[81] W. Alliance, "MultiBand OFDM Physical Layer Specification," August 2009.

[82] T. Keller and L. Hanzo, "Adaptive multicarrier modulation: a convenient framework for time-frequency processing in wireless communications," *Proceedings of the IEEE*, vol. 88, no. 5, pp. 611–640, May 2000.

[83] R. Puerta, J. Yu, X. Li, Y. Xu, J. J. V. Olmos, and I. T. Monroy, "Demonstration of 352 Gbit/s Photonically-enabled D-Band Wireless Delivery in one 2×2 MIMO System," in *Optical Fiber Communication Conference*, 2017, p. Tu3B.3.

[84] R. Puerta, J. Yu, X. Li, Y. Xu, J. J. V. Olmos, and I. T. Monroy, "Single Carrier PDM Radio-over-Fiber 328 Gb/s Wireless Transmission in a D-band Millimeter Wave 2 × 2 MU-MIMO System," submitted to *J. Light. Technol.*, June 2017.

[85] X. Zhou, L. E. Nelson, P. Magill, R. Isaac, B. Zhu, D. W. Peckham, P. I. Borel, and K. Carlson, "High Spectral Efficiency 400 Gb/s Transmission Using PDM Time-Domain Hybrid 32-64 QAM and Training-Assisted Carrier Recovery," *J. Light. Technol.*, vol. 31, no. 7, pp. 999–1005, Apr. 2013.

[86] R. Puerta, S. Rommel, J. J. V. Olmos, and I. T. Monroy, "Ultra Wideband Technology Comeback: Prospective Solution for 5G Next Generation Networks," submitted to *IEEE Commun. Mag.*, Apr. 2017.

[87] R. Puerta, S. Rommel, J. A. Altabas, L. Pyndt, R. Idrissa, A. K. Sultanov, J. J. Vegas Olmos, and I. Tafur Monroy, "Multiband carrierless amplitude/phase modulation for ultrawideband high data rate wireless communications," *Microw. Opt. Technol. Lett.*, vol. 58, no. 7, pp. 1603–1607, 2016.

[88] R. Puerta, S. Rommel, J. J. Vegas Olmos, and I. Tafur Monroy, "10Gb/s ultra-wideband wireless transmission based on multi-band carrierless amplitude phase modulation," in *2016 IEEE 17th Annual Wireless and Microwave Technology Conference (WAMICON)*, April 2016, pp. 1–4.

[89] R. Puerta, S. Rommel, J. J. Vegas Olmos and I. Tafur Monroy, "Up to 35 Gbps ultra-wideband wireless data transmission links," in *2016 IEEE 27th Annual International Symposium on Personal, Indoor, and Mobile Radio Communications (PIMRC)*, Sept 2016, pp. 1–5.

[90] N. Ledentsov Jr., V. A. Shchukin, J.-R. Kropp, M. Agustin, N. N. Ledentsov, "Oxide-Confined Leaky Vertical-Cavity Surface-Emitting

Lasers for Single Mode Operation," *SPIE Newsroom*, May 2016.

[91] D. A. Morero and M. R. Hueda, "Efficient concatenated coding schemes for error floor reduction of LDPC and turbo product codes," in *Global Communications Conference (GLOBECOM)*, 2012 IEEE, 2012, pp. 2361–2366.

[92] N. Eiselt, J. Wei, H. Griesser, A. Dochhan, M. H. Eiselt, J.-P. Elbers, J. J. V. Olmos, and I. T. Monroy, "Evaluation of Real-Time 8×56.25 Gb/s (400G) PAM-4 for Inter-Data Center Application Over 80 km of SSMF at 1550 nm," *J. Light. Technol.*, vol. 35, no. 4, pp. 955–962, Feb. 2017.

[93] M. Minowa *et. al.*, "5G R&D Activities for High Capacity Technologies with Ultra High-Density Multi-Band and Multi-Access Layered Cells," *IEICE Technical Report*, vol. RCS2015–250, Dec, 2015.

[94] S. T. Abraha, C. Okonkwo, P. Gamage, E. Tangdiongga, and T. Koonen, "Routing of 2Gb/s Wireless IR-UWB and 1.25Gb/s Wired Services for In-Building Networks," in *Optical Fiber Communication Conference*, 2012, p. OTh3G.4.

[95] J. B. Jensen, T. B. Gibbon, X. Yu, R. Rodes, and I. T. Monroy, "Bidirectional 3.125 Gbps Downstream / 2 Gbps Upstream Impulse Radio Ultrawide-band (UWB) over Combined Fiber and Wireless Link," in *Optical Fiber Communication Conference*, 2010, p. OThO5.

[96] S. Pan and J. Yao, "UWB-Over-Fiber Communications: Modulation and Transmission," *J. Light. Technol.*, vol. 28, no. 16, pp. 2445–2455, Aug. 2010.

[97] Cisco, "802.11ac: The Fifth Generation of Wi-Fi, Technical White Paper," March 2014.

List of Acronyms

5G	Fifth Generation
AM	Amplitude Modulation
B2B	Back-to-back
BER	Bit Error Rate
C-RAN	Cloud Radio Access Network
CAGR	Compound Annual Growth Rate
CAP	Carrierless Amplitude Phase
CD	Chromatic Dispersion
CN	Cellular Network
CSPR	Carrier-to-signal Power Ratio
DAC	Digital-to-analog Converter
DAN	Distributed Antenna Network
DCF	Dispersion-compensating Fiber
DCI	Datacenter Interconnect
DFE	Decision Feedback Equalizer
DMD	Differential Modal Delay
DML	Directly Modulated Laser
DMT	Discrete Multi-tone
DPD	Digital Pre-distortion
DSB	Double Sideband
DSP	Digital Signal Processing
ECC	Electronic Communications Committee
EIRP	Effective Isotropic Radiated Power
ENOB	Effective Number of Bits

FCC	Federal Communications Commission
FEC	Forward Error Correction
FFE	Feedforward Equalizer
FFT	Fast Fourier Transform
FIR	Finite Impulse Response
FSPL	Free-space Path Loss
FTTH	Fiber-to-the-home
I	In-phase
IF	Intermediate Frequency
IFFT	Inverse Fast Fourier Transform
IM/DD	Intensity Modulation and Direct Detection
IoE	Internet of Everything
IP	Internet Protocol
ISB	Independent Sideband
ISI	Intersymbol Interference
IT	Information Technology
KK	Kramers-Kronig
LMS	Least Mean Squares
LO	Local Oscillator
LPDC	Low-density Parity-check
M2M	Machine-to-machine
M-PAM	M-ary Pulse Amplitude Modulation
MB-CAP	Multiband Carrierless Amplitude Phase
MB-OFDM	Multiband Orthogonal Frequency Division Multiplexing
MD	Modal Dispersion
MIMO	Multiple-input Multiple-output
MMF	Multi-mode Fiber
mmWave	Millimeter-wave
MU-MIMO	Multi-user Multiple-input Multiple-output
MZM	Mach-Zehnder Modulator
NRZ	Non-return to Zero
OOK	On-off Keying
PAPR	Peak-to-average power Ratio

PD	Photo-detector
PDM	Polarization Division Multiplexing
PHY	Physical Layer
PMD	Polarization Mode Dispersion
Q	Quadrature
RC	Raised Cosine
RDE	Radius Directed Equalization
RF	Radio Frequency
RLS	Recursive Least Squares
RoF	Radio-over-fiber
RRC	Root-raised Cosine
RRU	Remote Radio Unit
SC-QAM	Single-carrier Quadrature Amplitude Modulation
SCRF	State Committee for Radio Frequencies
SDM	Spatial Division Multiplexing
SISO	Single-input Single-output
SMSR	Side-mode Suppression Ratio
SNR	Signal-to-noise Ratio
SOP	State-of-polarization
SSB	Single Sideband
SSBP	Signal-to-signal Beating Products
SSMF	Standard Single-mode Fiber
UWB	Ultra-wideband
VCSEL	Vertical-cavity Surface-emitting Laser
WDM	Wavelength-division Multiplexing
WPAN	Wireless Personal Area Network
ZB	Zettabyte